Novel Process for Removal and Recovery of Vapor Phase Mercury

Final Report for Phase I
Contract DE-AC22-95PC95257--32

March 9, 1998

Prepared by
ADA Technologies, Inc.
304 Inverness Way South, Suite 365
Englewood, CO 80112

Daryl L. Roberts, Jason Albiston, Tom Broderick, Collin Greenwell, and Robin Stewart

Prepared for
Department of Energy
Federal Energy Technology Center
P. O. Box 10940
Pittsburgh, PA 15236-0940

DOE Contracting Officer's Representative
Mr. Thomas Brown

Disclaimer

This report was prepared as an account of work sponsored by an agency of the United States Government. Neither the United States Government nor any agency thereof, nor any of their employees, makes any warranty, express or implied, or assumes any legal liability or responsibility for the accuracy, completeness, or usefulness of any information, apparatus, product, or process disclosed, or represents that its use would not infringe privately owned rights. Reference herein to any specific commercial product, process, or service by trade name, trademark, manufacturer, or otherwise does not necessarily constitute or imply its endorsement, recommendation, or favoring by the United States Government or any agency thereof. The views and opinions of authors expressed herein do not necessarily state or reflect those of the United States Government or any agency thereof.

Contents

I. Executive Summary 1
II. Introduction 2
III. Task I-1 Screen Sorbent Configurations in the Laboratory 5
A. Thermal Stability 5
B. Repeated Sorption and Desorption of Mercury with Particulate Form of Sorbent 8
C. Repeated Sorption and Desorption of Mercury with Monolithic Form of Sorbent 12
IV. Task I-2 Design and Fabricate Bench-Scale Equipment 16
V. Task I-3 Test Bench-Scale Equipment on Pilot Combustor 19
A. Scope of Pilot Testing 22
B. Overview of Pilot Testing Results 25
C. Sorption Results 25
D. Desorption Results 32
E. Monolith Tests After Field Work 36
VI. Task I-4 Evaluate Economics Based on Bench-Scale Results 36
A. Approximate Cost Analysis 36
B. Economic Benefits of Mercu-RE Process 39
VII. Conclusions and Recommendations 40
VIII. References 41
IX. Appendices
A. Mercury Analyzer Data Reduction 43
B. Permeation Tubes and Diffusion Vials as Calibration Sources 55
C. Investigation of Flow Distribution and Heating Efficiency during Regeneration 60
D. Example Data Records from Continuous Mercury Analyzer 65
E. Iodated Carbon Trap and Wet Chemistry Results for Testing in March, 1997 75
F. Excerpt of Paper Explaining Fundamentals of Mercury Analyzer 77
G. Laboratory Results with Monoliths Returned from the Field Test Unit 83

Figures

Figure 1 Fates of Mercury in Various Control Schemes 4
Figure 2 History of Crystallite Size for Sorbent BI 6
Figure 3 History of Crystallite Size for Sorbent BVI..... 7
Figure 4 History of Crystallite Size for Sorbent BIV..... 7
Figure 5 Schematic Diagram of Laboratory Test Apparatus..... 9
Figure 6 Accelerated Sorption and Desorption Test for Particulate Form of Sorbent .. 10
Figure 7 Effect of Bed Residence Time on Mercury Capture Efficiency 11
Figure 8 Flow Resistance of 4”-Deep Bed of Particulate Sorbent 12
Figure 9 Repeated Sorption and Desorption with Monolithic Form of Sorbent 13
Figure 10 Simultaneous Sorption of Elemental Mercury and Mercuric Chloride 15
Figure 11 Schematic Diagram of 20 ACFM Pilot Unit 16
Figure 12 Skid-Mounted 20 ACFM Unit Near Completion at ADA 17
Figure 13 Mercury Analyzer and Skid Installed at Consol, Library, PA 20
Figure 14 Internals of ADA’s Mercury Analyzer 21
Figure 15 Flow Resistance of Skid-Mounted Sorbent Module at 70°F 22
Figure 16 Quantitative Uptake of Elemental Mercury in Unit 2; 6/5 and 6/6/97 26
Figure 17 Performance of Unit 2 with Low Sulfur Pittsburgh Seam Coal; 6/10/97 27
Figure 18 Performance of Unit 2 with Low Sulfur Pittsburgh Seam Coal; 6/11/97..... 27
Figure 19 Performance of Unit 1 with High Sulfur Pittsburgh Seam Coal; 3/6/97 29
Figure 20 Performance of Unit 1 with High Sulfur Pittsburgh Seam Coal; 3/12/97..... 30
Figure 21 Performance of Unit 2 with High Sulfur Pittsburgh Seam Coal; 3/11/97..... 31
Figure 22 Performance of Unit 1 with High Sulfur Illinois #6 Coal; 1/31/97 32
Figure 23 Desorption of Non-Elemental Mercury; Original Regeneration Cycle..... 33
Figure 24 Desorption of Unit 2 with Auxiliary Heater 34
Figure 25 Continued Desorption Unit 2 with Auxiliary Heater..... 34
Figure 26 Quantitative Desorption of Unit 1 with Clean Regeneration Sampling Line.... 35
Figure 27 Concept of Full-Scale Mercury Monolith Cassettes 38

Tables

Table 1 Desorption Time-Temperature Profile 14

Table 2 Comparison of Mercury Sorbed to Mercury Desorbed in Monolith Test 14

Table 3 Process Data Monitored by PLC-1 18

Table 4 Coals Burned During Testing of 20 ACFM Skid at Consol 23

Table 5 Operational History of 20 ACFM Skid 23

Table 6 Projected Process Costs for 250 MW Facility 39

Executive Summary

We demonstrated in the Phase I program all key attributes of a new technology for removing mercury from flue gases, namely,

a) removal of greater than 95% of both elemental and oxidized forms of mercury, both in the laboratory and in the field

b) regenerability of the sorbent

c) ability to scale up, and

d) favorable economics.

The Phase I program consisted of four tasks other than project reporting:

Task I-1 – Screen Sorbent Configurations in the Laboratory

Task I-2 – Design and Fabricate Bench-Scale Equipment

Task I-3 – Test Bench-Scale Equipment on Pilot Combustor

Task I-4 – Evaluate Economics Based on Bench-Scale Results

In Task I-1, we demonstrated that the sorbents are thermally durable and are regenerable through at least 55 cycles of mercury uptake and desorption. We also demonstrated two low-pressure-drop configurations of the sorbent, namely, a particulate form and a monolithic form. We showed that the particulate form of the sorbent would take up 100% of the mercury so long as the residence time in a bed of the sorbent exceeded 0.1 seconds. In principle, the particulate form of the sorbent could be imbedded in the back side of a higher temperature bag filter in a full-scale application. With typical bag face velocities of four feet per minute, the thickness of the particulate layer would need to be about 2000 microns to accomplish the uptake of the mercury.

For heat transfer efficiency, however, we believed the monolithic form of the sorbent would be the more practical in a full scale application. Therefore, we purchased commercially-available metallic monoliths and applied the sorbent to the inside of the flow channels of the monoliths. At face velocities we tested (up to 1.5 ft/sec), these monoliths had less than 0.05 inches of water pressure drop. We tested the monolithic form of the sorbent through 21 cycles of mercury sorption and desorption in the laboratory and included a test of simultaneous uptake of both mercury and mercuric chloride.

Overall, in Task I-1, we found that the particulate and monolith forms of the sorbent were thermally stable and durable and would repeatedly sorb and desorb 100% of the mercury, including mercuric chloride, with low pressure drop and short residence times at realistic flue gas conditions.

Under Task I-2, we then built a test unit that incorporated the monolithic form of the sorbent and that would treat 20 ACFM of flue gas. The unit was designed for testing at Consol's 100 lb/hr coal combustor in Library, PA. The test unit was automated insofar as practical so that we could monitor and control it from our offices in Englewood, CO, through computers and telephone lines. The unit contained two sorbent modules in a "heat exchanger" configuration. Each sorbent module contained 51 monoliths, each with one milligram of active noble metal.

Under Task I-3, we shipped the unit to Consol and installed it along with ADA's continuous mercury analyzer to monitor the performance of the unit. The unit ran for over 700 hours while testing flue gas from the combustion of four different coals (January through June, 1997). The unit quantitatively sorbed the flue gas mercury. Desorption was not problematic but was difficult to quantify. After overcoming some problems, in the one test we did with full control over all of the equipment variables, we verified quantitative desorption of one of the sorbent beds. We removed one monolith from each of the sorbent modules near the end of the test program and found in laboratory testing that the monoliths had retained their capacity for mercury even though they had been through hundreds of hours of testing in the field and were covered with a thin ash layer. The field test program was difficult but successful.

Under Task I-4, we assessed the economics of a 250 MW installation of the mercury sorption technology. We concluded that the technology is highly advantageous economically, in comparison to the injection of activated carbon, even if we are substantially underestimating the costs of our technology ($866,000 annualized cost for our technology versus $4.2 million or more annually for activated carbon). This economic assessment is approximate given the early stage of our technology but is encouraging for the eventual commercial implementation of the technology.

Considering the ability of the ADA's mercury removal process to collect all chemical forms of mercury, to generate no secondary wastes, and to regularly remove over 95% of the mercury, the process has clear technical and economic advantages over available technologies. The proposed Phase II work, described in a separate document, is aimed at bringing these performance and cost benefits closer to reality for the electric power industry.

Introduction

ADA's developmental mercury removal process relies on the ability of noble metals to sorb mercury and its common compounds at ordinary flue gas temperatures and to desorb the mercury at elevated, but reasonable, temperatures, such as 600°F to 700°F. The technology offers several potential advantages to the electric power industry. First, because all chemical forms of mercury are removed from the flue gas, the user does not need to know the chemical form of the mercury nor be concerned that changes in the fuel, in the firing conditions, or in the flue gas temperature (either seasonally or with load swings) will alter the efficiency of mercury removal. Second, the mercury is recovered in a form that is suitable for commercial distillation and recycling, eliminating disposal costs, secondary wastes, and any associated liabilities. Finally, the technology offers significant cost savings with respect to options such as injection of activated carbon or related sorbents at the same time as eliminating possible adverse effects of these sorbents on electrostatic precipitators or other particle control devices.

The technology uses a **re**generable sorbent that allows for **re**covery of liquid elemental **mercury** from the flue gas. For these reasons, we call our technology the "Mercu-RE process."

The Mercu-RE process has the following advantages:

1) mercury removal efficiencies exceeding 90% regardless of the chemical form of the mercury compared with 25% to 75% efficiency of alternative technologies,

2) a substantial reduction in the cost of mercury control compared with alternative approaches,

3) elimination of mercury-contaminated solid or liquid wastes, and

4) removal of mercury from the biosystem.

Figure 1 contrasts the fate of mercury in the Mercu-RE process with the fate of mercury in an uncontrolled coal-fired combustor and in a system using state-of-the-art carbon injection for mercury control. The quantities of ash and mercury shown in Figure 1 are those generated annually by a 500 MW coal-fired combustor. The end product of the Mercu-RE process **is liquid, elemental mercury,** which is suitable for recycle and re-use and is thereby not available to be distributed into the biosystem. Further, no secondary wastes are made. In contrast, state-of-the-art carbon injection technology produces a mercury-contaminated carbon, with approximately 300 times the mercury concentration of the original coal, mixed with fly ash. As a minimum, the mercury on this carbon is susceptible to eventual leaching, introducing the mercury into the biosystem. In the worst case, the fly ash with the highly contaminated carbon would be considered a hazardous waste, requiring costly, special disposal practices.

In commercial practice, the Mercu-RE process would involve multiple sorbent modules treating approximately 100,000 ACFM each and would encompass the following steps:

1. Capturing approximately 10 $\mu g/m^3$ of Hg for one month from 100,000 ACFM of flue gas at 300^oF to 400^oF;
2. Taking one sorbent module off-line;
3. Regenerating the sorbent module for eight hours at 500^oF to 700^oF, passing less than 100 ACFM of hot purge gas through the module, thereby creating a highly concentrated mercury stream;
4. Condensing the mercury contained in the purge gas;
5. Putting the sorbent module back on-line; and
6. Sale or safe disposal of the liquid mercury.

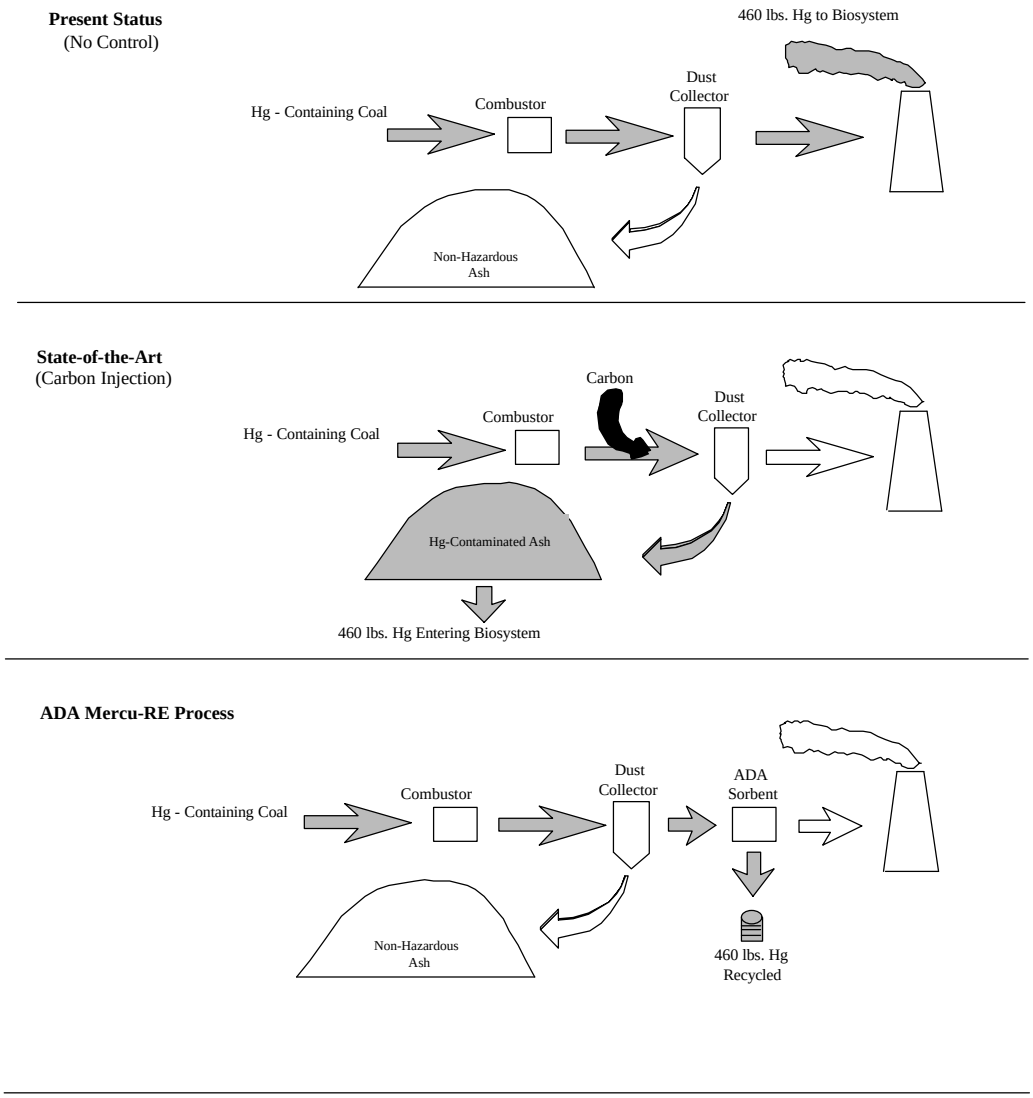

Figure 1 – Fate of Mercury in Various Control Schemes

(Assumes 500 MW Plant, 2 MMACFM, 10 μg Hg/Nm^3)

The following sections describe the results of the Phase I work that ADA conducted under contract DE-AC22-95PC95257 wherein our objective was to move the technology from an early stage of development (Maturity Level 2 in terms of the original PRDA) to a pilot demonstration (Maturity Level 3). This objective was met in the Phase I work.

The Phase I work consisted of four tasks:

Task I-1 – Screen Sorbent Configurations in the Laboratory

Task I-2 – Design and Fabricate Bench-Scale Equipment

Task I-3 – Test Bench-Scale Equipment on Pilot Combustor

Task I-4 – Evaluate Economics Based on Bench-Scale Results

The following sections describe the results of each of these tasks.

Task I-1 – Screen Sorbent Configurations in the Laboratory

This task was designed to determine whether the sorbents would be durable under conditions typical of coal-fired power plants and whether the sorbent could be configured in a low pressure drop, compact manner so as to minimize both the operating and capital expense of an eventual full-scale system.

Thermal Stability

The sorbent is a dispersion of noble metal on a microporous, metal oxide substrate, typical of conventional catalysts. We wanted to know whether the noble metal crystallites themselves would be stable under the temperatures anticipated for this process, namely, as high as 700°F. A source of instability could, for example, be coalescence by surface diffusion of the metal crystallites at the higher temperatures of the process. Such coalescence would decrease the amount of noble metal surface area available to sorb the mercury and likely lead to decreased sorbent performance.

The size of small crystals can be determined with x-ray diffraction (XRD) line broadening methods (e.g., Cullity, 1978). The particulate form of the sorbent provides a convenient sample for XRD. We therefore chose the particulate form of the sorbent for the thermal durability tests. We decided to expose the sorbent constantly to the maximum regeneration temperature of our process (700°F) so as the accelerate any degradation processes. The Chemistry Department of the Colorado School of Mines (Golden, CO) performed the XRD analyses.

To make the particulate form of the sorbent, we crushed commercially-available alumina beads and sieved them to be smaller than about one millimeter. We then dispersed the noble metal on these fine alumina particles using wet impregnation (e.g., Stiles, 1983). We made three different forms of the sorbent with different preparation methods. We placed 10 grams of each sorbent in an oven at the regeneration temperature of 700°F continuously for 180 days. In real operation the sorbent would be exposed to the regeneration temperature for at most 50% of the time, so the 180 days of exposure represented at least one year of operation. We removed one-

gram samples of the sorbent from the oven periodically and examined the size of the noble metal crystallites using x-ray diffraction line broadening.

Two of the sorbent formulations were quite stable for the 180-day test (Figures 2, 3, and 4). The "x" axis on these figures is the length of time that the sorbent was held in the oven at 700°F. The "y" axis is the ratio of the crystallite diameters to the initial crystallite diameters. The crystallite diameters of one of the formulations grew and then began to reach a steady condition (the last data point is likely an anomaly). We are planning to measure the crystallite diameters of these sorbents again at 365 days and at 730 days. Sorbents BVI and BI were clearly thermally stable, and we used the sorbent BVI formulation in the rest of our work.

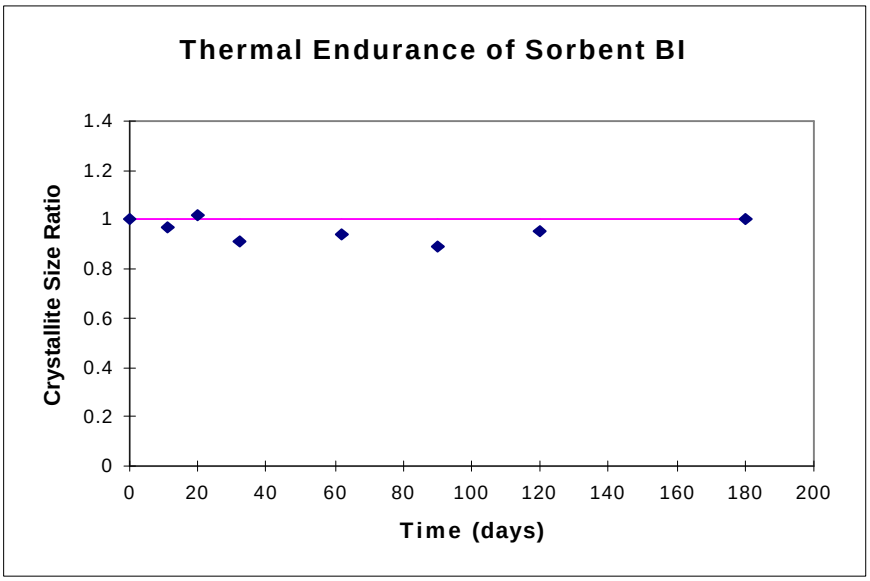

Figure 2 – History of Crystallite Size for Sorbent BI

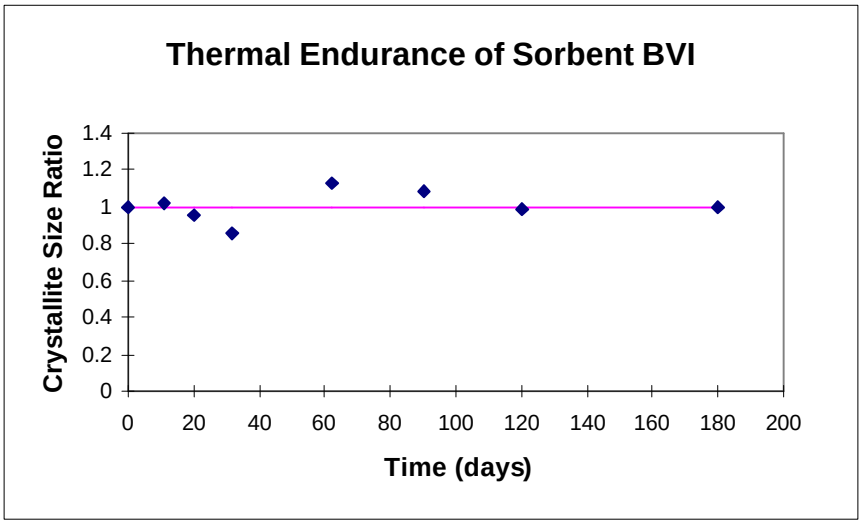

Figure 3 – History of Crystallite Size for Sorbent BVI

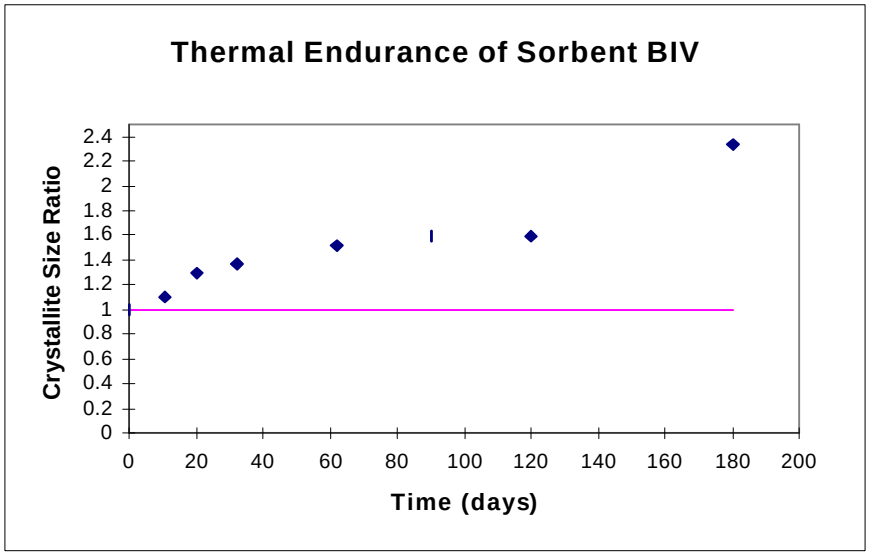

Figure 4 – History of Crystallite Size for Sorbent BIV

Repeated Sorption and Desorption of Mercury with Particulate Form of Sorbent

Another important laboratory test was to determine whether the sorbent would repeatedly take up mercury and give off mercury when thermally regenerated. For these tests, we made a laboratory sorption apparatus that allowed us to pass a mercury-containing synthetic flue gas through the sorbent and then to heat up the sorbent to drive off the mercury. We automated this apparatus so we could do repeated sorption and desorption tests. Achieving quantitative, high quality data with an essentially automatic apparatus involving low levels of mercury was quite challenging.

We made mercury-containing synthetic flue gas by passing dry nitrogen at 100 standard cubic centimeters per minute (sccm) over a calibrated permeation tube that contains elemental mercury or over a calibrated diffusion vial that contains mercuric chloride. We maintained more than 20 permeation tube and diffusion vials at a constant temperature and weighed them once per month so that whether we needed a high concentration of mercury or a low concentration of mercury, we would have a confident calibration without changing the temperature of the permeation device (see Appendix B). Changing the temperature of the permeation device means that the emission rate is not really known with a high confidence for about three months because the mass loss rates of mercury are so small.

To make a low concentration of mercury typical of coal fired power plants, we used a permeation tube or diffusion vial with a mercury emission rate of approximately 50 ng/min. The nitrogen carrier gas with the mercury was then mixed with the other flue gas components that were themselves mixed with conventional mass flow controllers (Figure 5). The total flow rate of the synthetic gas mixture was one to five liters/min. The synthetic flue gas typically contained 15 $\mu g/m^3$ of elemental mercury, 4% oxygen, 50 ppm HCl, 1500 ppm SO_2, 10% CO_2, 8% water, and the balance nitrogen at 300°F and ambient pressure (620 torr).

We used a laboratory version of ADA's continuous mercury analyzer to measure the concentration of mercury at both the inlet and outlet of the sorbent bed (Schlager, et al., 1995). We did substantial work on verifying the quality of the data in this sorption apparatus, including finding materials of construction and temperatures where mercury is not sorbed by the equipment surfaces. We chose electropolished stainless steel as the material to make the most of the system. The exception was the sorbent holder itself, which was quartz.

Beds of the particulate form of the sorbent were held in 0.87-inch inside diameter, 4-inch long quartz cylinder at the top of the quartz sorbent holder. The flow was laminar in the lab as is anticipated for the full-scale implementation of this technology (Reynolds number of the flow based on the inside diameter of the sorbent holder was about 130). With one to five grams of the particulate sorbent and with flows from one to five liters per minute, we were able to vary the bed residence time from less than 0.1 seconds to over one second. Similarly a single monolith could be held in the quartz vessel, and the typical residence time for a monolith test was 0.3 to 1.0 seconds (see below).

The concentration of mercury in the gas downstream of the sorbent bed was measured continuously with our UV-based mercury analyzer. In this way, the breakthrough characteristics of the sorbent could be obtained. The key output of an experiment was a curve showing when and how the sorbent bed began to lose its efficiency for mercury uptake. Since the inlet concentration of mercury was known, the capacity at any point on the breakthrough curve could also be determined.

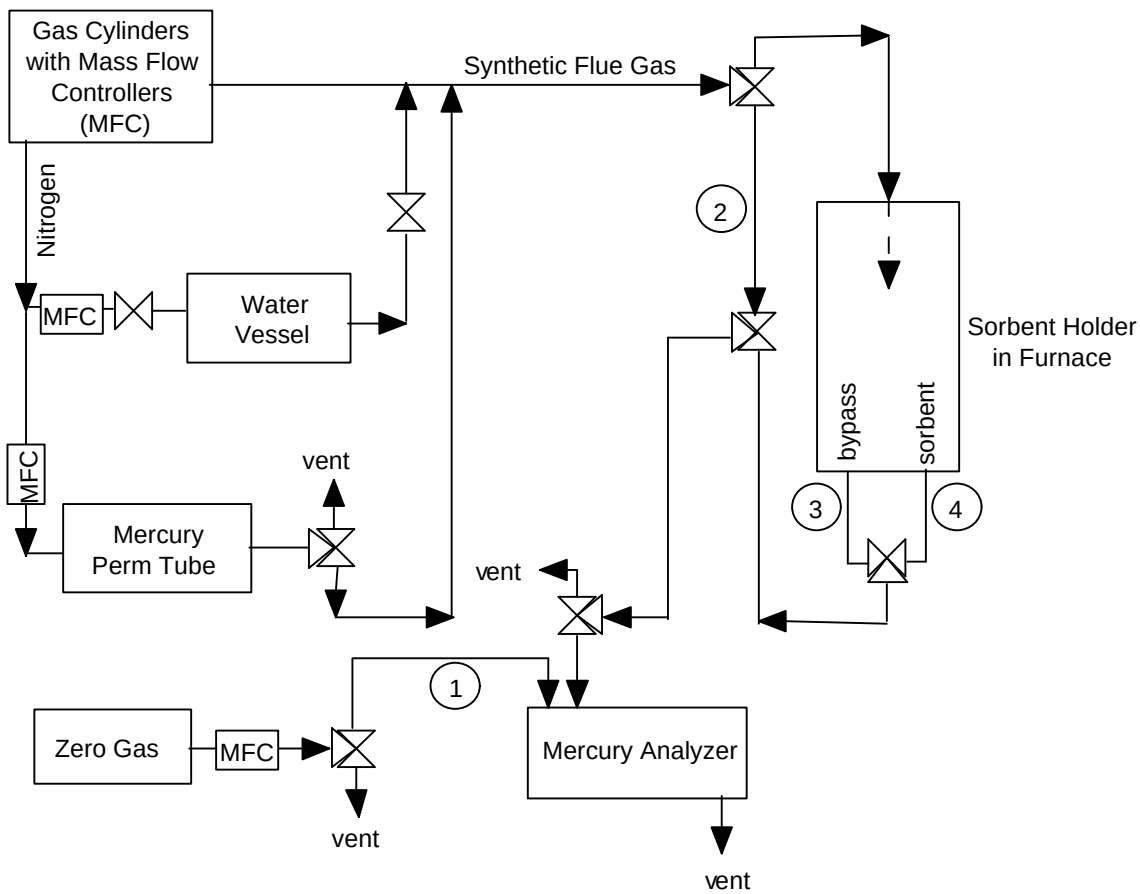

Figure 5 – Schematic Diagram of Laboratory Test Apparatus

At first, we decided to do sorption and desorption of mercury at an elevated mercury concentration. We did so because some metallurgists advised us that one of the failure mechanisms for the sorbent could be the formation of a liquid amalgam on the surface of the sorbent and the spreading and coalescing of the noble metal crystallites. By choosing a high concentration of mercury, our tests were an accelerated durability test. We chose a mercury concentration of 3,000 $\mu g/m^3$ for these tests (baseline gas was air with seven percent water vapor at 275°F).

We found that after a "break-in" period of about 20 cycles, the sorbent breakthrough time remained consistent through 55 cycles, which is when we stopped the test (Figure 6). Because the mercury concentration in these tests was about 300 times that expected in coal fired power plants, the sorbent has seen as much mercury as if it had undergone 1600 cycles in a coal-fired power plant. If the mercury itself was going to adversely affect the sorbent behavior in a coal-fired power plant application, it would have done so in the 55 cycles that we tested. While we cannot say that Figure 6 proves that the sorbent would last for over 1500 cycles in coal-fired power plant flue gas, we can at least say that the sorbent is robust in the presence of much higher concentrations of mercury than will ever be encountered in the coal-fired application.

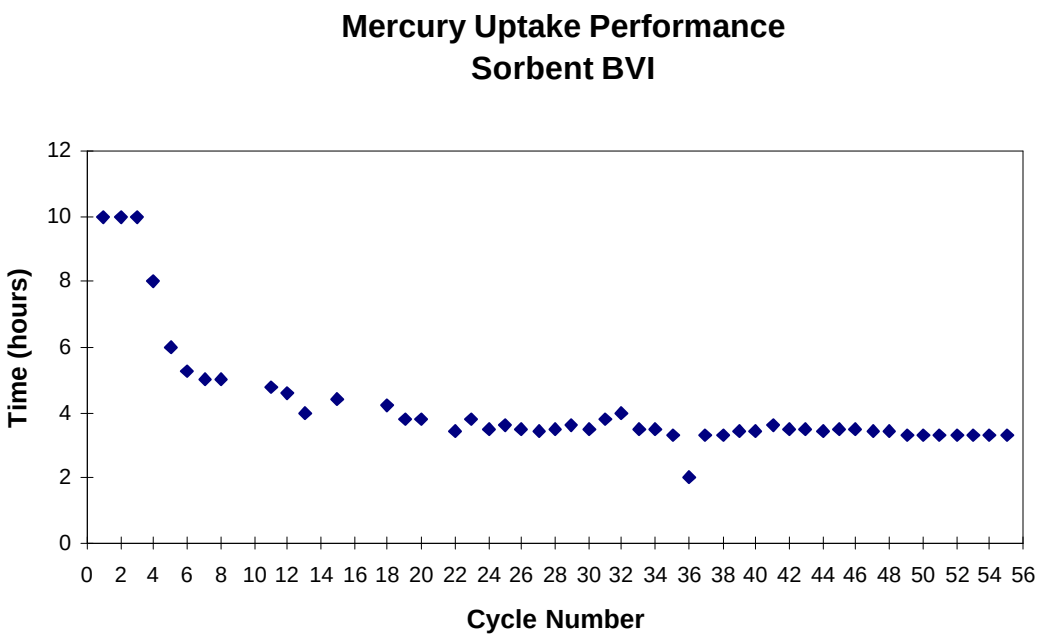

Figure 6 – Accelerated Sorption and Desorption Test for Particulate Form of Sorbent

We also wanted to know how fast we could flow the gas through a bed of the sorbent and still have 100% uptake of the mercury. The effect of the residence time of the gas in the sorbent bed was measured by varying the feed gas flow rate between one and eight standard liters per minute and by varying the mass of sorbent in the bed from 0.8 to 4.5 grams. With these flow rates and masses of sorbent, the residence time ranged from three to 156 milliseconds. Tests were done with 8% water vapor in air, with and without 100 ppm HCl at 300°F and with 1,800 µg/m^{3} of mercury. The results (Figure 7) indicate that when the residence time exceeds 100 milliseconds, the mercury uptake is complete. The mercury capture with HCl in the feed gas exceeds, in most cases, that found without HCl but not by enough to be an important consideration.

The fluid flow approaching the bed in these tests is laminar (Reynolds number between 90 and 720). The Reynolds number based on particle diameter for this bed is between 23 and 181. In packed beds laminar flow is defined as Re<10, thus the sorbent bed was in transition or turbulent flow. Matching the flow conditions between the laboratory tests and the field-scale work is important to the ability to scale the process up to full-scale. By matching flow profiles we can assert that the 0.1 second residence time "rule of thumb" should prevail in full-scale applications as well as in the laboratory.

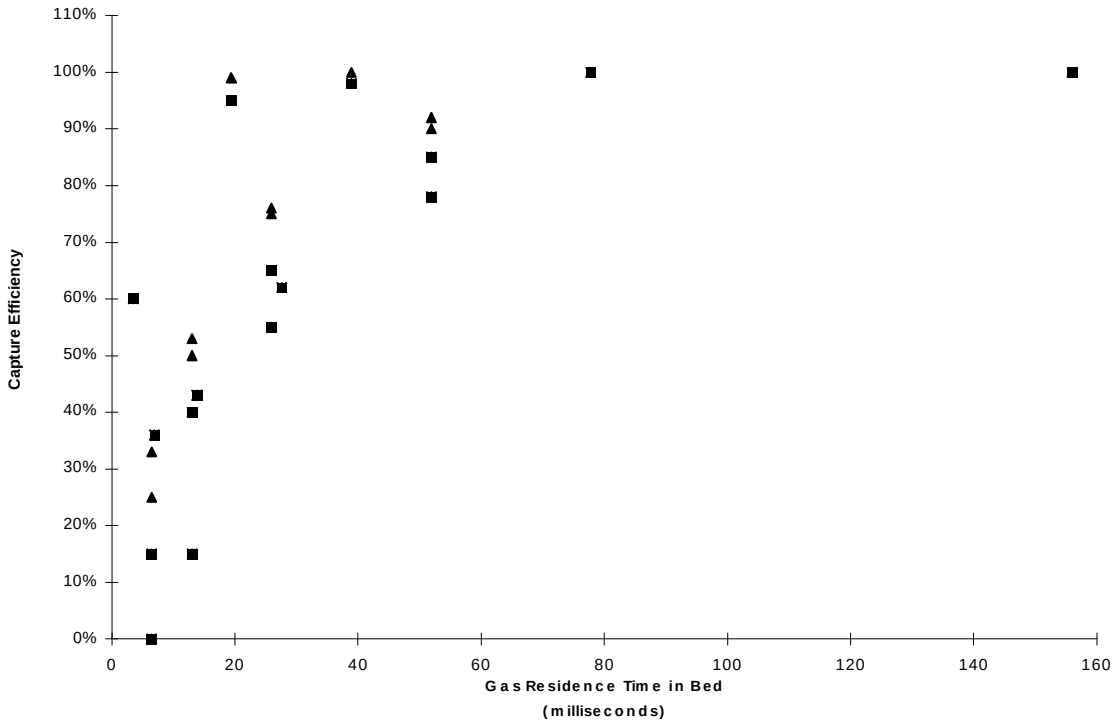

Figure 7 – Effect of Bed Residence Time on Mercury Capture Efficiency

We recorded the pressure drop through the sorbent bed during the residence time tests. Figure 8 shows the pressure drop through a 4”-deep bed of the particulate sorbent. With realistic superficial velocities of 1 ft/sec to 2 ft/sec, the pressure drop of the particulate form of the sorbent was found to be quite low.

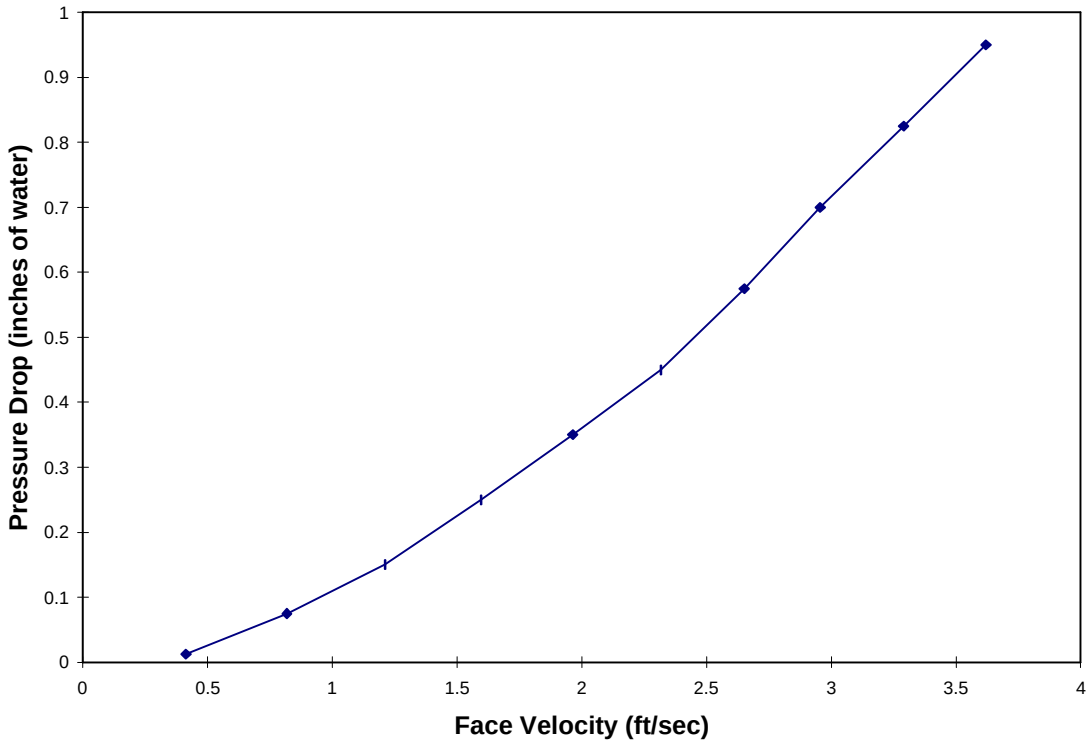

Figure 8 – Flow Resistance of 4”-deep Bed of Particulate Sorbent

Repeated Sorption and Desorption of Mercury with Monolithic Form of Sorbent

Once we proved the stability of the sorbent in the particulate form, we then turned our attention to what we believed would be a more practical form of the sorbent for a coal-fired power plant, namely, a monolithic configuration. The monoliths are made commercially by placing a corrugated piece of metal on top of a flat sheet of metal and rolling the sheets up like a roll of carpet. The gas flow path in the finished monolith is along the corrugations. The flow channels themselves measure about 1/16th of an inch in maximum dimension, and there are about 100 flow channels per square inch of monolith cross section. We chose metallic monoliths because of their superior heat transfer characteristics compared with standard ceramic monoliths that are commonly used in automobile catalytic converters. To make the monoliths active for mercury sorption, we coated the inside walls of the monolith with the sorbent.

We subjected the monolithic form of the sorbent to 21 cycles of sorption and regeneration in a synthetic flue gas containing 18 µg/m^3 of elemental mercury, 4% oxygen, 6% water vapor, 34 ppm HCl, 1020 ppm SO_2, 7.6 % CO_2, and the balance nitrogen. The sorption temperature was

300°F, and the regeneration temperature followed a profile that peaked at 700°F. We varied the ratio of sorption time to desorption time until we found a ratio that worked well. The monolith showed no permanent loss of performance over these 21 cycles, and it seemed to be refreshed by two 19-hour desorptions at 700°F (Figure 9).

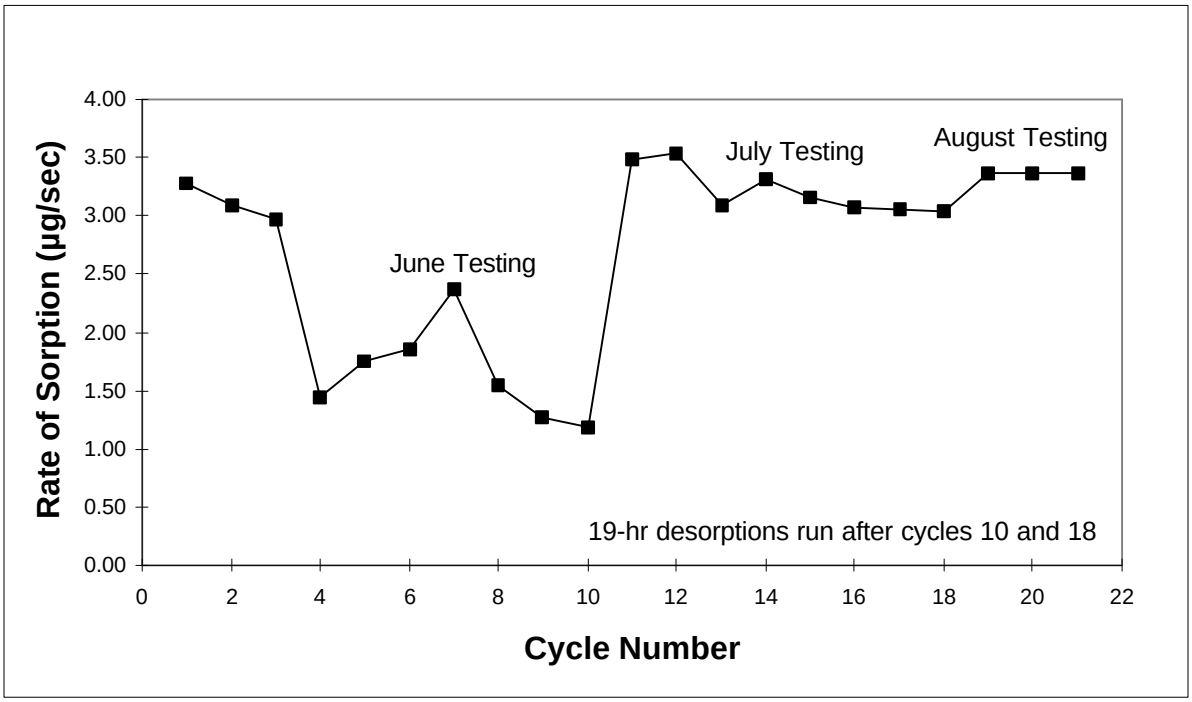

Figure 9 – Repeated Sorption and Desorption with Monolithic Form of Sorbent

During the individual desorption cycles, the oven temperature was ramped up to 600°F according to the schedule shown in Table 1. The concentration of mercury desorbing from the monolith could be followed with our mercury analyzer, if we kept the flow rate high through the monolith, and this desorption curve could be integrated to quantify the amount of mercury desorbed. It took several attempts before we had a procedure for quantifying the mercury desorption process. Because the amounts of mercury were so small (approximately 50 µg) and we did not know at the outset how high of a mercury concentration we would see, we were able to get a good quantitative procedure working well only for cycles 13 through 17 (see below).

During cycles 13 through 17, we were able to perform a mass balance on the mercury taken up and given off by the monolith (Table 2). There appeared in general to be slightly less mercury desorbed than sorbed, but within experimental error, the mercury was quantitatively desorbed.

Table 1 -- Desorption Time-Temperature Profile

Time at Desorption Temperature (min.)	Desorption Temperature (^oF)
5	300
10	350
20	400
15	450
10	500
5	550
175	600

Table 2 – Comparison of Mercury Sorbed to Mercury Desorbed in Monolith Test

Cycle Number	Amount Sorbed (µg)	Amount Desorbed (µg)
13	50.4	63.1
14	57.9	52.2
15	56.2	48.1
16	54.4	49.2
17	56.7	51.3
Total	**276**	**264**

We also tested the monolithic form of the sorbent for ability to take up mercuric chloride simultaneously with elemental mercury. We used the same monolith that had been through 21 cycles of sorption and desorption, and we used the same mercury concentration (half elemental and half mercuric chloride) and the same concentrations of the other flue gas constituents. Mercuric chloride is much more difficult to work with, and with the time constraints we were facing, we did only a brief test, depicted in Figure 10. One hundred percent of the elemental mercury and the $HgCl_2$ was removed by the monolith. A similar test was done with a monolith that had been in the field for six months and a similar result was found (see below). Hence, even though our laboratory time with $HgCl_2$ was brief, the monoliths sorbed this common oxidized form of mercury.

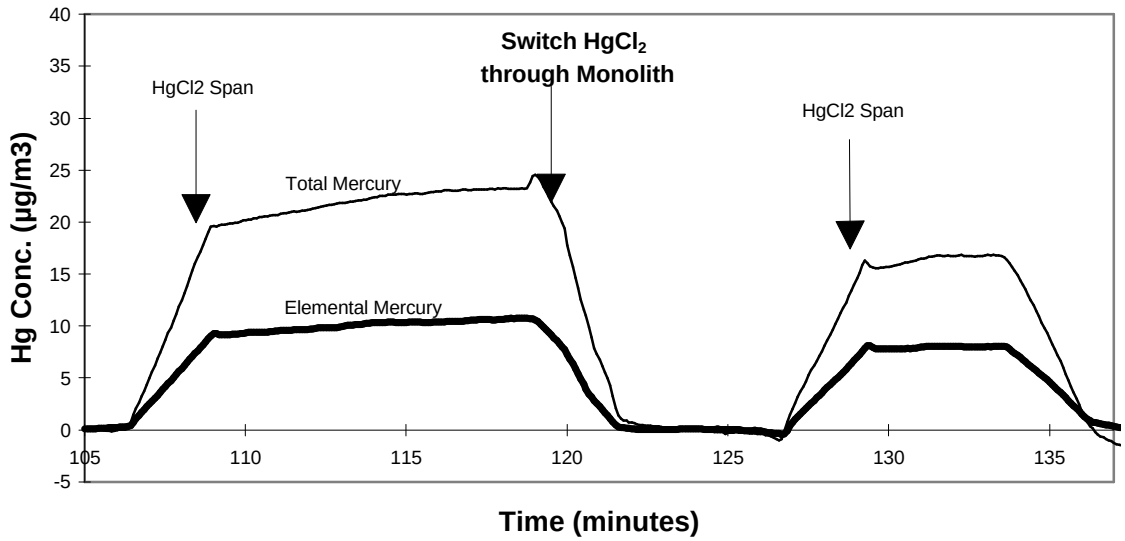

Figure 10 – Simultaneous Sorption of Elemental Mercury and Mercuric Chloride

We did not have the time to perform similar tests on the effect of residence time on mercury uptake for the monolithic form of the sorbent. We did, however, measure the pressure drop as a function of flow rate and found that the pressure drop was less than 0.1 inches of water for face velocities up to 1.5 ft/sec. Given that we could run as fast as a 0.1-second residence time with the particulate form of the sorbent, we could likely run the monoliths faster than the one second residence time of our typical lab test and still get good mercury uptake. The field unit was conservatively designed with a 1.5 second residence time (and had very low pressure drop, as described below). This residence time is about 1/10th that found in a typical electrostatic precipitator, insuring that the full scale system will be small compared to the ordinary flue gas control equipment found in power plants.

To summarize the laboratory work, we found that the particulate and monolith forms of the sorbent were thermally stable and durable and would repeatedly sorb and desorb 100% of the mercury, including mercuric chloride, with low pressure drop and short residence times at realistic flue gas conditions.

Task I-2 – Design and Fabricate Bench-Scale Equipment

We devised a skid-mounted test unit to treat 20 ACFM of flue gas that consisted of a particulate filter, two sorbent vessels, a flue gas blower, an air heater and blower to regenerate each bed, and the associated controllers, valves, and electrical equipment to operate the test unit (Figure 11). The base of the skid measured 4' by 8'. With heavy duty casters on the base of the skid, the unit was transportable. The test unit itself was accompanied by ADA's continuous mercury analyzer (see Task I-3 and Appendix A). The test unit was computer controlled, as was the analyzer, and both could be operated remotely from ADA's offices in Englewood, CO. In practice, we ended up on site a fair amount to overcome various operating issues that arose, but the remote operation capability increased the rate at which we were able to obtain data.

Each sorbent module consisted of 17 tubes in a shell-and-tube heat exchanger design. The tubes were 18" long with an inside diameter of 1.87" and an outside diameter of 2". There were 51 monoliths, each 1.75" in outer diameter and 6" long, stacked three per tube in the 17 tubes of each sorbent module. Each sorbent module was designed to handle 20 ACFM of flue gas taken as a slip stream from Consol's pilot coal combustor. The direction of flow was upward during sorption; regeneration gas flowed at typically three standard liters per minute in the opposite direction during desorption. The superficial velocity in each of the 17 tubes during sorption was about 1 ft/sec at 300°F and one atmosphere pressure, and the empty bed residence time was about 1.5 seconds. The slip stream itself was taken downstream of Consol's electrostatic precipitator.

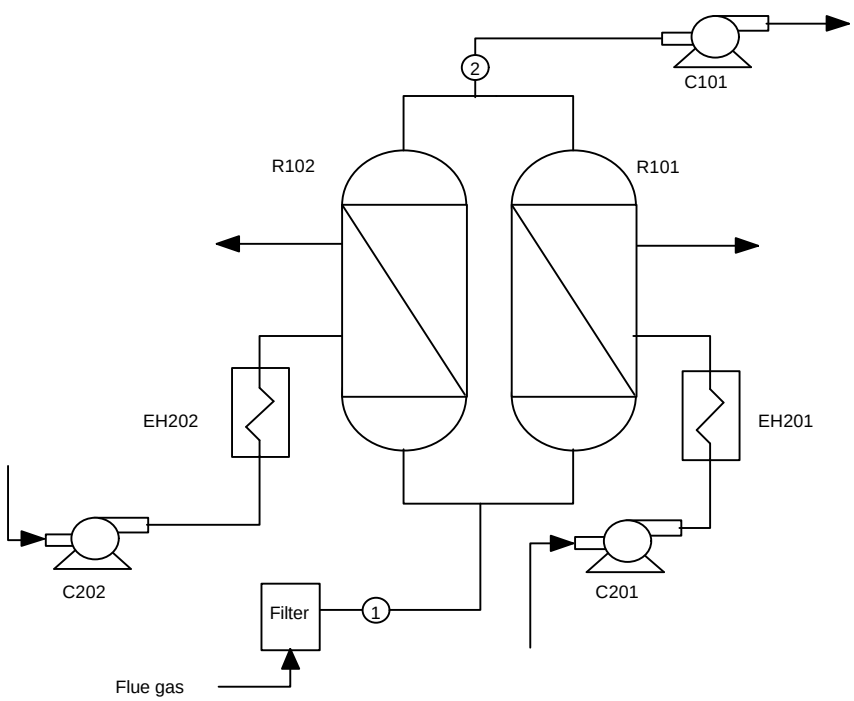

Figure 11 – Schematic Diagram of 20 ACFM Pilot Unit

Each of the monoliths contained a total of one milligram of noble metal on the monolith surfaces. With a typical inlet mercury concentration of 10 $\mu g/m^3$, this amount of noble metal could be expected to last for 20 hours before reaching breakthrough. In this way, we hoped to achieve several sorption/desorption cycles in the 90 hours of run time in a week of operation of the Consol pilot combustor.

Figure 12 shows the skid nearing completion at ADA Technologies.

Some explanation of the flow path during regeneration is useful at this point so that some of the regeneration results are better understood. During regeneration, a small flow of purge gas (three liters per minute) was delivered in a ¼" line to the top cone. The regeneration gas then flowed down through the monoliths to the bottom cone where another ¼" line was attached. This line connected to a condenser. In practice, the amount of mercury being desorbed in any one cycle was expected to be about 5 milligrams (368 liquid nanoliters if condensed). What actually happened during operation is that the mercury accumulated on the walls of the regeneration line and likely the condenser as well, although we tested only the regeneration line. Further, the bottom cone of the unit was exposed to very high concentrations of mercury during regeneration. This fact may account for some of the unexpected results we observed in some of the tests since the exact skin temperature of this cone was not directly measured, only the flue gas inlet and outlet temperatures.

Late in the program (June, 1997), we replaced the regeneration line with electropolished stainless tubing and heated it to 400°F so that we could sample through this line without losses. Only under this circumstance were we able to quantify the amount of mercury desorbed.

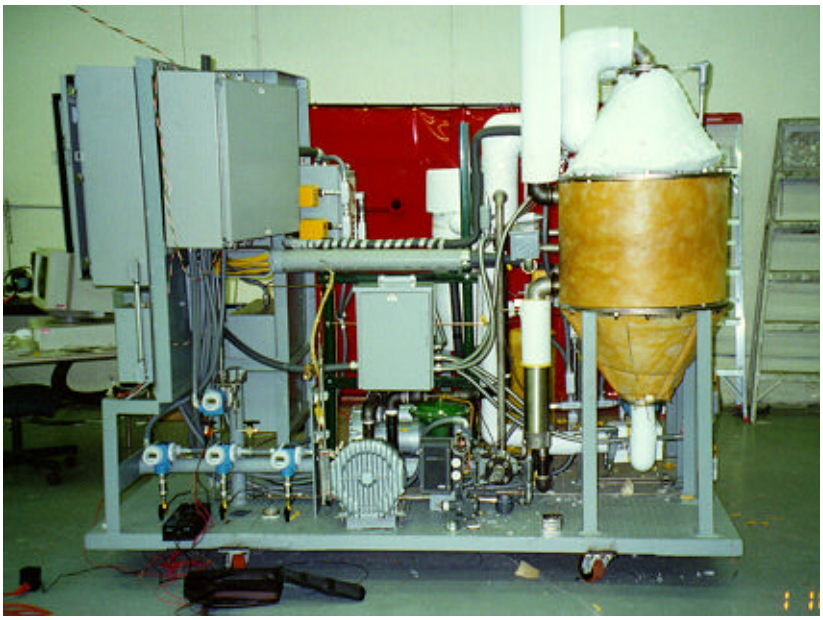

Figure 12 – Skid-Mounted 20 ACFM Unit Near Completion at ADA

The following paragraphs describe the design operation of the unit.

Electric resistance air heaters were used to maintain the sorption vessels at sorption and desorption temperatures. The heaters were capable of heating 40 CFM of air to a temperature of 1000°F (we typically used 850°F; plant steam would be used at an operating utility installation). This air was piped to the shell-side of the sorbent vessel and discharged to the room through a vertical tailpipe. Each sorbent vessel had its own air blower and resistance heater so that the vessels could be maintained at different temperatures. Typically, one vessel was in a sorption mode while the other vessel was in a desorption mode. The monolith temperatures for sorption and desorption modes were 300°F and 700°F, respectively. Heating the shell side of the sorbent module was important even during the sorption mode to maintain flue gas temperature in the unit since with a small unit, heat losses would otherwise lead to non-representative test conditions.

Process control and data acquisition for the skid was handled by two PLCs. One PLC (PLC-2) was dedicated to the control of 12 heat trace circuits used to maintain the temperature of the vessels and flue gas piping at 300°F. The other PLC (PLC-1) was responsible for controlling the flue gas flow rate through the skid, monitoring pressures and temperature throughout the process, and coordinating valve sequencing and air heater temperatures for the sorption and desorption cycles. Process data monitored by PLC-1 are listed in Table 3. The pressure drop across a venturi flow meter was used to control the flow through the unit at approximately 20 ACFM.

Table 3 – Process Data Monitored by PLC-1

Process Parameter Description	Normal Operation Condition	
	Sorption	Desorption
Hot Air Temperature of Heater 1	296 °F	846 °F
Hot Air Temperature of Heater 2	296 °F	847 °F
R-101 Tube #9 Temperature	263 °F	692 °F
R-101 Tube #3 Temperature	260 °F	703 °F
R-102 Tube #9 Temperature	258 °F	670 °F
R-102 Tube #1 Temperature	258 °F	685 °F
R-101 Hot Air Out Temperature	194 °F	434 °F
R-102 Hot Air Out Temperature	197 °F	428 °F
C-201 Outlet Air Pressure	5” WC	
C-202 Outlet Air Pressure	5” WC	
Flue Gas Temperature	250 °F	
Venturi Differential Pressure	2.5” WC	
Flue Gas Pressure	-16” WC	

Upon startup, the PLC-1 program energized the two hot air blowers. After a short delay, power was supplied to the air heater controllers, and air was heated to the sorption temperature of 300°F. When the air temperatures were within 25°F of the setpoint temperature, the flue gas blower was energized. From this point, the operator monitored the tube temperatures of the sorbent vessels until the vessels equilibrated at the sorption temperature. The desorption cycle was started by pressing either the "Start R-101 Desorption Cycle" or "Start R-102 Desorption Cycle" buttons. This initiated the 24-hour desorption cycle for one of the sorbent vessels.

Several activities happened when a desorption cycle was started. First, two valves were repositioned to direct flue gas through the vessel used for mercury sorption. Simultaneously, two other valves were rotated to flow purge gas through the vessel undergoing desorption. The purge gas transported the liberated mercury to a condenser and carbon trap downstream. The purge gas was routed to the inlet of the flue gas blower and blown into the outlet of the ESP with the treated flue gas.

While the temperature of the sorption vessel was held at the sorption temperature of 300°F, a temperature program was started in the hot air controller for the desorption vessel. The program gradually increased the air temperature to 850°F over a period of one hour. This temperature was sufficient to heat the tubes to roughly 700°F. The controller program maintained the air temperature at 850°F for typically 21 hours. When the program expired the air temperature returned to the sorption temperature of 300°F, and the vessel cooled. The cool-down time was usually two hours. The PLC program operated in this mode until the desorption cycle was finished. Then, the desorption cycle for the second vessel was started automatically.

PLC-1 was connected to a computer using an RS-232 cable for data acquisition and to monitor the operation of the skid. A data acquisition software package logged data to a file at a time interval specified by the user. Usually data was written to the file every five minutes. The computer was equipped with a 28.8 kilobyte per second modem and "PC Anywhere" software to download data to ADA's offices in Englewood, CO. The communication equipment was also used to operate the skid remotely and if necessary, to modify the PLC program.

Task I-3 – Test Bench-Scale Equipment on Pilot Combustor

We installed the bench-scale equipment at the pilot combustion facility of Consol, Inc., in Library, PA (Figure 13). Consol burns its coals in this facility for about 90 hours per week and for about 32 weeks per year to evaluate fouling, slagging, and emissions behavior of its coals in support of its coal business. Consol's combustor burns about 150 pounds of coal per hour (about 1.5 million Btu/hr). We installed the skid downstream of Consol's electrostatic precipitator.

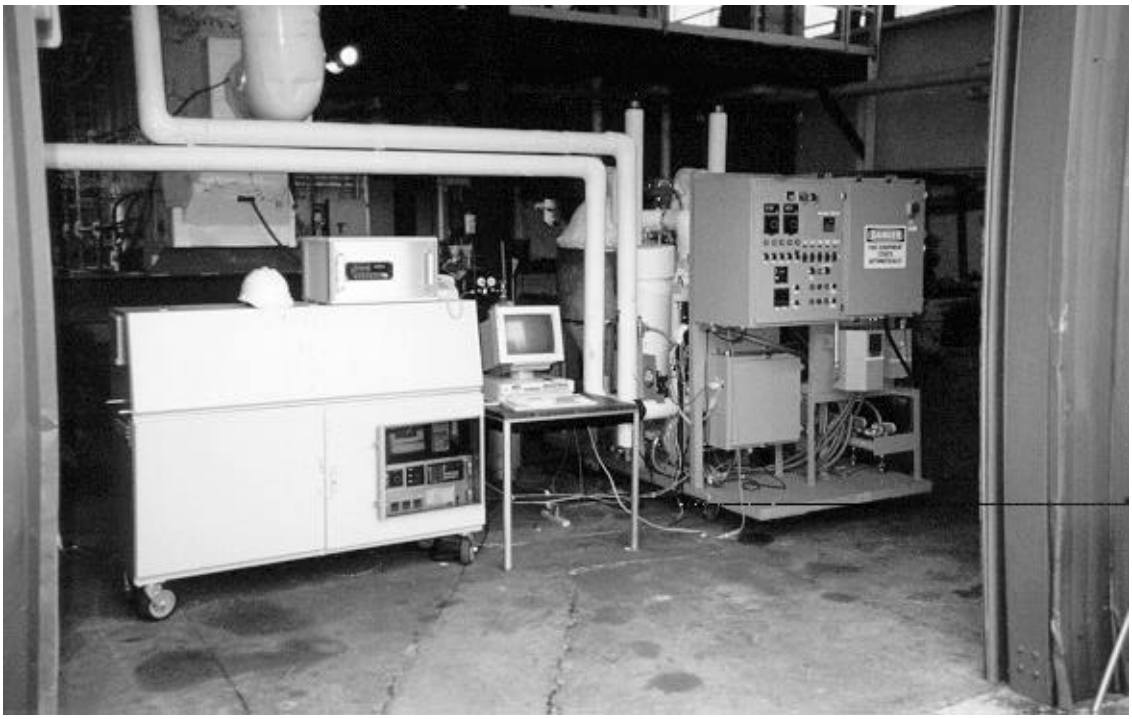

Figure 13 – Mercury Analyzer and Skid Installed at Consol, Library, PA

The mercury analyzer itself, explained further in Appendix F, contains two sample cells. One of these is held at the flue gas temperature, approximately 300°F. The other is maintained at about 1600°F so that all mercury-containing species are converted thermally to elemental mercury. In this way, the instrument simultaneously reports the elemental mercury and the total mercury concentrations in real time. One can subtract these two numbers to derive the non-elemental mercury concentration if desired.

Figure 14 shows the analyzer under construction where the two sample cell ovens are evident. The left hand side of the analyzer contains two on-board permeation tube holders, one for elemental mercury and one for mercuric chloride, and it also contains a set of automatic valves. With these valves, we can send span gas, zero gas, or sample gas to the sample cells. We can also pass span gas outside of the analyzer to check to see if the sample line plumbing alters the mercury signal or not. All of these functions are controlled by the on-board computer. The computer program, written with LabView software from National Instruments (Austin, TX), displays the mercury concentration in real time on the screen and allows for various data storage and manipulation functions.

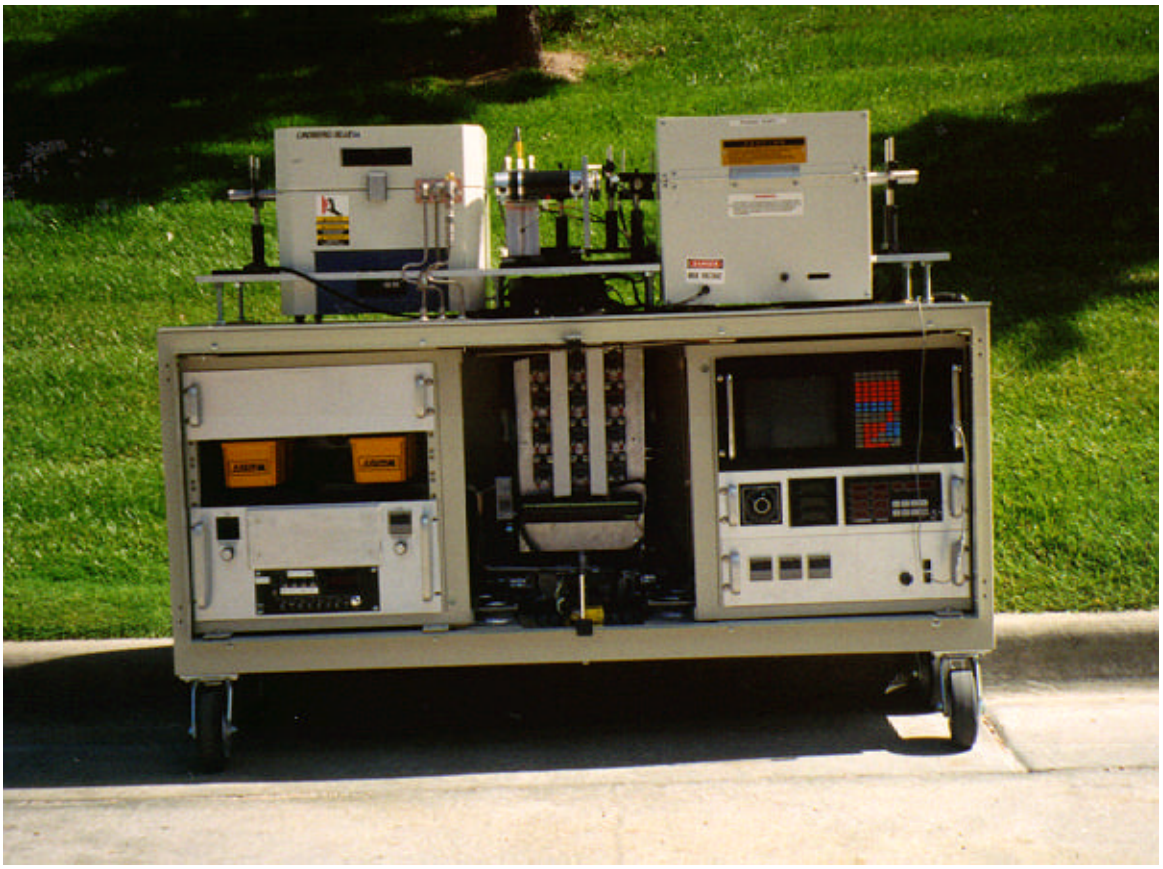

Figure 14 – Internals of ADA's Mercury Analyzer

Before we began to pass flue gas through the test skid, we determined the flow resistance with room air flowing through the unit (Figure 15). We found a low pressure drop, consistent with our laboratory testing. The flow is laminar, and the pressure drop is proportional to the first power of the superficial velocity. This contrasts with the flow regime of the particle-bed configuration where the flow within the bed was not laminar (Figure 8). At 20 ACFM, the design flow rate of the skid unit, the superficial velocity is 1 ft/sec. With these low pressure drops, we probably could have tested mercury uptake on the skid at flows up to 50 ACFM but did not have time to do so.

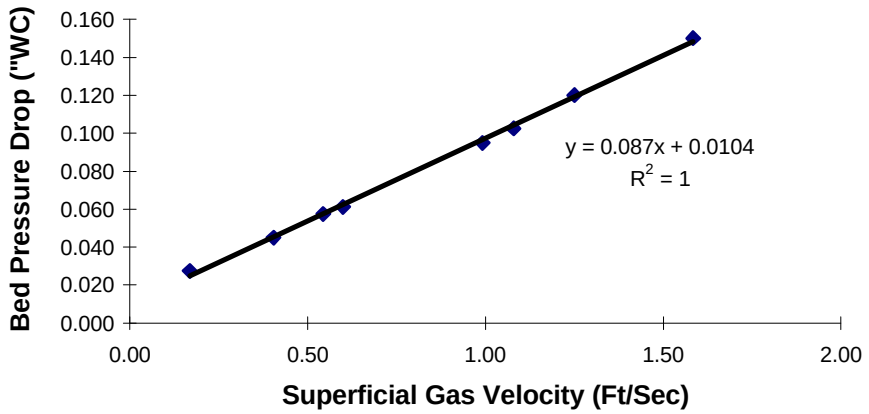

Figure 15 – Flow Resistance of Skid-Mounted Sorbent Module at 70°F

Scope of Pilot Testing

The bench-scale equipment treated the flue gas from four coals over eight calendar weeks in which we achieved approximately 440 hours of operation on sorbent vessel number 1 and 610 hours of operation on sorbent vessel number 2 (Tables 4 and 5; total skid "on" time was about 700 hours). Each of the coals had approximately 0.1 ppm by weight mercury but varied in their sulfur and chlorine contents.

During the two weeks of the higher sulfur Pittsburgh Seam tests, Consol personnel sampled both before and after our skid using a modified Ontario Hydro impinger train, a derivative of EPA method 29 that is a leading contender to being a "reference method" for measuring oxidized and elemental mercury in flue gases. At this same time, ADA personnel sampled with iodated carbon traps provided by Frontier Geosciences (Seattle, WA). These traps were then analyzed for "total" mercury by Frontier Geosciences. Briefly stated, none of the techniques agreed, but we concluded that the main point of our study is mercury control technology, not mercury measurement technology (although of course the two are logically intertwined); consequently, we did not pursue further comparison of measurement methods.

Table 4 – Coals Burned During Testing of 20 ACFM Skid at Consol

Dates Tested	Coal Name	Sulfur Content	Chlorine Content
1/27 through 1/31; 5/5 through 5/8	Illinois #6 Seam, High Sulfur	3.6-3.8%	0.06%
2/3 through 2/14	Illinois #6 Seam, Low Sulfur	1.0-1.1 %	0.42 %
3/3 through 3/13	Pittsburgh Seam, High Sulfur	2.5-2.7%	0.12%
6/4 through 6/20	Pittsburgh Seam, Low Sulfur	1.8 %	0.11%

During these four coals, sorbent module number one experienced 199 hours of sorption and 257 hours of desorption, and sorbent module two experienced 277 hours of sorption and 331 hours of desorption. These figures correspond to about 11 cycles of sorption and desorption on sorbent Unit Number 1 and 12 cycles on Unit Number 2. The 102 individual monoliths in the units remained in the unit throughout the testing with the exception of one monolith that was removed in April and two monoliths that were removed at the end of the program. These three monoliths removed from the unit were tested in the laboratory.

Table 5 – Operational History of 20 ACFM Skid

	Sorbent Unit Number 1		Sorbent Unit Number 2	
Date	Sorption Time (hours)	Desorption Time (hours)	Sorption Time (hours)	Desorption Time (hours)
1/31/97	10			12
February 1		20		
2/3			10	
2/4	20			20
2/5		20	20	
2/6	20			20
2/7		20	12	
2/8				20
2/10	10			20
2/11		20	20	
2/12	20			20
Jan/Feb Sub Total	80	80	62	112

Table 5 – Operational History of 20 ACFM Skid (continued)

	Sorbent Unit Number 1		Sorbent Unit Number 2	
Date	Sorption Time (hours)	Desorption Time (hours)	Sorption Time (hours)	Desorption Time (hours)
March 4			8	
3/5		20	12	
3/6	12			20
3/7		20	8	
3/8				20
3/10				20
3/11		20	20	
3/12	20			20
3/13		20	20	
Monthly Sub Total	32	80	68	80
May 5		20		
5/6	20			20
5/7	17	7	6	14
5/8		13	20	
5/21				2
5/22				24
5/23				6
Monthly Sub Total	37	40	26	66
June 4			12	
6/5			24	
6/6		8	12	
6/7		17		8
6/8				24
6/10			13	
6/11			24	
6/12	7		11	
6/13	8			8
6/14		8		13
6/15		13		
6/17			7	
6/18	4		18	4
6/19	24			16
6/20	7	11		
Monthly Sub Total	50	57	121	73
Total Hours	**199**	**257**	**277**	**331**

Overview of Pilot Testing Results

Substantial data were obtained during the 700 hours of run time. At the outset of the Phase I program, we had planned to do careful quantitative studies of the performance of the skid. However, quantitative mercury-related work in the field, especially with a new technology, is extremely challenging. We were able to quantify the uptake of mercury when all of the equipment was working well and have substantial verification of the unit's ability to sorb both elemental and non-elemental mercury, but in only one case were we able to quantify the desorption of the mercury. We have, however, qualitative desorption data that confirms the desorption of both elemental and non-elemental mercury.

We were sometimes fighting drift problems on the analyzer and crashes of the computers controlling the skid and the analyzer. These problems were overcome essentially by having an operator on-site (March, May, and June testing). Other operational issues that we investigated after the March tests were the flow distribution and the regeneration efficiency. The flow distribution turned out not to be a problem for the sorption of the mercury. The heating of the bed was, however, much less efficient than we had hoped although we have no firm evidence that this inefficiency was causing us a problem. A discussion of these two operational issues is included in Appendix C.

The mercury analyzer recorded data every second, and we stored a 30-second box car average every minute, creating rather large data records of the detector voltages. To mitigate the effect of thermal drift on the analyzer data, we incorporated automatic hourly instrument zeroing and calibrations for both SO_2 and mercury. Therefore data recorded by the analyzer includes these zeroes and calibrations, and the analyzer voltage records are rather "messy" looking to someone who does not regularly work with the analyzer (see Appendix D).

Despite these "realities" of working in the field with a new technology**, the simplest and most important result that we have from the six months of testing is that in every time period where we have high confidence in the data, the sorbent beds completely removed the mercury from the flue gas for all coals tested**. In the following sections, we cover first sorption data, then regeneration data, and finally the data taken back in the laboratory with monoliths that had been removed from the field unit in April and at the end of the field testing at the end of June.

Sorption Results

a) Low Sulfur Pittsburgh Seam Coal, June, 1997

We start first with the Low Sulfur Pittsburgh Seam coal burned in June because these data were taken after we improved the regeneration (Appendix C). To reiterate, however, we do not have any evidence that says the regeneration was not working before June, only that we are confident during June that is was working well.

In early June, we decided to spike elemental mercury into the flue gas just to test the unit performance. As expected, the sorbent unit (number 2) quantitatively removed this mercury from a concentration of about 10 to 30 $\mu g/m^3$ at the inlet to the noise level of the instrument at the

outlet (less than 1 µg/m^3; Figure 16). The concentration of the inlet mercury dropped with time, but we did not want to spend effort on improving its constancy since the goal of the test had been achieved.

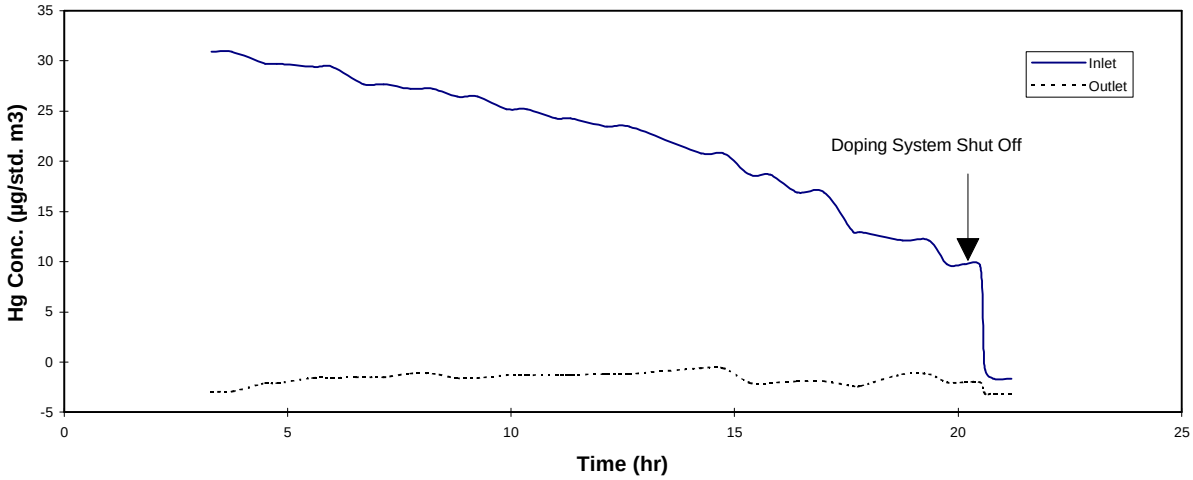

Figure 16 – Quantitative Uptake of Elemental Mercury in Unit 2; 6/5 and 6/6/97

After this test with spiked mercury, we then desorbed the unit for a total of 32 hours starting on 6/7 and ending on 6/8. Then we introduced flue gas again on the morning of 6/10 and sorbed for 48 hours.

Figure 17 shows a zero, span, inlet, and outlet data sequence on the afternoon of 6/10 when we had been sorbing on Unit 2 for about six hours. Adjusting for the zero offset of about two µg/m^3, the total inlet mercury concentration is approximately seven µg/m^3, 50% of which is non-elemental mercury. The total outlet mercury concentration is zero to within plus or minus one µg/m^3. This bed was still sorbing 15 hours later. The inlet concentration was still about seven µg/m^3, about 50% was non-elemental, and the outlet concentration was zero (Figure 18). Both of these figures show the simultaneous removal of essentially 100% of the elemental and non-elemental mercury.

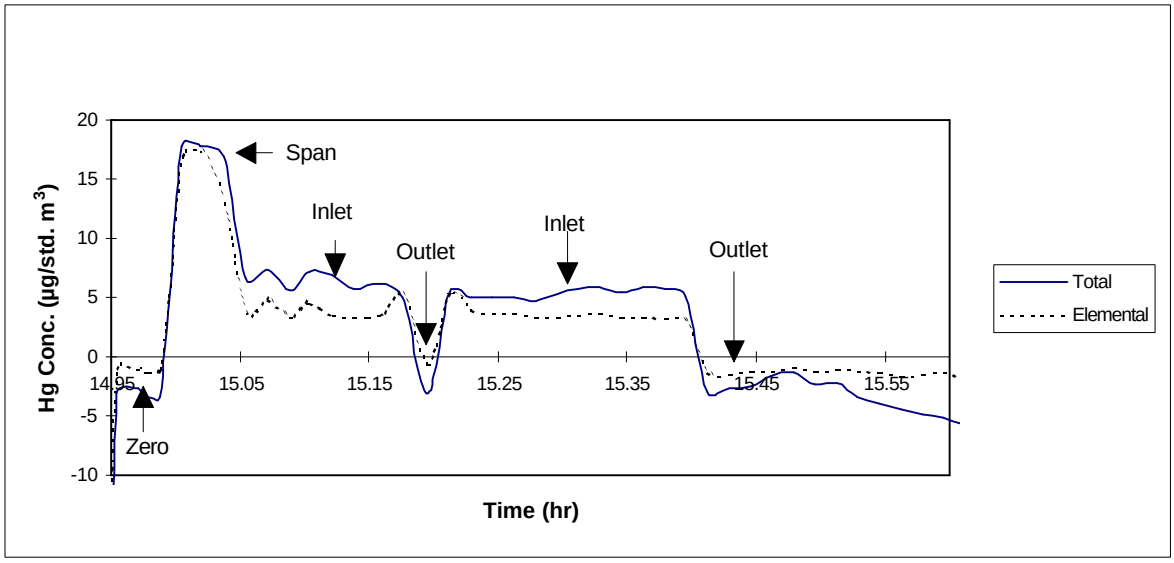

Figure 17 – Performance of Unit 2 with Low Sulfur Pittsburgh Seam Coal; 6/10/97, approximately 3 pm.

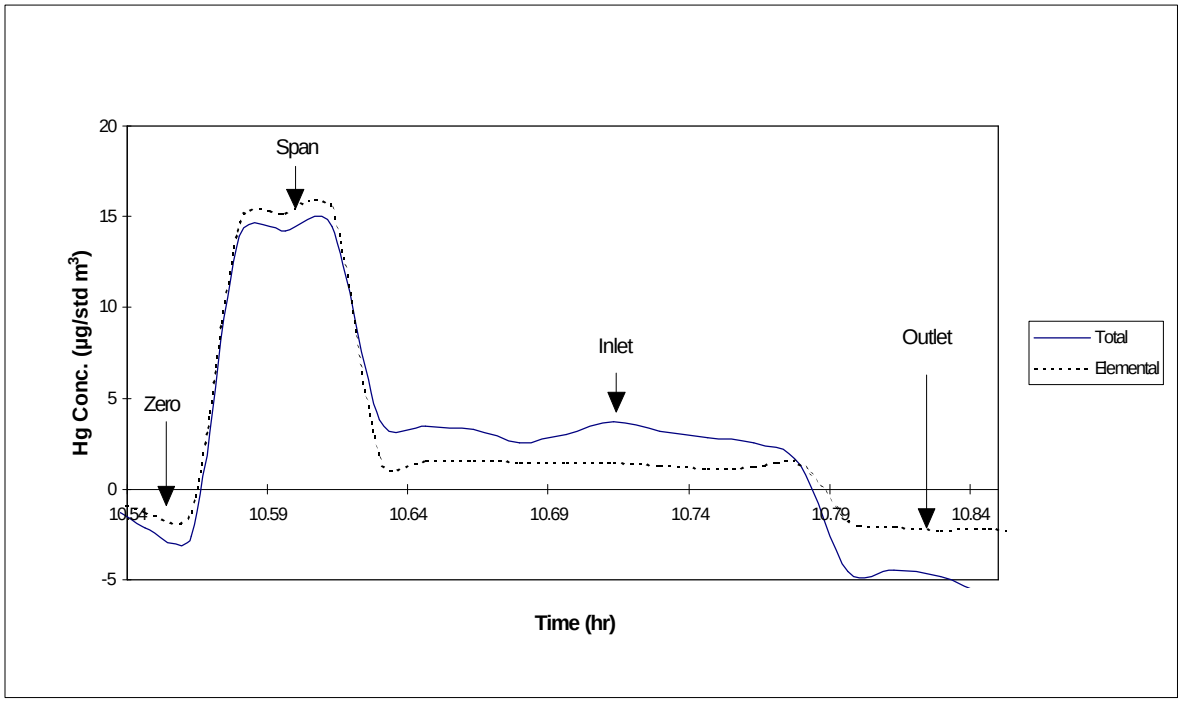

Figure 18 – Performance of Unit 2 with Low Sulfur Pittsburgh Seam Coal; 6/11/97, approximately 10:30 am

The unit continued to sorb mercury through the entire 48 hours of testing, and the entire record of the mercury analyzer during this run is included in Appendix D. Given the inlet concentration of about seven µg per standard cubic meter and the inlet flow rate of 20 ACFM at 250°F, the total mercury going into the sorbent unit during the 48 hours was 7.9 milligrams. This ratio of this mass of mercury to the mass of active noble metal (51 milligrams of noble metal per sorbent module) is within the range we typically see in the laboratory before breakthrough. This run was the longest sorption period in the field tests.

b) High Sulfur Pittsburgh Seam Coal, March, 1997

During the two weeks between 3/3 and 3/13, we sorbed in Unit 1 twice and in Unit 2 four times. We sampled with our analyzer and with iodated carbon traps, and Consol personnel sampled with the Ontario Hydro impinger method ("wet chemistry;" see Appendix E). We had more baseline drift issues during these tests and also reported generally over 80% of the flue gas mercury as elemental. Consol reported 75% to 80% of the mercury as non-elemental. Recent studies with our analyzer at a federal laboratory have shown that under some conditions, the analyzer reports a greater fraction of the mercury as elemental but agrees well with the total mercury concentration, when compared to wet chemistry results (Hargis, 1997). This apparent skewing towards elemental mercury may be caused by the sampling line leading to the analyzer (i.e., the mercury really is elemental at the analyzer) or by some conversion in the analyzer itself. The meaning for our skid tests is that the inlet flue gas was probably a higher fraction oxidized mercury than that reported by the analyzer.

The skid appeared to remove essentially 100% of the mercury in these tests.

During the first sorption run of Unit 1 on 3/6/97, the removal of mercury across the bed appeared to be complete (12 µg/m^3 removal across the bed) although there is some possible baseline drift (Figure 19). The analyzer seems to under report the fraction non-elemental mercury. This run began at 1:30 pm, and Figure 19 shows the capture efficiency at two hours into the run. The complete mercury analyzer output for a five-hour section of this run is included in Appendix D.

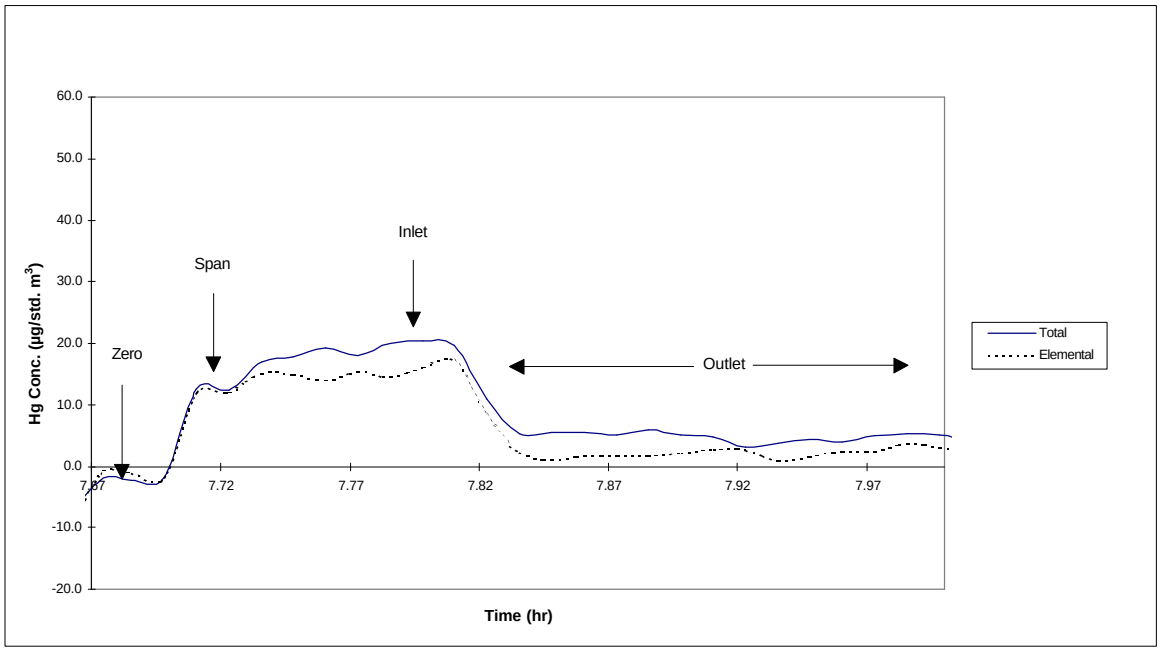

Figure 19 – Performance of Unit 1 with High Sulfur Pittsburgh Seam Coal; 3/6/97, approximately 3:40 pm

This bed then underwent two 20-hour desorptions before another sorption run was undertaken. Figure 20 shows Unit 1 removing mercury approximately four hours into its second sorption run. The inlet concentration of mercury seems to drift down for the 10 minutes between the time we switched from span to the inlet and then to the outlet. The best measure of the inlet mercury concentration is found at about 1.85 hours to 1.9 hours on Figure 20, where the total mercury concentration is about 12 µg/m^3, and the analyzer reports almost all of this mercury as elemental. The outlet mercury concentration is zero, again to within the precision of the analyzer. The mercury analyzer output for the last 12 hours of this 20-hour sorption run is included in Appendix D. In 20 hours with approximately 10 µg/m^3 of mercury in the flue gas, the mass of mercury going into the bed was 5.6 milligrams. So the fact that we did not see breakthrough is consistent with our laboratory data.

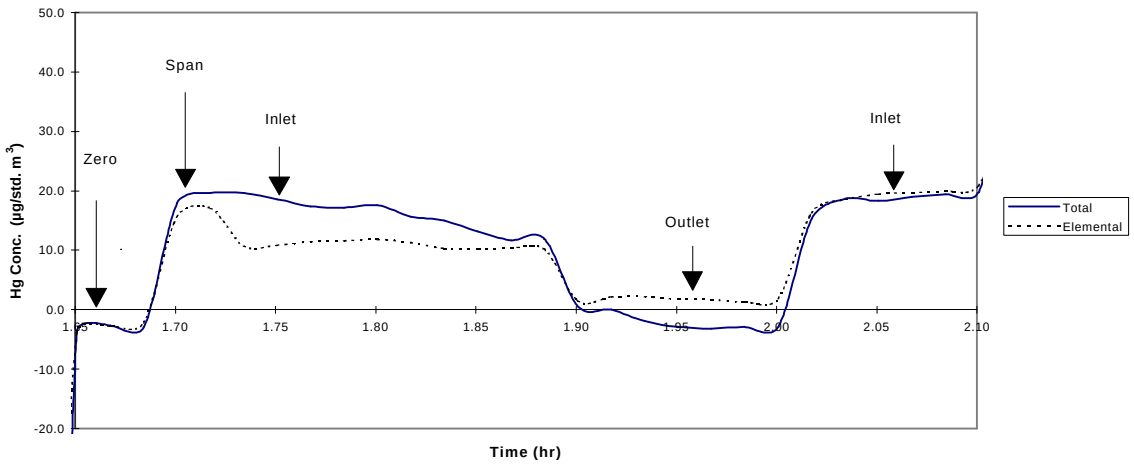

Figure 20 – Performance of Unit 1 with High Sulfur Pittsburgh Seam Coal; 3/12/97, approximately 10:30 am

The final example with the High Sulfur Pittsburgh coal is the third sorption cycle with Unit 2 on 3/11/97. There was approximately 90% removal of the total mercury and 100% removal of the four µg/m^3 of elemental mercury (Figure 21).

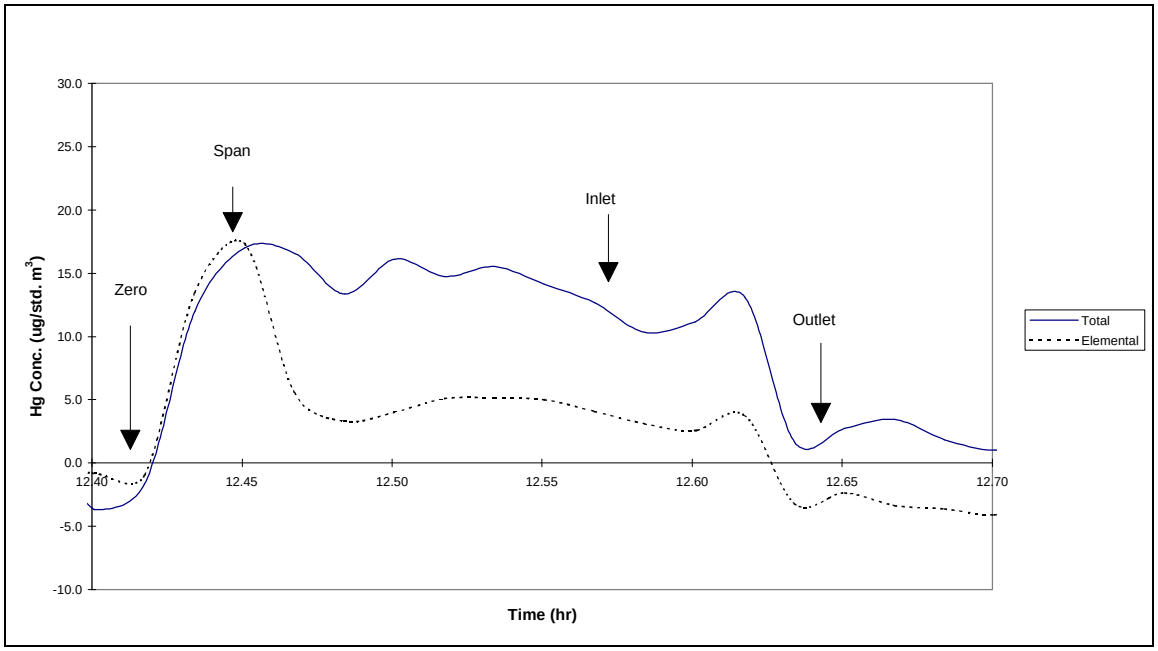

Figure 21 – Performance of Unit 2 with High Sulfur Pittsburgh Seam Coal; 3/11/97, approximately 12:30 pm

c) High Sulfur Illinois #6 Coal, January, 1997

Our first results were obtained in January with a high sulfur Illinois #6 coal. We had more baseline drift in January than we did later, but we saw a removal of about seven $\mu g/m^3$ of mercury across the bed, most of which the analyzer reported as elemental mercury (Figure 22).

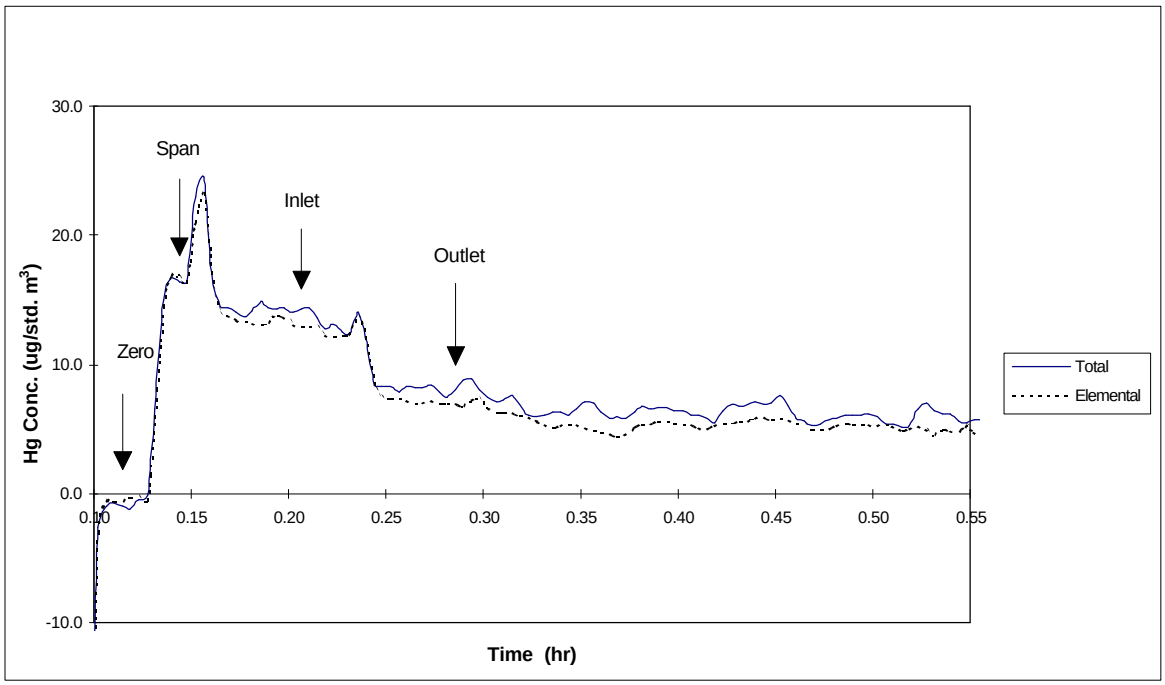

Figure 22 – Performance of Unit 1 with High Sulfur Illinois #6 Seam Coal; 1/31/97, approximately 1:00 pm

d) Low Sulfur Illinois #6 Coal, February, 1997

We had significant problems with the unit during February, including a crash of the analyzer's computer. Because the skid computer itself operated regardless of the analyzer, the unit continued to go through automatic sorption and desorption cycles as listed in Table 5. Whereas we monitored the analyzer output from our offices in Colorado and noted essentially complete removal of mercury across the skid, when the analyzer's computer crashed, the recorded data were lost.

Desorption Results

We found significant off-gassing of the regeneration line while we were investigating the regeneration conditions in May. That so much mercury desorbed from the regeneration exhaust line was a clear indication that mercury had been desorbing from the sorbent beds during the previous regenerations in the months of January, February, and March. In routine operation in the months of January, February, and March, we did not monitor the mercury in the regeneration

exhaust gas so did not have an opportunity before May to see the mercury coming through the regeneration line. Further, the regeneration exhaust line that connected to a small condenser was not heated until the end of May when we replaced the line and heated it. Hence, it made sense that mercury had accumulated in the line.

For example, on May 7, we began a desorption cycle on Unit 1 after 37 hours of sorption. About four hours into the desorption, copious amounts of mercury came off, almost all of it non-elemental mercury (Figure 23). The time delay in when we saw the desorption was reasonable because it takes two hours for the unit to heat up to the regeneration temperature and probably takes longer for the regeneration exhaust gas to heat up the regeneration exhaust line itself. The mercury off-gassing in Figure 23, therefore, could be a mix of mercury coming off of the bed and mercury coming off of the regeneration line itself. Since the flow rate of regeneration purge gas is only about five standard liters per minute in Figure 23, the total amount of mercury coming off integrated to only about 0.3 milligrams.

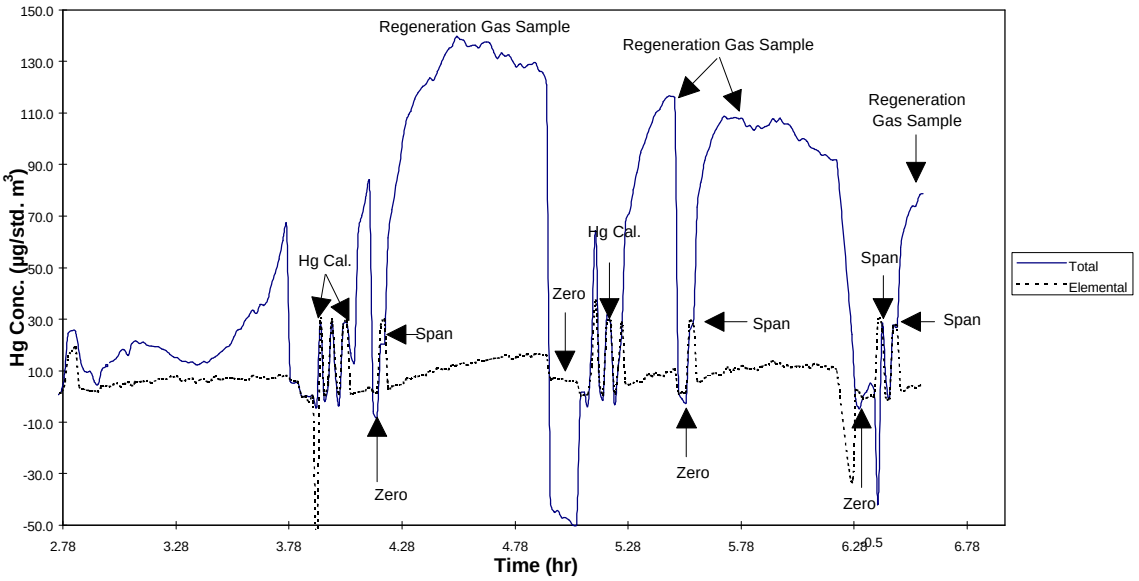

Figure 23 – Desorption of Non-Elemental Mercury; Original Regeneration Cycle; Unit 1; 5/7/97 approximately 8 PM; after sorbing High Sulfur Illinois #6 Flue Gas

After our investigation of the regeneration rate and conditions (Appendix C), we installed an auxiliary heater and increased the regeneration purge gas flow rate to 40 ACFM to insure that

the regeneration purge gas reached 700°F. At this time, the former regeneration exhaust line (a ¼" tube) became a line through which we sampled and the main flow exhausted back into the Consol flue gas duct. We had not yet replaced nor heated this regeneration gas sampling line. When we desorbed Unit 2 with this arrangement, we saw ample mercury coming off, but because the regeneration sampling line was not heated, we could not say for sure that all of this mercury was from the sorbent unit itself.

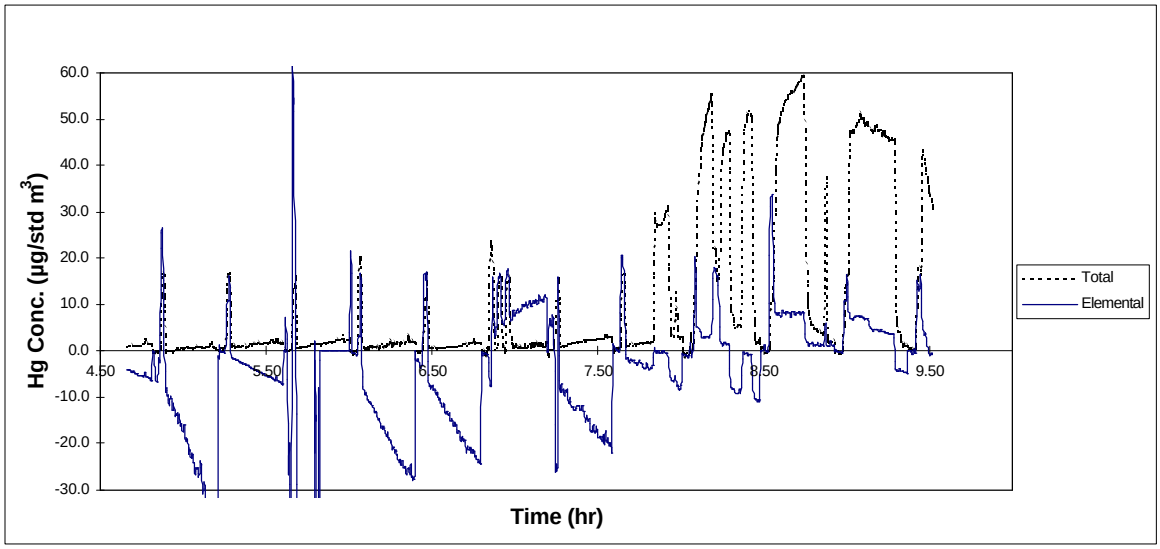

Figure 24 – Desorption of Unit 2 with Auxiliary Heater; 5/22/97

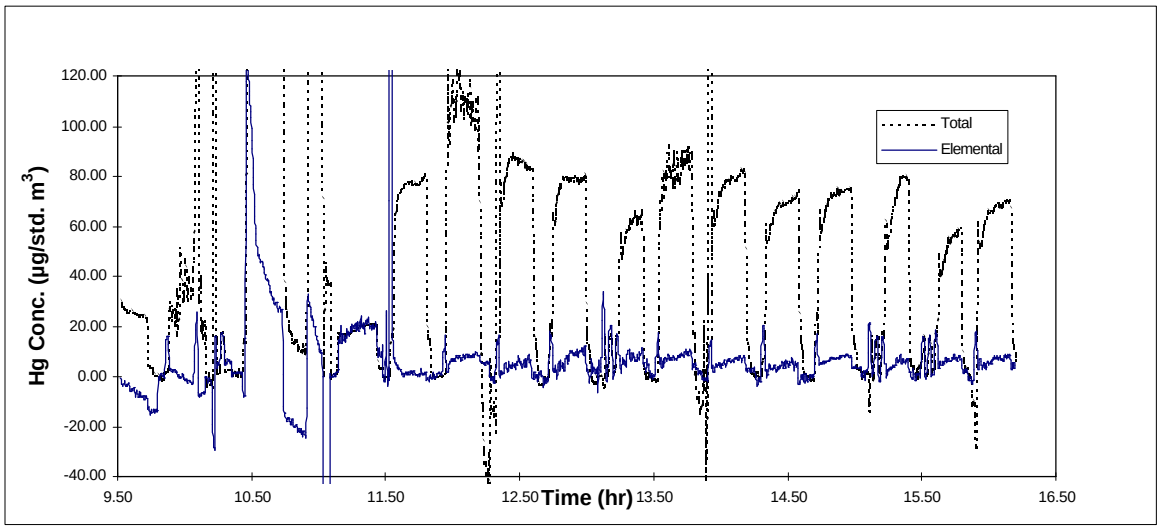

Figure 25 – Continued Desorption of Unit 2 with Auxiliary Heater; 5/23/97

Once we determined that so much mercury was desorbing during the regeneration, either from the desorbing bed or from the regeneration line itself, we determined that we should replace the regeneration sampling line with electropolished steel and that we should heat this line. In this way, we would be able to sample through this line to the continuous mercury analyzer with no concern that the signal was coming from the sampling line itself.

On 6/6 overnight (into 6/7), we regenerated Unit 1 with the improved regeneration conditions (Appendix C) wherein we were 100% sure that the regeneration gas temperature was 700°F. Under these conditions, we were able to quantify the desorbing mercury. We desorbed 5.1 mg of mercury from the bed almost precisely the capacity of mercury on the monoliths in the laboratory testing (Figure 26).

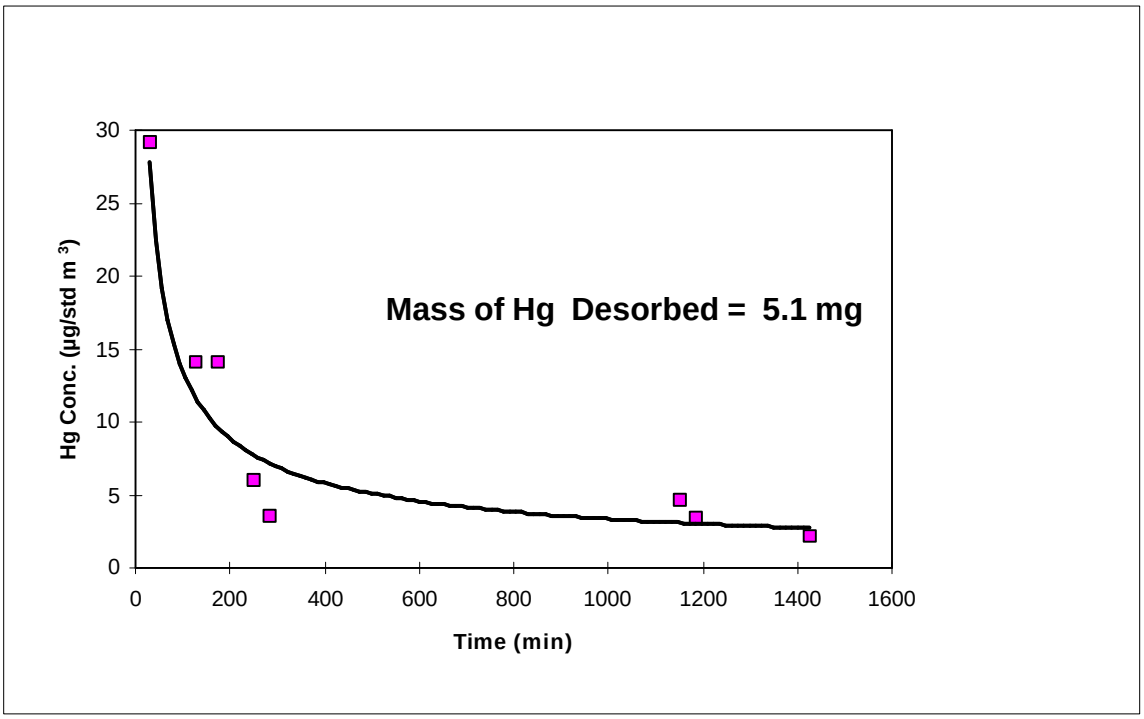

Figure 26 – Quantitative Desorption of Unit 1 with Clean Regeneration Sampling Line (6/6 and 6/7/97)

Although we would have loved to have ten figures like Figure 26, we were quite gratified to have finally worked through enough issues with the skid to get a good clean, quantifiable desorption and that it agreed with the amount of mercury that would be present on a fully-saturated monolith. The final interesting issue about Figure 26 is that all of the mercury detected was non-elemental. There may be a number of meanings to this observation, but it at least provided further confirmation that the monoliths removed non-elemental mercury from the flue gas.

Monolith Tests After Field Work

We brought back one monolith in April from Unit 1 and one monolith from both Unit 1 and Unit 2 at the end of June when the test program had concluded. We tested these monoliths in our laboratory test apparatus. All three monoliths quantitatively sorbed elemental mercury to the expected breakthrough point in the laboratory just as they had before going to the field, gave off the mercury upon regeneration, and quantitatively sorbed mercury again. We tested one of the monoliths also with mercuric chloride and saw complete removal of mercuric chloride as well. These results are detailed in Appendix G.

Task I-4: Evaluate Economics Based on Bench-Scale Results

Approximate Cost Analysis

The capital cost of a sorbent bed to treat a specific flue gas depends on the concentration of mercury in the gas and on how long the bed will last between regenerations. A simple relationship can be derived between the capital cost of sorbent and the time between sorbent regenerations. If essentially all of the mercury vapor is captured up to the point of breakthrough, the breakthrough time, τ_b, is related to the flow rate, **Q**, the mercury concentration, **C**, and the mass of sorbent in the bed, M_s, by

$$\tau_b = \frac{M_s}{Q}\frac{\Delta q\,\overline{W}}{C} \tag{1}$$

where $\overline{W}$ is the mass fraction gold on the sorbent and, Δq is the difference between the mass ratio of mercury to gold at the end of a sorption cycle and the mass ratio of mercury to gold at the beginning of a sorption cycle. The capital cost of the sorbent per unit of flue gas flow rate, ΔI_s, is related to the breakthrough time by

$$\frac{\Delta I_s}{\tau_b} = \frac{G \bullet C}{\Delta q} \tag{2}$$

Here, G is the cost of a unit mass of noble metal on the sorbent. Reasonable values of Δq and G are 0.1 and $10,000/lb; with these values, the capital cost per unit of breakthrough time can be written

$$\frac{\Delta I_s}{\tau_b} = 0.00898 \bullet C\left(\frac{m^3}{\mu g}\right)\left(\frac{\$}{ACFM}\right)\left(\frac{1}{day}\right) \tag{3}$$

As an example, equation 3 states that if the mercury concentration is 10 $\mu g/m^3$ and if the sorbent is regenerated once every day (τ_b = 1 day), the capital cost of the noble metal itself will be \$0.0898 for each ACFM of flue gas flow rate, or \$89,800 for a 1,000,000 ACFM facility (250 MW power plant). In the Phase I testing, the sorbent beds were designed to last for 24 hours, and therefore we consider that regenerating once per day is a reasonable design basis.

Based on these figures, we believe the major capital expense will not be the sorbent itself but the monoliths to support the sorbent, the vessels to hold the monoliths, and the ducting to connect the sorbent vessels to the power plant flue gas ducting.

The cost of the monoliths themselves is about \$50 per square foot of cross sectional area. The cost of putting the sorbent on the monoliths is about \$45 per square foot of cross sectional area. The cost of the sorbent itself is about \$90,000 as described above. For a 1,000,000 ACFM unit wherein the superficial face velocity is 1 ft/sec, we will need about 20,000 ft^2 of cross sectional area (includes 20% of the modules being regenerated at any given time). Therefore, the capital cost for the prepared monoliths is \$1.99 million.

The sorbent vessel itself, at full-scale, is likely have tens of monolith cassettes (Figure 27) with alternating inlet and outlet flow passages. The flue gas will enter the cassette, take a 90° turn to flow through the monoliths, and then take another 90° turn to exit the cassette. The monoliths themselves would likely be 12” diameter circles or squares with a depth of 6” to 12” in the direction of flow, and there would be multiple monoliths per cassette. Although it is not possible to give a firm cost for this vessel at this stage of the technology development, the vessel has similar characteristics to an electrostatic precipitator. For example, an ESP has hanging electrodes spaced about 12 inches apart much like the monolith cassettes may be arranged in our unit. The inlet to an ESP requires much the same manifolding that we will require. Some mechanical equipment will need to be on top of our unit to open and close shutters as the monolith cassettes go into a desorption mode much like mechanical equipment on top of an ESP is needed for the electrical service and for rapping.

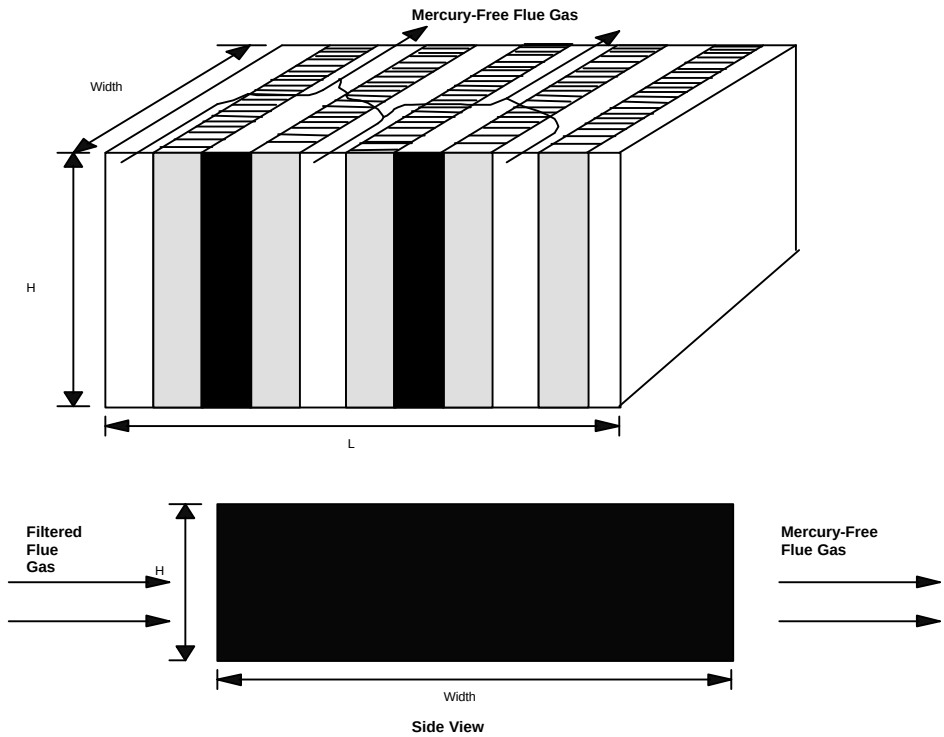

Figure 27 – Concept of Full-Scale Mercury Monolith Cassettes

We believe our best estimate of the cost of the vessel to hold the monolith cassettes can be derived from known electrostatic precipitator costs. The difference is that our vessel will be much smaller than an ESP. For example, Sloat, Gaikwad, and Chang (1993) indicate that the electrode and flow chamber for an ESP treating 950,000 ACFM of flue gas occupies a volume of about 245,000 cubic feet (a 15 second residence time). Our vessel will occupy a volume of about 20,000 cubic feet. This factor of 12 reduction in size will lead to a factor of approximately 5.1 reduction in cost. Sloat, et al., report a capital cost of $8.5 million in 1991 dollars for an ESP processing 950,000 ACFM. Therefore, we can expect the capital cost of our sorbent vessel to be about $2.24 million in 1997 dollars (5% inflation per year from 1991 to 1997).

The total capital cost of our system to treat 1,000,000 ACFM (250 MW facility) therefore is approximately $4.53 million when duct work is included (Table 6).

The operating costs include electricity for overcoming the system pressure drop, heat for regeneration, and maintenance. The cost of the electricity to run the fan to push the flue gas through the sorbent bed depends on the bed pressure drop. With superficial velocities near 1 ft/sec, the bed pressure drop in the 20 ACFM test unit was about 0.2 inches of water. This low of a pressure drop is important because, as long as the pressure drop remains less than an inch of

water, the fan or fans already being used at an operating power plant will be sufficient to push the gas through the unit. We believe that 1" of water pressure drop is realistic for our full-scale system given the low pressure drop observed in the 20 ACFM testing. A pressure drop of 1" of water corresponds to a power consumption of 1.96 kWh per million actual cubic feet of gas flow. At 5¢ per kWh, this power will cost $46,300 per year in a plant that processes 1,000,000 ACFM of flue gas (one year assumed to be 7884 operating hours).

Table 6 -- Projected Process Costs for 250 MW Facility

	Initial Capital Cost	Annualized Cost (15% of capital cost)
Capital Items		
Sorbent Monoliths	$1,990,000	$298,500
Sorbent Vessel	$2,240,000	$336,000
Duct Work	$300,000	$45,000
Total Capital Cost	$4,530,000	$679,500
Operating Costs		
Fan Power		$46,300
Heat for Regeneration		$50,000
Maintenance (2% of Initial Capital Cost)		$90,600
Total Operating Costs		$186,900
Total Annualized Cost		**$866,400**

The cost of heat for regeneration is not fully known at this point, but at a coal-fired power plant, plenty of steam is available compared to the needs of this process, and the actual cost of this energy may be quite small. We have estimated the regeneration energy cost to be on the order of the fan power cost. The amount of mercury needing to be removed and condensed in the regeneration step is so small (e.g. one liquid quart of mercury condensed every month in a system treating 1,000,000 ACFM with 10 $\mu g/m^3$ of mercury) that no substantial cooling loads will be required. Further, the condensation downstream of the regeneration vessel can be with cooling water at about 60°F, and the heat load is so small so as to be negligible. Hence, with our estimate for the fan power cost and the regeneration heating cost, we likely have identified the major operating costs of the system.

Economic Benefits of Mercu-RE Process

Carbon injection is the only established technology for mercury control available for flue gas treatment today (Bustard and Chang, 1994; Chang and Offen, 1995; Sjostrom, et al, 1997). According to this literature, to achieve a mercury capture efficiency above 75%, approximately 10,000 pounds of injected carbon are needed per pound of mercury removed. The price of an appropriate activated carbon is about $0.55/lb in the large quantities needed for a large flue gas application. Therefore, to treat 1,000,000 ACFM containing 10 $\mu g/m^3$ of mercury (295 pounds of mercury) will require three million pounds of activated carbon at a cost of $1,620,000 per year. Annualized capital and additional maintenance and operating costs bring the total annualized cost

of a carbon injection system to $14,400 to 38,200 per pound of mercury removed, or $4.25 million to $11.3 million in this case (Chang and Offen, 1995).

Costs for both the Mercu-RE process and for carbon will be reduced as the mercury concentration is reduced, but carbon works less well at lower mercury concentrations while the Mercu-RE process is independent of the mercury concentration in the range tested to date. Therefore, the cost comparison will be more favorable to the Mercu-RE process at lower mercury concentrations. Even if our approximate economic analysis for the Mercu-RE system is off by a factor of three, the Mercu-RE process will be less than half the low-end costs for a carbon injection system. Considering the ability of the Mercu-RE process to collect all chemical forms of mercury, to generate no secondary wastes, and to regularly remove over 95% of the mercury, the Mercu-RE process has clear technical and economic advantages over available technologies.

Conclusions and Recommendations

The Phase I work showed that the monolithic form of the sorbent will take up and desorb mercury repeatedly after exposure to a variety of realistic flue gases. The monoliths worked well for both non-elemental mercury and elemental mercury, both in the laboratory and in the field.

Our future work must focus on recovering mercury in a routinely operating unit. To this end, we have recommended to DOE that the next phase of the work emphasize routine operation of a 20 ACFM skid at Consol's pilot facility including desorbing mercury at condensable concentrations and then doing the same with a 50 ACFM unit at an operating coal-fired power plant.

References

Bustard, C. J., R. Chang, "Sorbent Injection for Flue Gas Mercury Control," presented at the 87th Annual Air and Waste Management Meeting, Cincinnati, OH, June 19-24, 1994.

Chang, R., G. R. Offen, "Mercury Emission Control Technologies," *Power Engineering*, November, 1995; pp 51-56.

Cullity, B. D., Elements of X-Ray Diffraction, Addison Wesley Publishing Company, New York, NY, 1978.

Hargis, R., Federal Energy Technology Center, Pittsburgh; personal communication, July, 1997.

Schlager, R. J., K. G. Wilson, A. D. Sappey, K. E. Baldrey, "Continuous Monitors for Measuring Emissions of Mercury and Particulate Matter," presented at EPRI/DOE International Conference on Managing Hazardous and Particulate Air Pollutants, Toronto, Ontario, Canada, August 15-18, 1995.

Sjostrom, S., J. Smith, T. Hunt, R. Chang, T. D. Brown, "Demonstration of Dry Carbon-Based Sorbent Injection for Mercury Control in Utility ESPs and Baghouses," 90th Annual Meeting of the Air and Waste Management Assn., Toronto, Canada, June 8-13, 1997.

Sloat, D. G., R. P. Gaikwad, R. L. Chang, "The Potential of Pulse-Jet Baghouses for Utility Boilers, Part 3: Comparative Economics of Pulse-Jet Baghouse, Precipitators, and Reverse-Gas Baghouses," *Air and Waste*, 43, 120-27, January, 1993.

Stiles, A. B., Catalyst Preparation and Manufacture, Marcel Dekker, New York, NY, 1983; pp. 68-98.

Appendix A

Mercury Analyzer Data Reduction

The appendix describes the equations that are necessary to relate the voltages recorded by the analyzer to mercury concentrations. There are a substantial amount of mathematics in Appendix A, but we wanted to include all of this information so that the data reduction method is recorded in one place.

The basis of the analyzer's ability to detect mercury is simply the "Beer-Lambert" law of light extinction. This law says that when light travels through a medium where an absorbing species resides at a concentration "C," that the incident light is decreased in proportion to the concentration of the absorbing species. The proportionality constant is a physical property of the species for a given wavelength of light and is known as the molar absorptivity.

ADA's mercury analyzer produces two wavelengths of light from a mercury lamp by placing the lamp in a magnetic field. The Zeeman effect dictates that these two wavelengths will be polarized 90° with respect to each other and displaced by only fractions of an Angstrom in wavelength from each other. Both wavelengths are passed alternatively through two detection cells. One wavelength of light is attenuated by elemental mercury. The other is essentially not attenuated by mercury. However, broad band interfering species such as SO_2 attenuate both wavelengths of light essentially equally, allowing cancellation of interfering species. Sjostrom, et al., (1997) have explained the functioning of the analyzer in detail, and an excerpt of this paper is included in Appendix F.

In the following discussion, we explain the algebra behind the data reduction routine. We will refer to the two wavelengths of light emitted by the mercury lamp as "vertical" and "horizontal" with the subscripts "v" and "h."

The basic equations relating the detector voltages to the sample gas concentration are

$$\frac{\mathbf{V_v}}{\mathbf{V_{v,o}}} = \mathbf{exp}\left(-\mathbf{L}\sum_{\mathbf{i=1}}^{\mathbf{N}} \mathbf{k_{i,v}C_i}\right) \qquad \text{(A-1)}$$

and

$$\frac{\mathbf{V_h}}{\mathbf{V_{h,o}}} = \mathbf{exp}\left(-\mathbf{L}\sum_{\mathbf{i=1}}^{\mathbf{N}} \mathbf{k_{i,h}C_i}\right) \qquad \text{(A-2)}$$

Here, L is the length of the cell through which the sample gas flows, $\mathbf{V_v}$ is the detector voltage corresponding to the intensity of vertically-polarized light at the detector, $\mathbf{V_h}$ is the detector voltage corresponding to the intensity of horizontally-polarized light at the detector, $\mathbf{V_{v,o}}$ is the voltage corresponding to the incident vertical light, and $\mathbf{V_{h,o}}$ is the detector voltage corresponding to the incident horizontal light. The coefficients $\mathbf{k_{i,v}}$ and $\mathbf{k_{i,h}}$ are the molar absorptivities of species "i" for vertical light and horizontal light, respectively.

In a system where only SO_2 and Hg are responsible for the light attenuation, equations A-1 and A-2 represent two equations for the two unknowns $\mathbf{C_{SO_2}}$ and $\mathbf{C_{Hg}}$. It is helpful, because of the possible uncertainties in the system, to modify equations A-1 and A-2 to include an "expected" or "reference" value of the SO_2 concentration. These equations then become

$$\ell n\left(\frac{\mathbf{V_v}}{\overline{\mathbf{V}}_\mathbf{v}}\right) = -\mathbf{Lk_{SO_2,v}}\left(\mathbf{C_{SO_2}} - \overline{\mathbf{C}}\right) - \mathbf{Lk_{Hg,v}C_{Hg}} \qquad \text{(A-3)}$$

and

$$\ell n\left(\frac{\mathbf{V_h}}{\overline{\mathbf{V}}_\mathbf{h}}\right) = -\mathbf{Lk_{SO_2,h}}\left(\mathbf{C_{SO_2}} - \overline{\mathbf{C}}\right) - \mathbf{Lk_{Hg,h}C_{Hg}} \qquad \text{(A-4)}$$

Here, the symbol $\overline{\mathbf{C}}$ denotes the expected value of the SO_2 concentration and $\overline{\mathbf{V}}_\mathbf{v}$ and $\overline{\mathbf{V}}_\mathbf{h}$ represent the detector voltages corresponding to the vertical and horizontal light intensities measured when **mercury-free, SO_2-containing gas** is sent to the analyzer with a concentration of SO_2 equal to $\overline{\mathbf{C}}$.

We can immediately write the solution to these equations as follows:

$$\frac{\left\{\left(\frac{k_{SO_2,v}}{k_{SO_2,h}}\right)\bullet \ell n\left(\frac{V_h}{\overline{V}_h}\right)-\ell n\left(\frac{V_v}{\overline{V}_v}\right)\right\}}{\left[1-\frac{k_{SO_2,v}}{k_{SO_2,h}}\bullet\frac{k_{Hg,h}}{k_{Hg,v}}\right]}=Lk_{Hg,v}C_{Hg} \qquad \text{(A-5)}$$

and

$$\frac{\left\{\ell n\left(\frac{V_h}{\overline{V}_h}\right)-\left(\frac{k_{Hg,h}}{k_{Hg,v}}\right)\ell n\left(\frac{V_v}{\overline{V}_v}\right)\right\}}{\left[1-\frac{k_{SO_2,v}}{k_{SO_2,h}}\bullet\frac{k_{Hg,h}}{k_{Hg,v}}\right]}=Lk_{SO_2,h}\left(\overline{C}-C_{SO_2}\right) \qquad \text{(A-6)}$$

Equation A-6 can be rearranged into a highly useful dimensionless form as follows:

$$\frac{C_{SO_2}}{\overline{C}}=1-\frac{1}{Lk_{SO_2,h}\overline{C}}\bullet\left\{\frac{\ell n\left(\frac{V_h}{\overline{V}_h}\right)-\left(\frac{k_{Hg,h}}{k_{Hg,v}}\right)\ell n\left(\frac{V_v}{\overline{V}_v}\right)}{1-\frac{k_{SO_2,v}}{k_{SO_2,h}}\bullet\frac{k_{Hg,h}}{k_{Hg,v}}}\right\} \qquad \text{(A-7)}$$

Equation A-5 gives the concentration of mercury in terms of known quantities, and equation A-7 gives the concentration of SO_2 in terms of known quantities. Equation A-5 corresponds to our intuition that the concentration of mercury is given largely by the extinction of vertically-polarized light in that the second term in the denominator of equation A-5 is small compared to 1.0. Equation A-7 says that the concentration of sulfur dioxide can be deduced largely from the extinction of horizontally-polarized light (the first term in the numerator inside the brackets in dominant).

We next turn our attention to obtaining the molar absorptivities $\mathbf{k_{Hg,v}}$, $\mathbf{k_{Hg,h}}$, $\mathbf{k_{SO_2,v}}$, and $\mathbf{k_{SO_2,h}}$, and the detector voltages $\overline{\mathbf{V}}_\mathbf{v}$, and $\overline{\mathbf{V}}_\mathbf{h}$ from calibrations with SO_2 and with mercury and obtaining the quantities $\mathbf{V_v}$ and $\mathbf{V_h}$ from the experimental data when running live sample gas.

We will proceed from the simple to the complex. First, we cover getting the values of $\mathbf{V_v}$ and $\mathbf{V_h}$ when running live sample gas. Next we cover getting $\overline{\mathbf{V}}_\mathbf{v}$ and $\overline{\mathbf{V}}_\mathbf{h}$ during an SO_2 calibration ("ZRBB") or during a mercury zeroing. Then we cover getting $\mathbf{k_{Hg,v}}$ and $\mathbf{k_{Hg,h}}$ during a mercury zero and span. Finally, the most challenging thing of all, we cover obtaining $\mathbf{k_{SO_2,v}}$, $\mathbf{k_{SO_2,h}}$, and $\hat{\mathbf{V}}_\mathbf{d}$ during ZRBB.

A) Obtaining $\mathbf{V_v}$ and $\mathbf{V_h}$ when Analyzing Live Sample Gas

The quantities $\mathbf{V_v}$ and $\mathbf{V_h}$ are related to voltages put out by the demod box by the following equations

$$\mathbf{V_v = V_a\left(1 - \varepsilon\right) = V_a \bullet \left(1 - \Delta\varepsilon - \frac{1}{2}\frac{\hat{V}_d}{V_a}\right)} \qquad \text{(A-8)}$$

and

$$\mathbf{V_h = V_a\left(1 + \varepsilon\right) = V_a \bullet \left(1 + \Delta\varepsilon + \frac{1}{2}\frac{\hat{V}_d}{V_a}\right)} \qquad \text{(A-9)}$$

The quantities $\Delta\varepsilon$ and $\mathbf{V_a}$ are known in terms of the demod box outputs. The multipliers in equations A-10, A-11, A-12, and A-13 are SPECIFIC TO EACH WAVE DEMODULATOR BOX, and the ones we list below refer ONLY to the instrument used on this program.

Elemental Circuitry

V_a is related to the measured values of V_1 and $\Delta \mathbf{V_1}$ by the following equation:

$$\mathbf{V_a} = \frac{\mathbf{V_1}}{\mathbf{459}} + \Delta \mathbf{V_1} \qquad \text{(A-10)}$$

The quantity $\Delta\varepsilon$ is related to measured voltages by the following equation:

$$\Delta\varepsilon = \frac{\frac{\mathbf{1}}{\mathbf{48.5}}\left[\frac{\mathbf{1}}{\mathbf{5.5}}\mathbf{V_2} + \Delta \mathbf{V_2}\right]}{\frac{\mathbf{V_1}}{\mathbf{459}} + \Delta \mathbf{V_1}} \qquad \text{(A-11)}$$

Total Circuitry

The same considerations apply, but with different multipliers. First, V_a is given by

$$\mathbf{V_a} = \frac{\mathbf{V_1}}{\mathbf{445}} + \Delta \mathbf{V_1} \qquad \text{(A-12)}$$

Next, $\Delta\varepsilon$ is given by

$$\Delta\varepsilon = \frac{\frac{\mathbf{1}}{\mathbf{45.7}}\left[\frac{\mathbf{1}}{\mathbf{5.5}}\mathbf{V_2} + \Delta \mathbf{V_2}\right]}{\frac{\mathbf{V_1}}{\mathbf{445}} + \Delta \mathbf{V_1}} \qquad \text{(A-13)}$$

B) **Obtaining $\overline{\mathbf{V}}_\mathbf{v}$ and $\overline{\mathbf{V}}_\mathbf{h}$ during ZRBB procedure**

The quantities $\overline{\mathbf{V}}_{\mathbf{v}}$ and $\overline{\mathbf{V}}_{\mathbf{h}}$ are recorded during the ZRBB procedure when the value of the SO_2 concentration equals the expected SO_2 concentration, $\overline{\mathbf{C}}$. In the current ZRBB procedure, this concentration is the fourth one in the sequence ($0.0\overline{\mathbf{C}}$, $0.1\overline{\mathbf{C}}$, $0.5\overline{\mathbf{C}}$, $1.0\overline{\mathbf{C}}$, $1.5\overline{\mathbf{C}}$).

One obtains the values of $\overline{\mathbf{V}}_{\mathbf{v}}$ and $\overline{\mathbf{V}}_{\mathbf{h}}$ from the measured quantities just as in the above equations, namely,

$$\overline{\mathbf{V}}_{\mathbf{v}} = \overline{\mathbf{V}}_{\mathbf{a}}\left(\mathbf{1} - \varepsilon\right) = \overline{\mathbf{V}}_{\mathbf{a}} \bullet \left(\mathbf{1} - \Delta\varepsilon - \frac{\mathbf{1}}{\mathbf{2}}\frac{\hat{\mathbf{V}}_{\mathbf{d}}}{\overline{\mathbf{V}}_{\mathbf{a}}}\right) \tag{A-14}$$

and

$$\overline{\mathbf{V}}_{\mathbf{h}} = \overline{\mathbf{V}}_{\mathbf{a}}\left(\mathbf{1} + \varepsilon\right) = \overline{\mathbf{V}}_{\mathbf{a}} \bullet \left(\mathbf{1} + \Delta\varepsilon + \frac{\mathbf{1}}{\mathbf{2}}\frac{\hat{\mathbf{V}}_{\mathbf{d}}}{\overline{\mathbf{V}}_{\mathbf{a}}}\right) \tag{A-15}$$

The values of $\overline{\mathbf{V}}_{\mathbf{a}}$ and $\Delta\varepsilon$ are obtained from the output of the demod box as per equations A-10 and A-11 (elemental circuitry) and A-12 and A-13 (total circuitry), above.

C) Obtaining $\mathbf{k}_{\mathbf{Hg,v}}$ and $\mathbf{k}_{\mathbf{Hg,h}}$ from the Calibration with Mercury

Our mercury calibration consists of passing to the sample cells first a mercury-free gas with the expected SO_2 concentration and then a mercury-containing gas with the same expected SO_2 concentration. To obtain $\mathbf{k}_{\mathbf{Hg,v}}$ and $\mathbf{k}_{\mathbf{Hg,h}}$ from the mercury calibration data, we apply Beer's Law to both the horizontal and vertical light and find

$$\ell\mathbf{n}\left(\frac{\overline{\mathbf{V}}_{\mathbf{v}}}{\mathbf{V}_{\mathbf{v}}}\right) = \mathbf{L}\mathbf{k}_{\mathbf{SO_2,v}}\left(\mathbf{C}_{\mathbf{SO_2}} - \overline{\mathbf{C}}\right) + \mathbf{L}\mathbf{k}_{\mathbf{Hg,v}}\mathbf{C}_{\mathbf{Hg}} \tag{A-16}$$

and

$$\ell\mathbf{n}\left(\frac{\overline{\mathbf{V}}_{\mathbf{h}}}{\mathbf{V}_{\mathbf{h}}}\right) = \mathbf{L}\mathbf{k}_{\mathbf{SO_2,h}}\left(\mathbf{C}_{\mathbf{SO_2}} - \overline{\mathbf{C}}\right) + \mathbf{L}\mathbf{k}_{\mathbf{Hg,h}}\mathbf{C}_{\mathbf{Hg}} \tag{A-17}$$

When we send into the analyzer the mercury-free gas with the SO_2 concentration equal to $\overline{\mathbf{C}}$, we get the values of $\overline{\mathbf{V}}_{\mathbf{v}}$ and $\overline{\mathbf{V}}_{\mathbf{h}}$ for use on the left hand side of equations A-16 and A-17. Presumably, these values have not changed since they were determined in the ZRBB procedure. **However, one should use the most recent value at all times**. Now, when the mercury concentration $\mathbf{C}_{\mathbf{Hg,cal}}$ is added to the gas, along with the same SO_2 concentration, equations A-16 and A-17 yield values for $\mathbf{k}_{\mathbf{Hg,v}}$ and $\mathbf{k}_{\mathbf{Hg,h}}$ as follows:

$$\mathbf{k}_{\mathbf{Hg,v}} = \frac{\mathbf{1}}{\mathbf{LC}_{\mathbf{Hg,cal}}} \ell\mathbf{n}\left(\frac{\overline{\mathbf{V}}_{\mathbf{v}}}{\mathbf{V}_{\mathbf{v}}}\right) \tag{A-18}$$

and

$$\mathbf{k}_{\mathbf{Hg,h}} = \frac{\mathbf{1}}{\mathbf{LC}_{\mathbf{Hg,cal}}} \ell\mathbf{n}\left(\frac{\overline{\mathbf{V}}_{\mathbf{h}}}{\mathbf{V}_{\mathbf{h}}}\right) \tag{A-19}$$

Note that the term $\mathbf{C}_{\mathbf{SO_2}} - \overline{\mathbf{C}}$ has dropped out because the mercury span gas contains the expected concentration of SO_2.

D) Obtaining $\mathbf{k}_{\mathbf{SO_2,v}}$, $\mathbf{k}_{\mathbf{SO_2,h}}$, and $\hat{\mathbf{V}}_{\mathbf{d}}$ from the Calibration with Sulfur Dioxide (ZRBB Procedure)

In the ZRBB procedure, essentially a calibration with SO_2, there is no mercury present. Equations A-16 and A-17 apply with $C_{Hg} = 0$, and we have

$$\ell\mathbf{n}\left(\frac{\overline{\mathbf{V}}_{\mathbf{v}}}{\mathbf{V}_{\mathbf{v}}}\right) = \mathbf{Lk}_{\mathbf{SO_2,v}}\left(\mathbf{C}_{\mathbf{SO_2}} - \overline{\mathbf{C}}\right) \tag{A-20}$$

and

$$\ell\mathbf{n}\left(\frac{\overline{\mathbf{V}}_{\mathbf{h}}}{\mathbf{V}_{\mathbf{h}}}\right) = \mathbf{Lk}_{\mathbf{SO_2,h}}\left(\mathbf{C}_{\mathbf{SO_2}} - \overline{\mathbf{C}}\right) \tag{A-21}$$

These equations can be rearranged to be explicit for $\mathbf{C_{SO_2}}$ as follows:

$$\frac{\mathbf{C_{SO_2}}}{\overline{\mathbf{C}}} = \mathbf{1} + \frac{\mathbf{1}}{\mathbf{Lk_{SO_2,v}}\overline{\mathbf{C}}}\,\ell\mathbf{n}\left(\frac{\overline{\mathbf{V}}_\mathbf{v}}{\mathbf{V_v}}\right) \tag{A-22}$$

and

$$\frac{\mathbf{C_{SO_2}}}{\overline{\mathbf{C}}} = \mathbf{1} + \frac{\mathbf{1}}{\mathbf{Lk_{SO_2,h}}\overline{\mathbf{C}}}\,\ell\mathbf{n}\left(\frac{\overline{\mathbf{V}}_\mathbf{h}}{\mathbf{V_h}}\right) \tag{A-23}$$

When doing the ZRBB procedure, $\mathbf{C_{SO_2}}$ takes on the values $0\overline{\mathbf{C}}$, $0.1\overline{\mathbf{C}}$, $0.5\overline{\mathbf{C}}$, $1.0\overline{\mathbf{C}}$, and $1.5\overline{\mathbf{C}}$. Therefore, equations A-22 and A-23 each represent four independent equations that we can use to calculate the unknown constants $\mathbf{k_{SO_2,v}}$, $\mathbf{k_{SO_2,h}}$, and $\hat{\mathbf{V}}_\mathbf{d}$. The constant $\hat{\mathbf{V}}_\mathbf{d}$ is imbedded in $\mathbf{V_v}$ and $\mathbf{V_h}$ and does not appear explicitly in equations A-22 and A-23.

For example, the method of least squares is a traditional method of doing the curve fitting. In this method, one tries to minimize the sum of the following two summations, denoted by $\mathbf{\Omega_1}$ and $\mathbf{\Omega_2}$:

$$\Omega_1^2 = \sum_{\mathbf{i=1}}^{\mathbf{k}}\left(\frac{\mathbf{C_{SO_2,i}}}{\overline{\mathbf{C}}} - \mathbf{1} - \frac{\mathbf{1}}{\mathbf{Lk_{SO_2,v}}\overline{\mathbf{C}}}\,\ell\mathbf{n}\left(\frac{\overline{\mathbf{V}}_\mathbf{v}}{\mathbf{V_{v,i}}}\right)\right)^2 \tag{A-24}$$

and

$$\Omega_2^2 = \sum_{\mathbf{i=1}}^{\mathbf{k}}\left(\frac{\mathbf{C_{SO_2,i}}}{\overline{\mathbf{C}}} - \mathbf{1} - \frac{\mathbf{1}}{\mathbf{Lk_{SO_2,h}}\overline{\mathbf{C}}}\,\ell\mathbf{n}\left(\frac{\overline{\mathbf{V}}_\mathbf{h}}{\mathbf{V_{h,i}}}\right)\right)^2 \tag{A-25}$$

The summations i = 1 to k in equations A-24 and A-25 include all of the values of the SO_2 concentration in the ZRBB procedure **OTHER THAN 1.0$\overline{\mathbf{C}}$.** The method of least squares says that the best values of $\mathbf{k}_{SO_2,v}$, $\mathbf{k}_{SO_2,h}$, and $\hat{\mathbf{V}}_d$ are found by adding Ω_1^2 and Ω_2^2 together and setting equal to zero the partial derivatives of this sum with respect to $\mathbf{k}_{SO_2,v}$, $\mathbf{k}_{SO_2,h}$, and $\hat{\mathbf{V}}_d$. That is,

$$\frac{\partial\left(\Omega_1^2 + \Omega_2^2\right)}{\partial \hat{\mathbf{V}}_d} = 0 \qquad \text{(A-26)}$$

$$\frac{\partial\left(\Omega_1^2 + \Omega_2^2\right)}{\partial \mathbf{k}_{SO_2,v}} = 0 \qquad \text{(A-27)}$$

and

$$\frac{\partial\left(\Omega_1^2 + \Omega_2^2\right)}{\partial \mathbf{k}_{SO_2,h}} = 0 \qquad \text{(A-28)}$$

Equations A-26, A-27, and A-28 represent three equations for the three unknowns $\hat{\mathbf{V}}_d$, $\mathbf{k}_{SO_2,v}$, and $\mathbf{k}_{SO_2,h}$.

Sparing the algebra, this procedure leads to the following equations:

$$\frac{\sum_{i=1}^{k} \mathbf{D}_{1,i}\left[\frac{\overline{\mathbf{V}}_v}{\mathbf{V}_{v,i}} - 1\right]}{\sum_{i=1}^{k}\left(\frac{\mathbf{k}_{SO_2,v}}{\mathbf{k}_{SO_2,h}}\right)\mathbf{D}_{2,i}\left[\frac{\overline{\mathbf{V}}_v}{\overline{\mathbf{V}}_h}\right]\left[\frac{\overline{\mathbf{V}}_h}{\mathbf{V}_{h,i}} - 1\right]} - 1 = 0 \qquad \text{(A-29)}$$

$$\mathbf{Lk_{SO_2,v}\overline{C}} = \frac{\sum_{i=1}^{k}\left[\ell n\left(\frac{\overline{V}_v}{V_{v,i}}\right)\right]^2}{\sum_{i=1}^{k}\left(\frac{C_{SO_2,i}}{\overline{C}} - 1\right)\ell n\left(\frac{\overline{V}_v}{V_{v,i}}\right)} \qquad \text{(A-30)}$$

and

$$\mathbf{Lk_{SO_2,h}\overline{C}} = \frac{\sum_{i=1}^{k}\left[\ell n\left(\frac{\overline{V}_h}{V_{h,i}}\right)\right]^2}{\sum_{i=1}^{k}\left(\frac{C_{SO_2,i}}{\overline{C}} - 1\right)\ell n\left(\frac{\overline{V}_h}{V_{h,i}}\right)} \qquad \text{(A-31)}$$

If we had an independent measure of the reference detector, the parameter $\hat{\mathbf{V}}_\mathbf{d}$ would be determined experimentally, and equations A-26 and A-29 would not apply. However, equations A-27, A-28, A-30, and A-31 would still apply and would be the proper way to determine the best values of $\mathbf{k_{SO_2,v}}$, and $\mathbf{k_{SO_2,h}}$ from SO_2 calibration data.

We have defined the terms $D_{1,i}$ and $D_{2,i}$ in equation A-29 for shorthand purposes as follows:

$$\mathbf{D_{1,i}} = \frac{C_{SO_2,i}}{\overline{C}} - 1 - \frac{1}{Lk_{SO_2,v}\overline{C}}\,\ell n\left(\frac{\overline{V}_v}{V_{v,i}}\right) \qquad \text{(A-32)}$$

and

$$\mathbf{D_{2,i}} = \frac{C_{SO_2,i}}{\overline{C}} - 1 - \frac{1}{Lk_{SO_2,h}\overline{C}}\,\ell n\left(\frac{\overline{V}_h}{V_{h,i}}\right) \qquad \text{(A-33)}$$

Now, how do we solve equations A-29, A-30, and A-31?

Recall that the values of $\overline{\mathbf{V}}_{\mathbf{v}}$, $\mathbf{V}_{\mathbf{v,i}}$, $\overline{\mathbf{V}}_{\mathbf{h}}$, and $\mathbf{V}_{\mathbf{h,i}}$ are related to the experimentally determined quantities $\Delta\varepsilon$, $\Delta\varepsilon_{\mathbf{i}}$, $\overline{\mathbf{V}}_{\mathbf{a}}$, and $\mathbf{V}_{\mathbf{a,i}}$ and to the quantity $\hat{\mathbf{V}}_{\mathbf{d}}$ by the following equations (see equations A-14 and A-15 above):

$$\overline{\mathbf{V}}_{\mathbf{h}} = \overline{\mathbf{V}}_{\mathbf{a}} \bullet \left(\mathbf{1} + \Delta\varepsilon + \frac{\mathbf{1}}{\mathbf{2}} \frac{\hat{\mathbf{V}}_{\mathbf{d}}}{\overline{\mathbf{V}}_{\mathbf{a}}} \right) \tag{A-34}$$

$$\overline{\mathbf{V}}_{\mathbf{h,i}} = \mathbf{V}_{\mathbf{a,i}} \bullet \left(\mathbf{1} + \Delta\varepsilon_{\mathbf{i}} + \frac{\mathbf{1}}{\mathbf{2}} \frac{\hat{\mathbf{V}}_{\mathbf{d}}}{\overline{\mathbf{V}}_{\mathbf{a}}} \frac{\overline{\mathbf{V}}_{\mathbf{a}}}{\mathbf{V}_{\mathbf{a,i}}} \right) \tag{A-35}$$

$$\overline{\mathbf{V}}_{\mathbf{v}} = \overline{\mathbf{V}}_{\mathbf{a}} \bullet \left(\mathbf{1} - \Delta\varepsilon - \frac{\mathbf{1}}{\mathbf{2}} \frac{\hat{\mathbf{V}}_{\mathbf{d}}}{\overline{\mathbf{V}}_{\mathbf{a}}} \right) \tag{A-36}$$

and

$$\overline{\mathbf{V}}_{\mathbf{v,i}} = \mathbf{V}_{\mathbf{a,i}} \bullet \left(\mathbf{1} - \Delta\varepsilon_{\mathbf{i}} - \frac{\mathbf{1}}{\mathbf{2}} \frac{\hat{\mathbf{V}}_{\mathbf{d}}}{\overline{\mathbf{V}}_{\mathbf{a}}} \frac{\overline{\mathbf{V}}_{\mathbf{a}}}{\mathbf{V}_{\mathbf{a,i}}} \right) \tag{A-37}$$

Now, we numerically solve for the quantity $\frac{\hat{\mathbf{V}}_{\mathbf{d}}}{\overline{\mathbf{V}}_{\mathbf{a}}}$, which is necessarily in the range -1 to +1.

We take an initial guess for $\frac{\hat{\mathbf{V}}_{\mathbf{d}}}{\overline{\mathbf{V}}_{\mathbf{a}}}$ and compute $\overline{\mathbf{V}}_{\mathbf{h}}$, $\mathbf{V}_{\mathbf{h,i}}$, $\overline{\mathbf{V}}_{\mathbf{v}}$, $\mathbf{V}_{\mathbf{v,i}}$, $\mathbf{k}_{\mathbf{SO_2,v}}$, $\mathbf{k}_{\mathbf{SO_2,h}}$, $D_{1,i}$, and $D_{2,i}$

from equations A-34, A-35, A-36, A-37, A-30, A-31, A-32, and A-33. We then use these values of the parameters to see if equation A-29 is satisfied to some arbitrary level of accuracy (such as the absolute value of left hand side of equation A-29 less than 10^{-5}). Because $\frac{\hat{V}_d}{\bar{V}_a}$ must lie between -1 and +1, the method of bisection will suffice to converge on the solution.

The best initial guess for $\frac{\hat{V}_d}{\bar{V}_a}$ can be had by the following approximation

$$\frac{\hat{V}_d}{\bar{V}_a} = \frac{1}{k}\sum_{i=1}^{k}\frac{2\left(\Delta\bar{\varepsilon} - \Delta\varepsilon_i\right)}{\left(1 - \frac{\bar{V}_a}{V_{a,i}}\right)} \qquad \text{(A-38)}$$

We have implemented the algebra given above into the data reduction routine in the ADA mercury analyzer.

Several interesting results were found during the six months of field testing. First, the molar absorptivity of mercury for the "vertically-polarized" light was essentially equal in the total cell and the elemental cell. For the elemental cell, the molar absorptivity of mercury for vertical light averaged $(277 \pm 51.3)\text{x}10^5$ L/mole/cm, and for the total cell, the molar absorptivity of mercury for vertical light averaged $(260 \pm 77)\text{x}10^5$ L/mole/cm over the five months of operation at Consol. This result is a good indication of the proper functioning of the instrument and of the

validity of the theory behind the data reduction method. The molar absorptivity of mercury for the horizontal light in the total and elemental cells actually calculated to be a negative number in most of the runs, a physical impossibility, but a result that indicated to us that the absorption of horizontal light by mercury was so small as to be negligible. This result is consistent with the theory and design of the instrument in that the molar absorptivity of mercury for the horizontal light is identically equal to zero in a perfect instrument.

Second, the molar absorptivity of SO_2 for the horizontally polarized light was about three times that for the vertically polarized light. For the elemental cell, the molar absorptivity of SO_2 averaged 167 ± 27 L/mole/cm for the horizontal light and 56.9 ± 5.5 L/mole/cm for the vertical light. For the total cell, the molar absorptivity of SO_2 averaged 233 ± 37 L/mole/cm for the horizontal light and 78.9 ± 16.5 L/mole/cm for the vertical light. This difference in the molar absorptivities of SO_2 for the two different polarizations of light is an important consideration in the data reduction and is properly accounted for in the method described above.

Appendix B: Permeation Tubes and Diffusion Vials As Calibration Sources

Elemental Mercury Permeation Tubes

We maintained several permeation tubes for making known concentrations of elemental mercury vapor. The permeation tubes were held in ovens at a constant temperature. With several calibrated permeation tubes, we could, if necessary, make a range of mercury concentrations without having to change the temperature of and re-calibrate any permeation tube.

The permeation tubes were weighed once per month. The mass loss rate was very constant for most tubes in that the standard deviation of the loss rate was less than 10% of the average value. Figure B-1 depicts a typical good permeation tube that emitted 72.2 ± 1.0 ng/min of mercury for fifteen months.

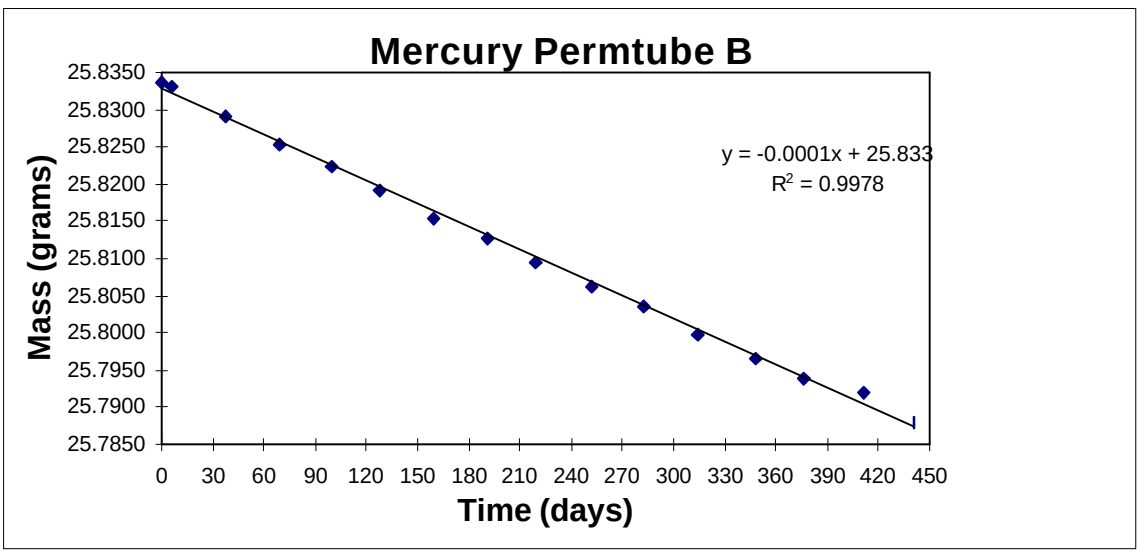

Figure B-1
Loss of Elemental Mercury from a Typical Permeation Tube

The surprising outcome of these tests was that the measured mass loss rates bore little resemblance to the mass loss rate estimated in the manufacturer's product literature (Table B-1). The manufacturer recommends that each permeation tube be weighed, but we were surprised to find how far off of the expected values the real mass loss rates were.

Table B-1 – Mass Loss Rates of Permeation Tubes Containing Elemental Mercury (Temperature 117°C)

Permeation Tube Identifier	Mercury Loss Rate (ng/min)	Manufacturer's Estimate (ng/min)
Hg-B	72.2 ± 1.0	20
Hg-C	49.4 ± 1.1	10
Hg-D	1878 ± 37.3	not available
Hg-E	1050 ± 18.1	not available
Hg-F	519± 24.0	355
Hg-G	3352 ± 26.2	not available
Hg-H	262 ± 7.1	100
Hg-I	437 ± 7.9	200
Hg-J	476 ± 14.9	400
Hg-K	36.8 ± 1.9	5
Hg-L	46.4 ± 1.8	10
Hg-M	132 ± 4.7	50

In trying to make concentrations of mercury in the range of 10 µg/m^3 while keeping the gas flow rates in the range of several liters per minute, it is desirable to have permeation tubes that emit mercury in the range of 30 to 50 ng/min. VICI Metronics was able to supply us with tubes that emitted in this range, but only after we asked for very low permeation rates (5 to 10 ng/min). In addition, we found that empty permeation tubes lost mass at a rate of about 5 to 9 ng/min. We did not correct our mass loss rates for the loss rate of the blank tubes because the correction was less than 10% for most of our tubes and because we believed that the overall accuracy of the data was not significantly influenced by this uncertainty. However, we also decided not to use permeation tubes that emit less than 50 ng/min so that the blank tube loss rate would not be a significant portion of the overall mass loss rate.

Mercuric Chloride Diffusion Vials

We made our own permeation devices for making up known concentrations of mercuric chloride vapors because none was available commercially. The mass loss rate of these diffusion vials was less constant than that of the elemental mercury permeation tubes, but in general the standard deviation of the loss rate was less than 10% of the average loss rate (Table B-2).

The diffusion vials themselves are "autosampler vials" sold by Cole-Parmer (Chicago, IL; product number E-98800-90). These vials come with a silicone rubber septum in a "crimp cap." One to four holes are made in the septum by penetrating the septum with a syringe needle (outside diameter 380 microns). These holes provide the means for the mercuric chloride vapor to escape from the diffusion vial. Approximately two grams of mercuric chloride (Puratronic Grade, 99.9995% purity, Alfa Aesar product #10808, Ward Hill, MA) is placed in the vial, and the cap is crimped into place.

Table B-2 – Mass Loss Rates of Mercuric Chloride Diffusion Vials

Diffusion Vial Identifier	Mass Loss Rate (ng/min)	Mercury Emission Rate (ng/min)
$HgCl_2$-6	109 ± 8.2	80.8
$HgCl_2$-7	154 ± 18.4	114
$HgCl_2$-8	157 ± 4.7	116
$HgCl_2$-9	369 ± 42.4	273
$HgCl_2$-10	241 ± 21.0	178
$HgCl_2$-11	91.5 ± 7.3	67.6
$HgCl_2$-12	145 ± 3.7	107
$HgCl_2$-13	184 ± 4.3	136

Figure B-2 shows a typical performance of a mercuric chloride diffusion vial wherein a slower rate of mass loss sets in after 200 days of testing. This diffusion vial was tested for over 600 days.

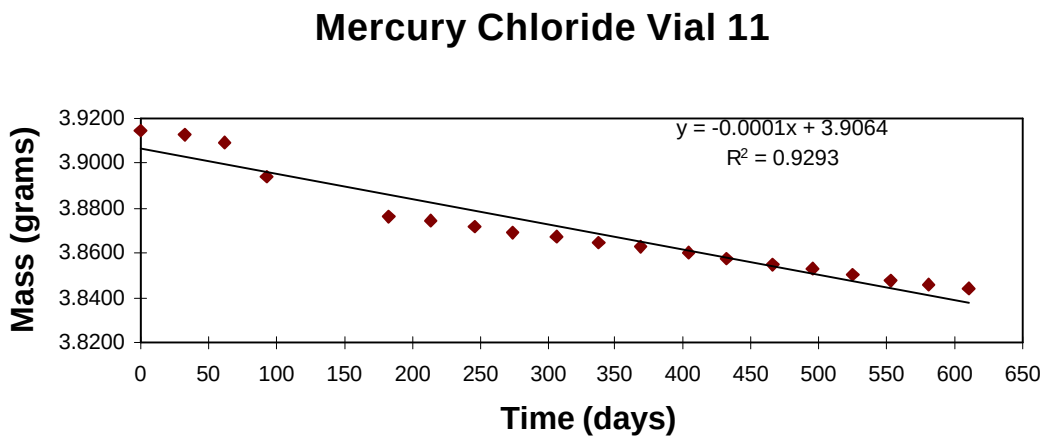

Figure B-2 – Loss of Mercuric Chloride from a Diffusion Vial

Mercuric Oxide Diffusion Vials

We made our own permeation devices for making up known concentrations of mercuric oxide vapors although we ended up not testing with HgO. The mass loss rate of these diffusion vials was less constant than that of the elemental mercury permeation tubes and of the mercuric chloride diffusion vials (Table B-3). These data were obtained for 140 days of permeation at 117°C. The mercuric oxide used in these diffusion vials was obtained from Alfa Aesar, Ward Hill, MA (Puratronic Grade, 99.998% purity, product #10810).

Table B-3 – Mass Loss Rate of Mercuric Oxide Diffusion Vials

Diffusion Vial Identifier	Mass Loss Rate (ng/min)	Mercury Emission Rate (ng/min)
HgO-4	139.8 ± 51.1	129
HgO-5	48.8 ± 5.3	45.2
HgO-6	45.2 ± 5.1	41.9

Figure B-3 shows a typical performance of a mercuric oxide diffusion vial. We were not 100% satisfied with how well these vials performed, but they are much improved over our first efforts.

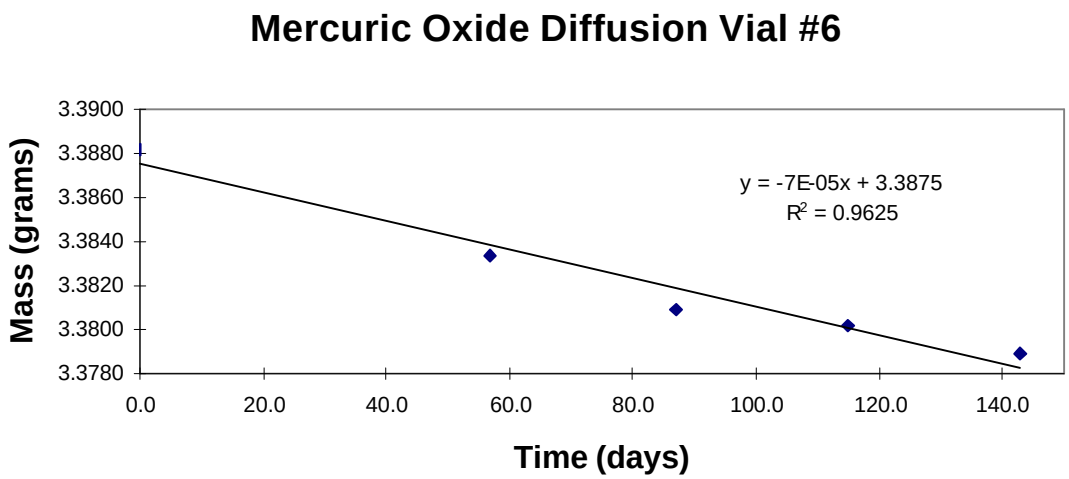

Figure B-3 – Mass loss from a mercuric oxide diffusion vial

Appendix C: Investigation of Flow Distribution and Heating Efficiency during Regeneration

In April and May, 1997, we examined in some detail the distribution of flow in the sorbent beds and whether the regeneration cycle was working as designed. We thought that perhaps one or both of these issues would explain some of the wet chemistry results obtained by Consol and/or the iodated carbon trap results that we obtained during the same time period (March, 1997). In summary, the flow distribution was not a problem, and the heating efficiency may or may not have been a problem. We believe, however, to be routinely effective in regeneration, the heat transfer problems found are a top priority to resolve in the Phase II work. Details of these flow and heat transfer investigations are described below.

Investigation of Flow Distribution (April, 1997)

We wanted to determine if the flue gas flowing through the sorbent modules was evenly distributed through the 17 tubes. To this end we removed the top cone of Unit 1 and measured the velocity of gas exiting each tube when 32 ACFM of air was flowing through the unit at room temperature. We found that the flow rate through each tube varied from 3.8% of the flow to 9.1% of the flow (Figure C-1). This range of flow variation means that at the design flow rate of 20 ACFM, the residence time in the 17 tubes varies from 0.9 seconds in the tube carrying the most flow to 2.3 seconds in the tube carrying the least flow. Our laboratory tests were done with a residence time of one second with the monolithic form of the sorbent, and tests with the particulate form of the sorbent showed 100% mercury uptake with any residence time longer than 0.1 seconds. Hence we believed that flow distribution during sorption was not causing us any problems.

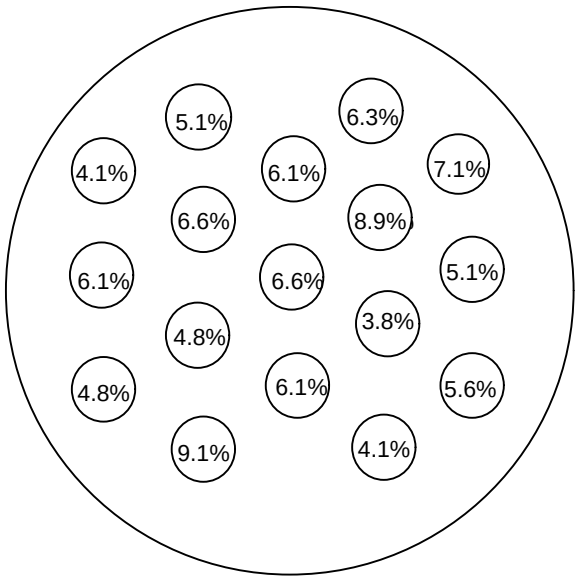

Figure C-1 – Portion of Total Flow Passing Through Each of 17 tubes in Module 1

Investigation of Regeneration Conditions (Early May, 1997)

Each sorbent vessel was instrumented with nine thermocouples placed on the outside of the tube walls on the shell side of the vessel to monitor the kinetics of the heating and cooling of the unit and to look for vertical and radial temperature variations. Before the skid left ADA in January, 1997, we tested the regeneration kinetics and found that the tube wall temperatures reached 650°F within two hours of the start of a regeneration. This temperature was thought to be sufficient since desorption in the laboratory is complete at about 600°F.

At Consol, we decide to look again at the regeneration kinetics since the wet chemistry and the iodated carbon trap data collected in March had a variety of curious features, including outlet concentrations as much as 10 times higher than the inlet concentrations (see Appendix E). We found that the regeneration kinetics were the same as they had been before. However, we also decided to monitor the inlet and outlet temperature of the regeneration gas itself, which flows at about three liters per minute during a regeneration. We found that both the inlet and outlet regeneration gas temperatures were reaching only about 500°F two hours into the desorption cycle (Figure C-2). This temperature is borderline for achieving good desorption, and we prefer to get to at least 600°F for complete desorption.

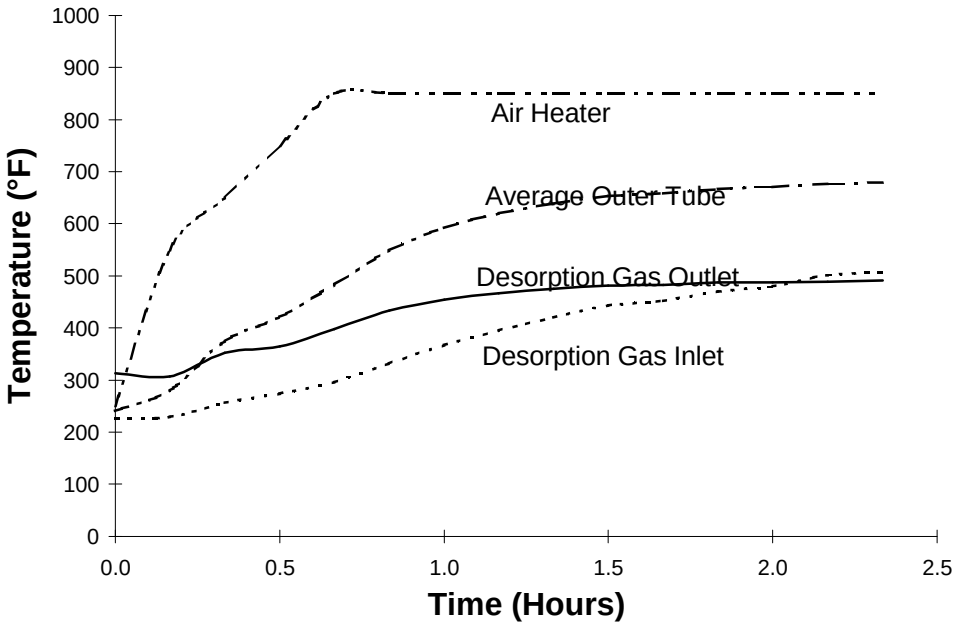

Figure C-2 – Temperature Profiles During Regeneration, Original Configuration

We had performed heat transfer rate studies on a 2" I.D. packed bed of the particulate form of the sorbent before designing the sorbent vessels and found that when the outer wall of the tube holding the sorbent was heated to 700°F, the center of the packed bed took only 15 minutes to reach 650°F. Since packed beds are notoriously poor at heat transfer because of the point contact between the individual particles. We reasoned that the metallic monoliths would not be worse at heat transfer.

We came to the conclusion that the poor heat transfer was because the monoliths were not actually touching the inside walls of the tubes of the sorbent vessel. To insert and hold the monoliths in the tubes, we had wrapped a layer of glass tape at the top edge. Consequently for most of the length of the monoliths there was an air gap, approximately 1/16th of an inch thick, between the monolith wall and the inner wall of the tubes. This air gap has a heat transfer resistance approximately 200 times that of the tube walls themselves. In the proposed Phase II work, we intend to fill this air gap with a thermally conductive paste, such as the PyroPutty product line offered by Aremco Products, Inc. (Ossinning, NY). One of these products has essentially the thermal conductivity of steel. Given that the temperature difference between the tube wall and the regeneration gas was about 150°F, eliminating the air gap with a high thermal conductivity paste will reduce the temperature difference between the monolith and the tube wall to about 1°F.

In Phase I, our only practical alternative to heating the beds more efficiently was to add an auxiliary heater and to route the hot gas exiting the shell side of the vessel through this auxiliary heater and then back through the monoliths themselves on the tube side of the vessel (Figure C-

3). In this configuration the regeneration gas temperature essentially tracked the temperature of the tube walls (Figure C-4), easily reaching 700°F. We had no further questions about the regeneration efficiency of the unit after this modification. The negative consequence of this configuration was that the flow rate of regeneration gas was so high (40 ACFM) that it was not representative of routine full-scale operation. However, we got our best data in June after this modification, so it seemed to be worthwhile.

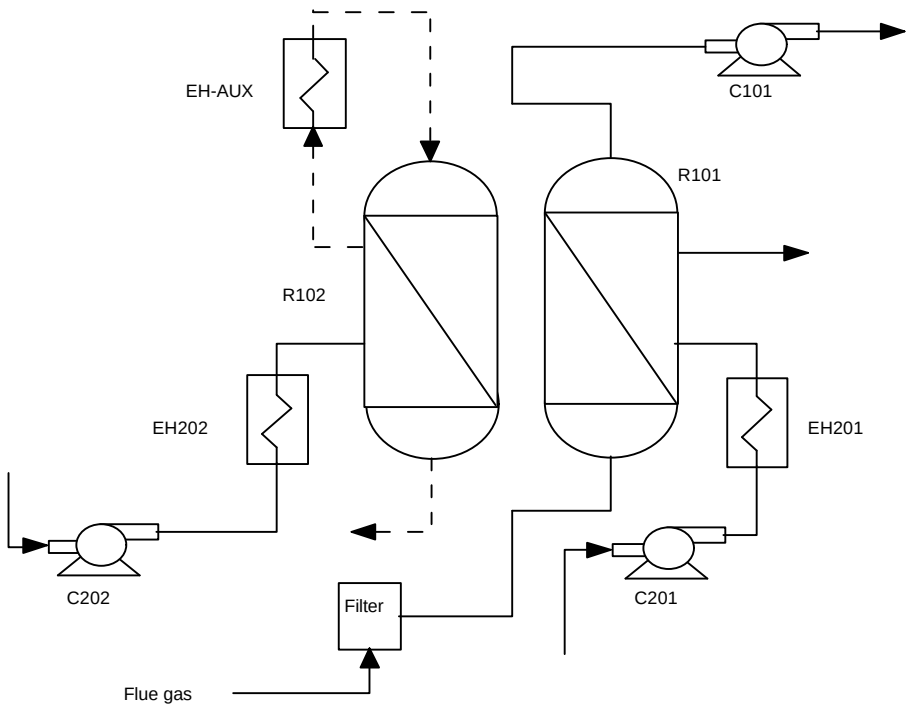

Figure C-3 – Addition of Auxiliary Heater to Skid

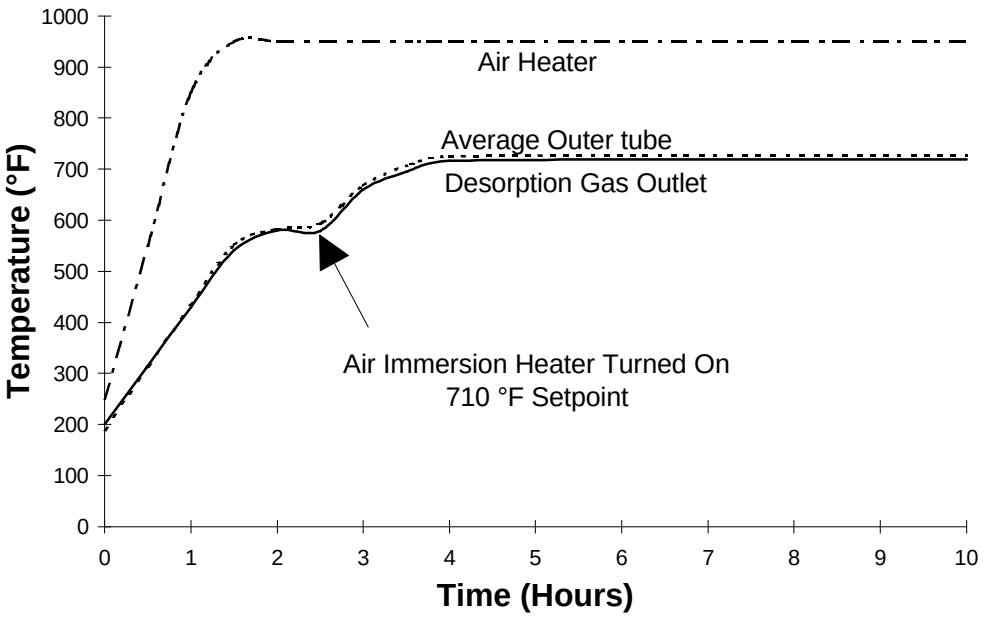

Figure C-4 – Temperature Profiles During Regeneration with Auxiliary Heater

Appendix D: Example Data Records from Continuous Mercury Analyzer

Appendix D

The following appendix contains the raw data collected with ADA's continuous mercury emissions monitor during combustion of specified coals.

A) High Sulfur, Illinois #6 Coal

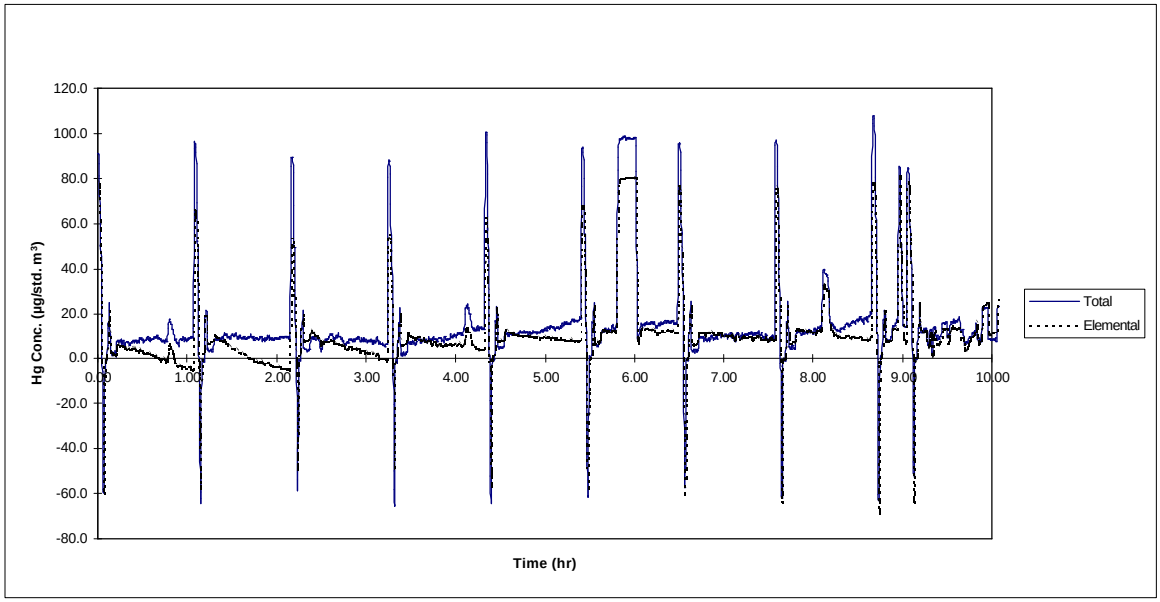

Figure D-1 – High Sulfur Illinois #6 Coal, 1/31/97 A.M.

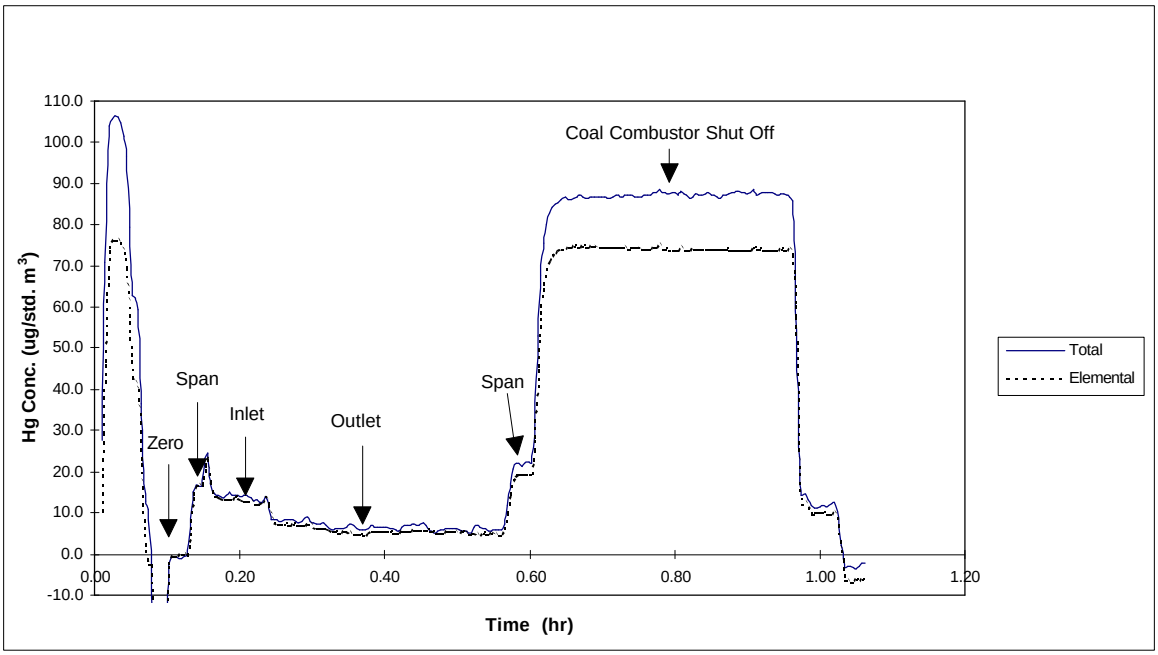

Figure D-2 – High Sulfur Illinois #6 Coal, 1/31/97 P.M.

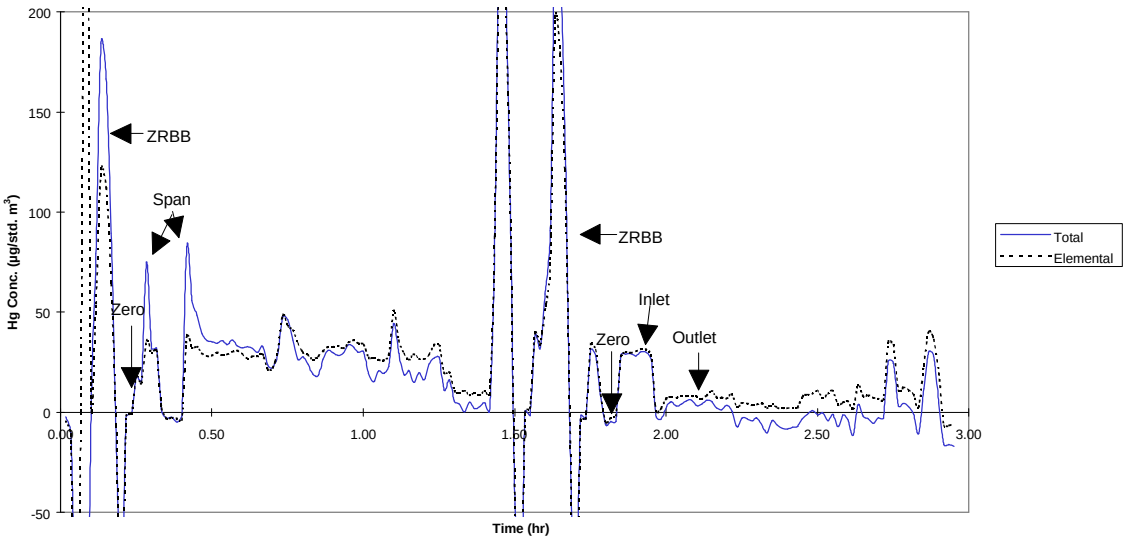

Figure D-3 – High Sulfur Illinois #6 Coal, 5/8/97

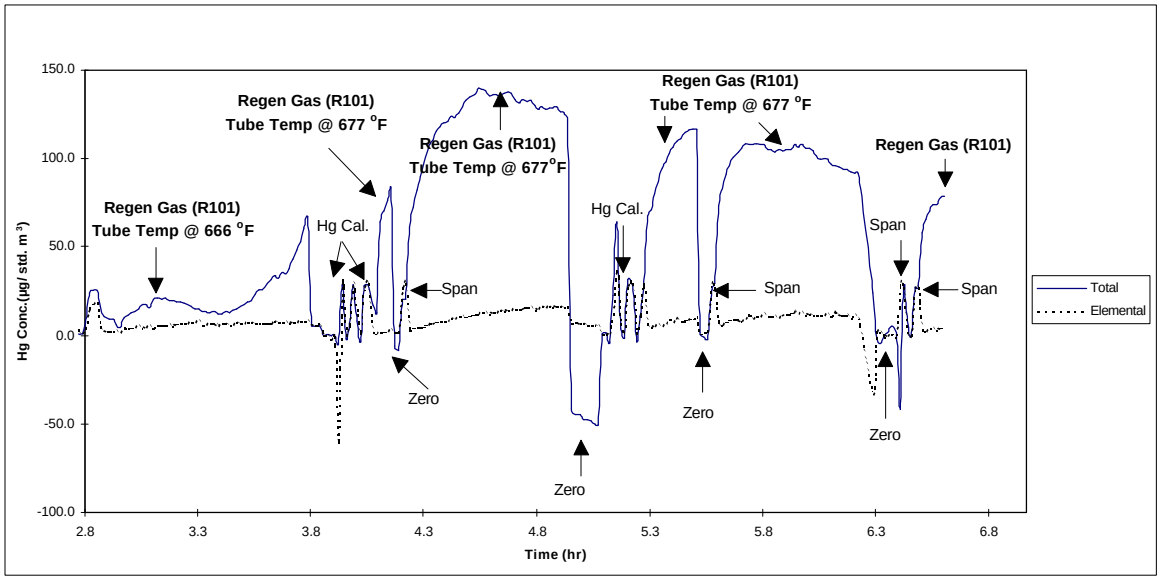

Figure D-4 – Regeneration of Unit 1, 5/7/97

B) High Sulfur, Pittsburgh Seam

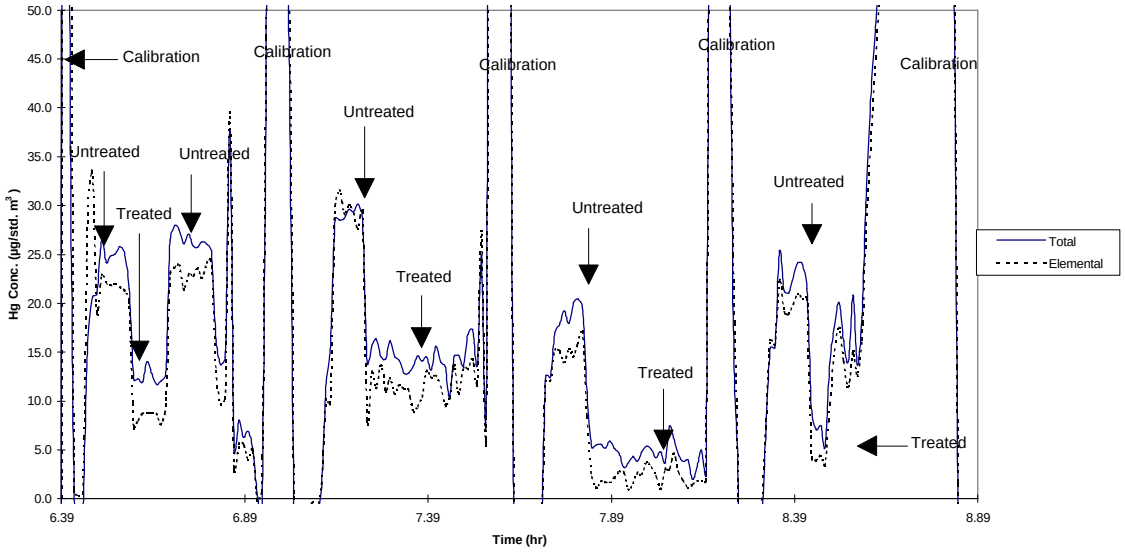

Figure D-5 – High Sulfur Pittsburgh Coal, 3/6/97

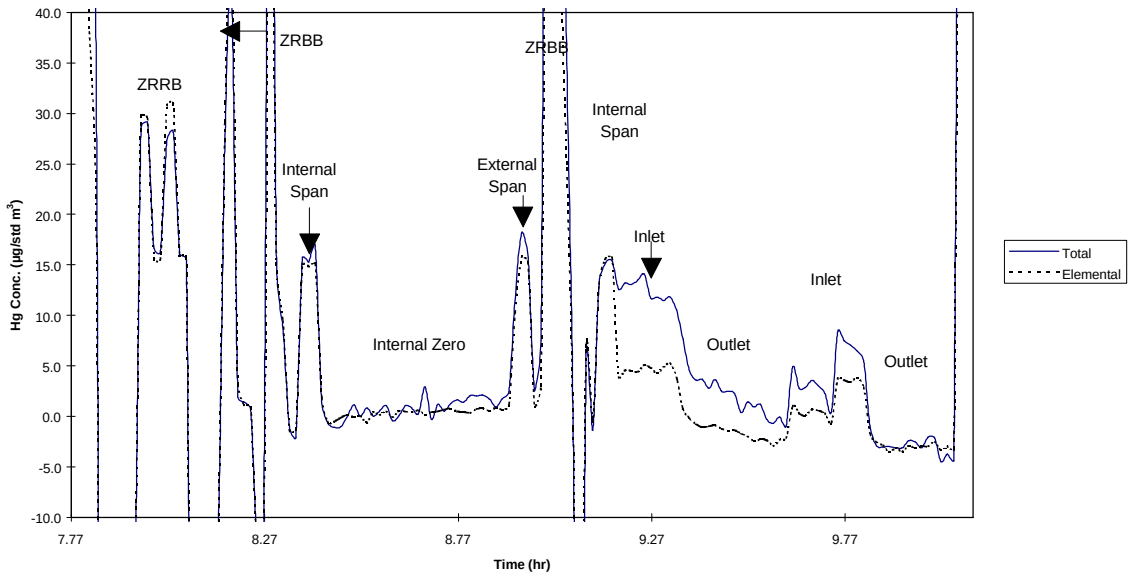

Figure D-6 – High Sulfur Pittsburgh Coal, 3/11/97

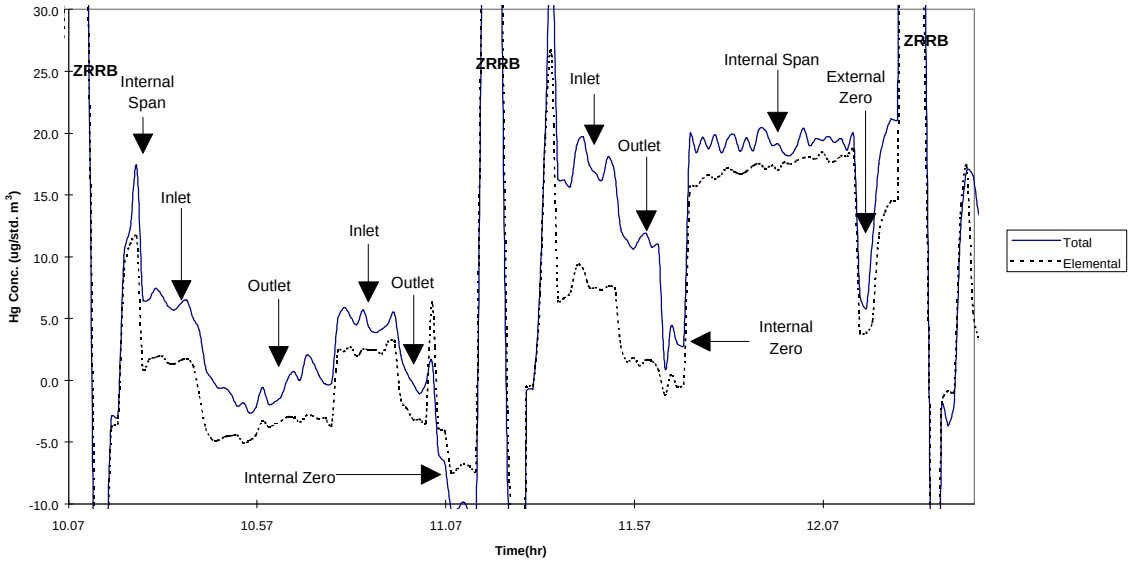

Figure D-7 – High Sulfur Pittsburgh Coal, 3/11/97

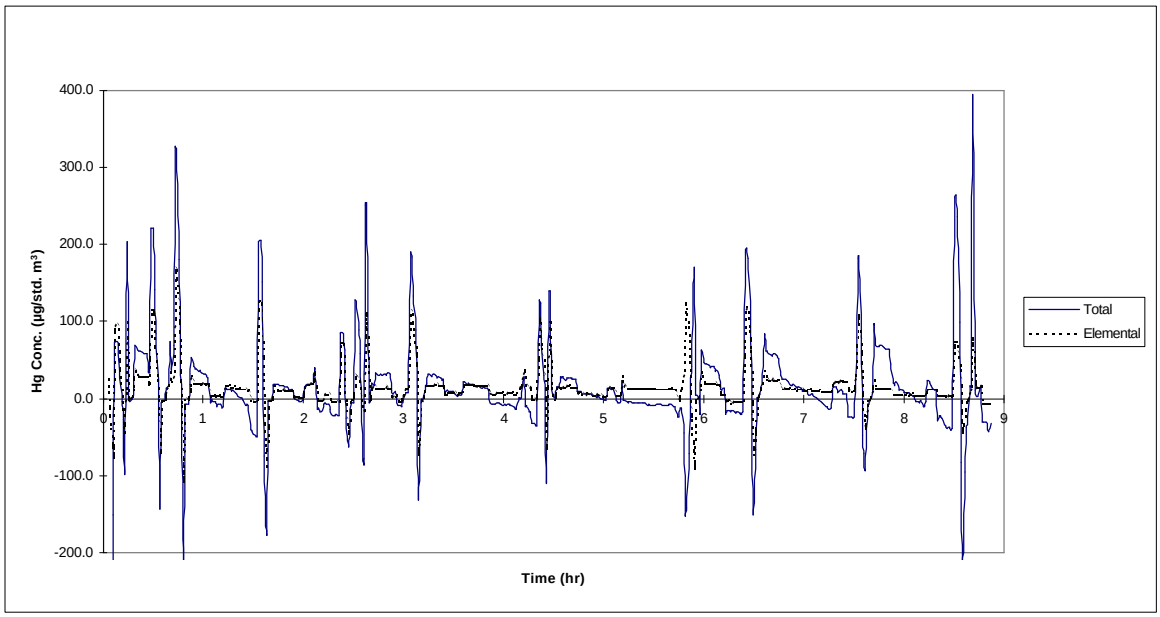

Figure D-8 – High Sulfur Pittsburgh Coal, 3/12/97

C) Low Sulfur, Pittsburgh Seam

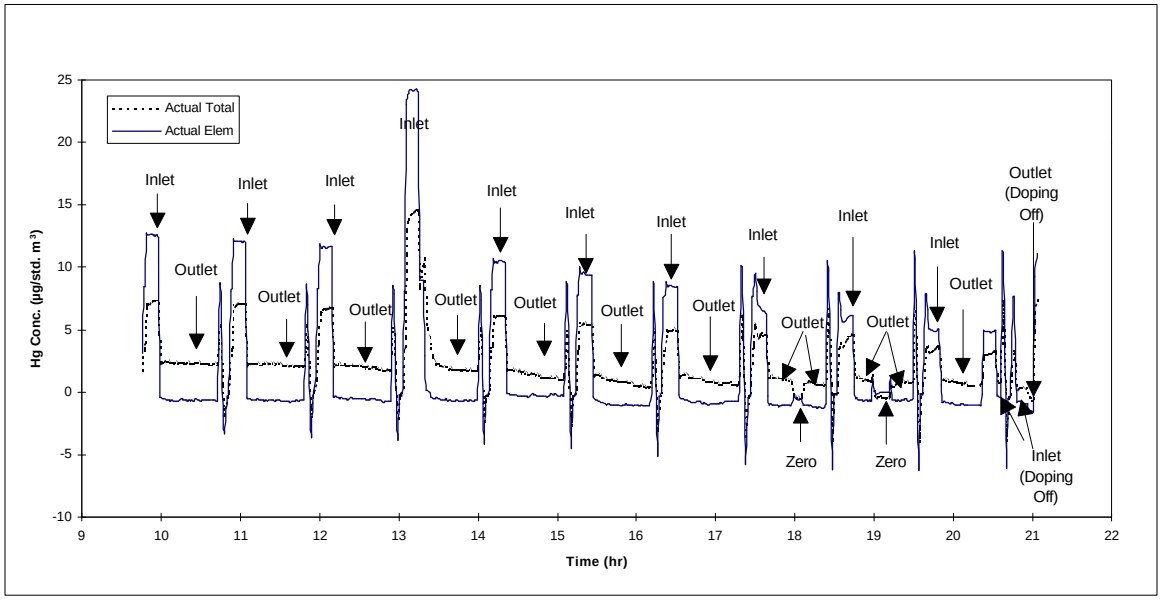

Figure D-9 – Low Sulfur Pittsburgh Coal, 6/6/97

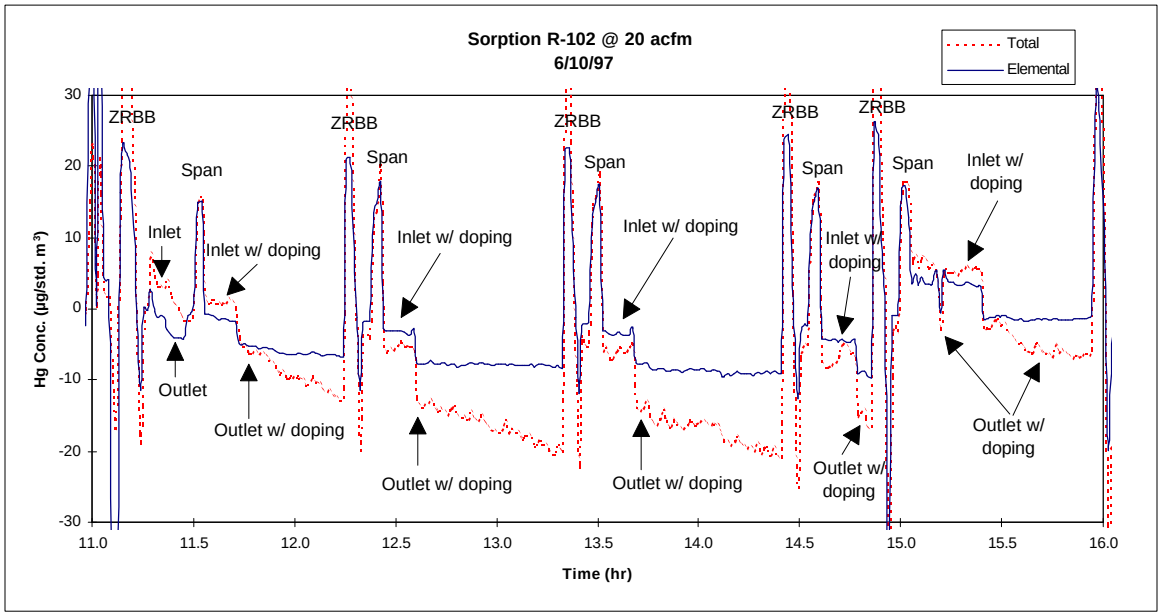

Figure D-10 – Low Sulfur Pittsburgh Coal, 6/10/97

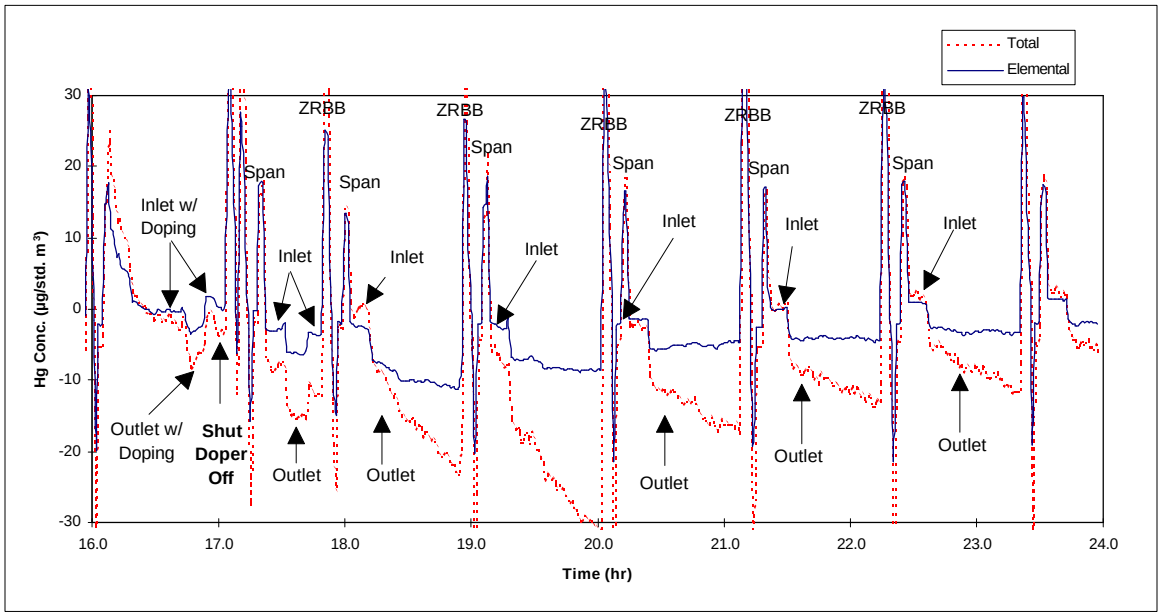

Figure D-11 – Low Sulfur Pittsburgh Coal, 6/10/97

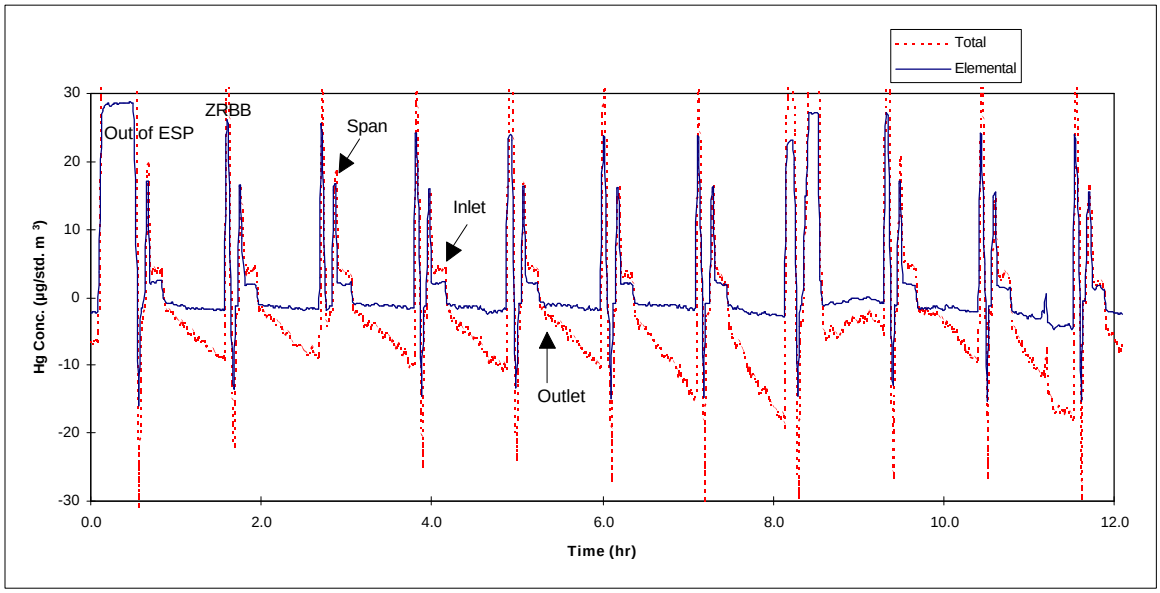

Figure D-12 – Low Sulfur Pittsburgh Coal, 6/11/97

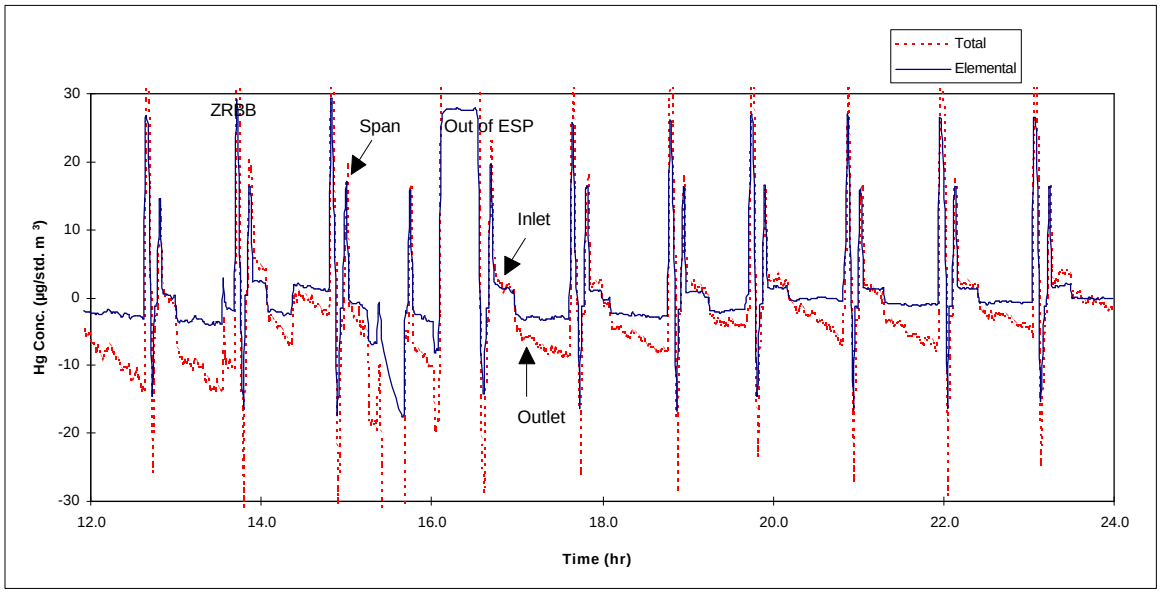

Figure D-13 – Low Sulfur Pittsburgh Coal, 6/11/97

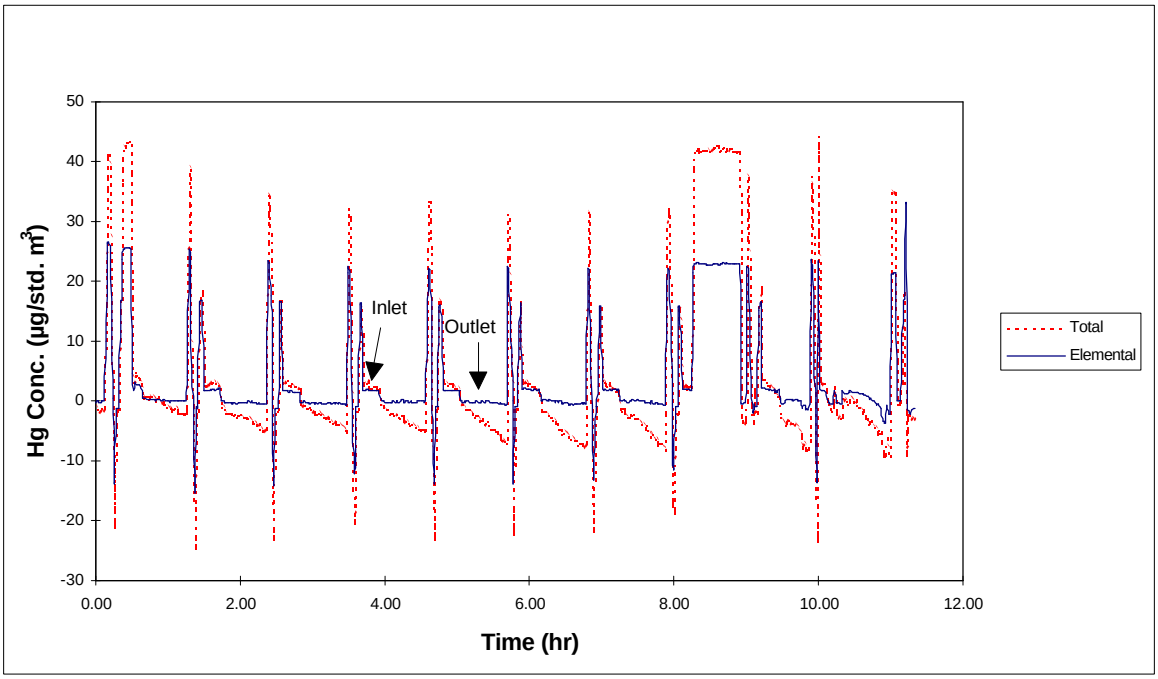

Figure D-14 – Low Sulfur Pittsburgh Coal, 6/12/97

The regeneration shown in the figure below illustrates thermal regeneration with air at 700 ^{o}F.

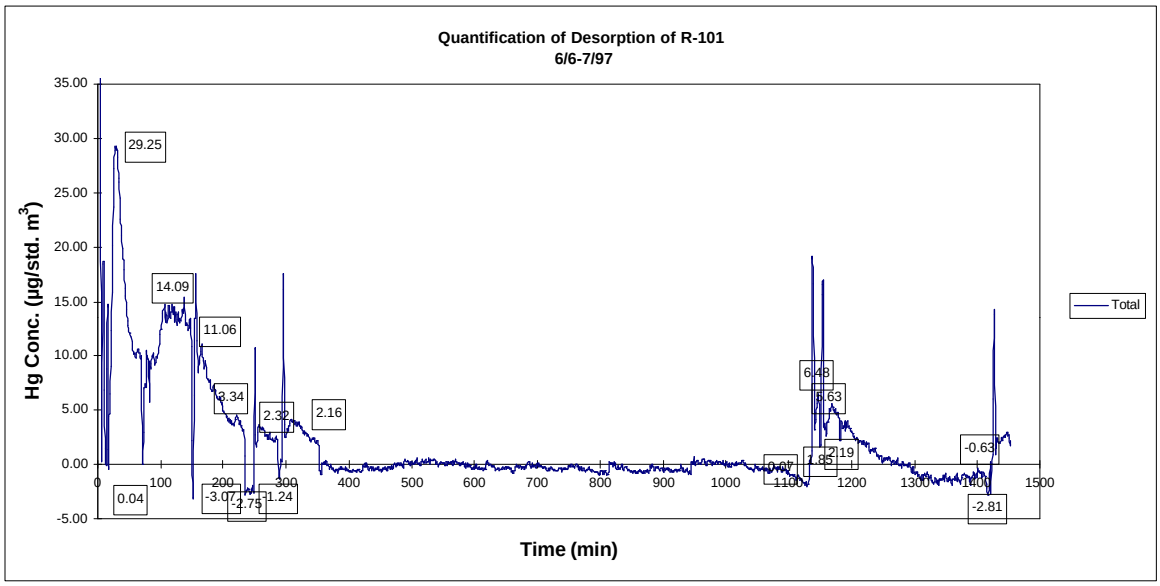

Figure D-15 – Desorption of Unit 1 with Clean Regeneration Sampling Lines, 6/6 - 6/7/97

Appendix E: Iodated Carbon Trap and Wet Chemistry Results for Testing in March, 1997

During the March, 1997, tests on High Sulfur Pittsburgh Seam coal, ADA Technologies sampled periodically with iodated carbon traps and Consol sampled with a modified Ontario Hydro "wet chemistry" method. The iodated carbon traps were provided and analyzed by Frontier Geosciences (Seattle, WA).

These tests basically disagreed with the ADA analyzer at the outlet of the sorbent beds and also disagreed with each other (Tables E-1 and E-2). However, we have no real reason to discard either the iodated carbon trap, the wet chemistry, or the analyzer results. One problem we faced in running the system was that periodically the flow would surge because of power problems at Consol or sparking from the Consol electrostatic precipitator. Temperature and flow surges could have actually desorbed some mercury from the beds during operation. The mercury analyzer would not necessarily see this phenomenon because it spends 10 minutes per hour zeroing and spanning. However, a burst of mercury can dominate the total mercury captured in time-average method like the iodated carbon traps or the wet chemistry technique (e.g., one minute at 1,000 $\mu g/m^3$ can look like 10 $\mu g/m^3$ in a 100 minute time-averaging sampling method). This explanation is only a hypothesis, but we believe that only something of this sort can explain the random high outlets seen by both the iodated carbon traps and the wet chemistry technique on completely different test days.

In general, the wet chemistry outlet concentrations are at least twice the inlet values. Further, on 3/12 and 3/13, virtually all of the outlet mercury is non-elemental. The results were of some concern to us which is why we investigated possible flow distribution and regeneration problems in April and May. However, we had no means in the Phase I program to investigate all of the implications of the iodated carbon and wet chemistry data. If the beds really were not working at all during the March tests, we are confident that they were working during June after our improvements to the regeneration. However, the analyzer data in March indicated good removal of mercury by the beds, and we had no reason to doubt the analyzer data in March.

Table E-1 –Iodated Carbon Measurements of Skid Performance (micrograms per standard cubic meter)

Date	Time	Inlet	Outlet
3/6/97	10:45 am to 11:30 am	18.1 µg/m^3	17.5 µg/m^3
3/11/97	9:50 am to 10:30 am	12.6 µg/m^3	53.9 µg/m^3
3/11/97	2:00 pm to 2:45 pm	11.0 µg/m^3	21.9 µg/m^3
3/12/97	2:20 pm to 3:05 pm	8.6 µg/m^3	10.0 µg/m^3
3/12/97	6 pm to 6:45 pm	14.8 µg/m^3	10.0 µg/m^3
3/13/97	5 pm to 5:50 pm	9.81 µg/m^3	10.6 µg/m^3

Table E-2 – Wet Chemistry Measurements of Skid Performance (micrograms per standard cubic meter; percentage oxidized mercury in parenthesis)

Date	Time	Inlet	Outlet
3/6/97	1 pm to 3 pm	10.4 µg/m^3 (75%)	32.3 µg/m^3 (86%)
3/11/97	9 am to 11 am	7.1 µg/m^3 (76%)	26.7 µg/m^3 (81%)
3/11/97	12:25 pm to 2:25 pm	5.9 µg/m^3 (76%)	15.1 µg/m^3 (76%)
3/12/97	Noon to 2:00 pm	6.4 µg/m^3 (83%)	12.5 µg/m^3 (95%)
3/12/97	3 pm to 5 pm	6.6 µg/m^3 (78%)	13.2 µg/m^3 (100%)
3/13/97	8 am to 10 am	6.9 µg/m^3 (80%)	65.0 µg/m^3 (93%)
3/13/97	11:30 am to 1:30 pm	7.3 µg/m^3 (80%)	21.0 µg/m^3 (98%)
3/13/97	2 pm to 4 pm	5.8 µg/m^3 (80%)	16.2 µg/m^3 (97%)

Appendix F

Excerpt of Paper Explaining Fundamentals of Mercury Analyzer

Full Paper given at 90th Annual Meeting of the Air and Waste Management Association, Toronto, Ontario, Canada

June 8-13, 1997

Development and Field Testing of a Continuous Real-Time, Speciating Mercury Analyzer

Ms. Sharon Sjostrom
Dr. Daryl L. Roberts
Mr. Gary Anderson
Mr. Frank Sagan
Mr. Justin Smith

ADA Technologies, Inc.
304 Inverness Way South, Suite 365
Englewood, CO 80112

Abstract

The mercury concentration in utility flue gas from coal-fired boilers is in the range of 0.1 to 1 part per billion. Wet chemical and solid sorbent measurement methods are available that can provide reasonable time-average measurements. However, a method that responds in real-time to mercury perturbations in the flue gas stream, can differentiate between elemental mercury and mercury compounds, is not affected by varying levels of SO_2, and that operates at typical stack temperatures to avoid sampling problems, would be a useful alternative to manual methods.

ADA Technologies has been developing such a continuous mercury analyzer for the past few years. The analyzer is based on absorption of ultraviolet light emitted by a mercury lamp. The lamp itself resides in a permanent magnetic field, creating two wavelengths of source light that are polarized 90° with respect to each other (Zeeman Effect). Mercury extinguishes only one of these wavelengths, and common interferents such as SO_2 extinguish both, allowing for on-line cancellation of the interfering species. The system consists of two sample cells each with sensitive photodetectors, a mercury species converter, and a calibration system. Elemental mercury is detected in the first sample cell. Sample gas exiting the first cell is passed through a "converter" to change speciated mercury compounds to elemental mercury that is then measured in a second cell (total mercury). Signals from both detectors are continually processed. The analyzer is calibrated regularly with known concentrations of mercury, and the operation is verified periodically by comparing to a manual mercury measurement method.

Extensive laboratory evaluation and field testing has recently been undertaken to optimize the performance of the analyzer. New developments in the calibration technique, sampling system,

measurement, and signal processing have resulted in a system capable of measuring mercury concentrations on a slipstream from a coal-fired power plant in real time (0.1 to 0.8 ppb mercury). The system is configured to automatically calibrate on a regular basis. We have found that we can also measure the SO_2 concentration because SO_2 absorbs UV light at the wavelength of the mercury lamp emission. With the Zeeman splitting of the light source, the SO_2 concentration does not affect the mercury signal except when the SO_2 varies more than 1000 ppm between calibrations. Descriptions of these recent developments and resulting field test data are included in this paper.

Introduction

Continuous monitoring of mercury emissions from combustion sources may be required by regulatory agencies in the near future. In addition, the effectiveness of research efforts aimed at mercury control technologies can be greatly enhanced with a continuous mercury monitor. For these reasons, ADA Technologies has been developing a continuous monitor for mercury found in flue gases and other combustion gases. The monitor has now undergone four months of testing at a coal-fired pilot facility and six months of field testing at a coal-fired power plant where the mercury concentrations have been in the range of 0.1 ppb to 0.8 ppb. The analyzer has also been configured to monitor SO_2 while recording total and elemental mercury concentrations. This paper describes the fundamentals behind the operation of the analyzer, the techniques used for calibration, non-ideal factors that influence operation, and an example of data collected from a coal-combustion flue gas stream.

Mercury Analyzer Fundamentals

Elemental mercury both emits and absorbs UV light in a very narrow wavelength range centered around 2537 A. Therefore a mercury lamp is the ideal source of light to pass into a sample cell that contains an unknown concentration of mercury. When elemental mercury vapor is in the light path between the lamp and a light detector, the mercury vapor absorbs light in the wavelength emitted by the lamp. The extinction of light gives a direct measure of the concentration of mercury through the application of Beer's law as has been practiced for "cold vapor atomic absorption" analyses for decades. The difficulty in applying this technique to flue gases is the presence of species, such as SO_2, that also absorb UV light in the same region. Since SO_2 is often present in concentrations that are one million times that of mercury, the extinction of light by SO_2 swamps that caused by the mercury, rendering conventional UV absorption spectroscopy useless.

ADA's approach to canceling the influence of such interferents in real time is based on the Zeeman effect on the UV emission spectrum of the mercury lamp (Figure 1). The mercury lamp shown in the figure emits light at 2537 Å with the subpeaks of several isotopes closely grouped. If the lamp is placed in a magnetic field, the spins of outer shell electrons will align, causing the emission profile to change. The new profile adds two "winglets" spaced a fraction of an angstrom on either side of the main emission grouping and orthogonally polarized to the main emission grouping.

The absorption profile of mercury is superimposed over the emission spectrum in Figure 1 (100% on this figure means 100% transmission and zero absorption). Elemental mercury vapor absorbs

the p wavelength (the main emission grouping) but does not significantly absorb the s^+ or s^- wavelengths (the "winglet" emissions). In contrast, SO_2 absorbs the p and s wavelengths almost equally. Application of Beer's law to both wavelengths (p and s) yields two equations that are solved simultaneously for the mercury concentration and the SO_2 concentration. Because the molar absorptivity of elemental mercury for the p wavelength exceeds that of SO_2 by a factor of about 1,000, the mercury concentration can be determined even though the SO_2 is present at concentrations one million times that of mercury.

To exploit this principle, it is necessary to introduce alternatively the p and then the s wavelength to the sample cells. The "switch" that chooses which wavelength enters the sample cell is a half-order waveplate rotating at approximately five rotations per second. The light coming through this waveplate follows the equation $\mathbf{I = I_\sigma \cos^2 2\theta + I_\pi \sin^2 2\theta}$, where θ is the angle of rotation of the waveplate. In one rotation of the waveplate, the light entering the sample cell has four peaks and four valleys corresponding to the intensity of either p-light or s-light emitted by the mercury lamp.

Figure 2 presents the photodetector response with zero gas, mercury span gas, and SO_2 present in the measurement cell. The photodetector response follows the sinusoidal equation of the waveplate. It does not matter if $\mathbf{I}_\sigma$ is greater than or less than $\mathbf{I}_\pi$, but for illustration purposes, Figure 2 shows a situation where $\mathbf{I}_\sigma$ is greater than $\mathbf{I}_\pi$. The first third of the figure represents the response with zero gas in the measurement cell. When mercury is in the measurement cell, the intensity of the p-light (main emission grouping) reaching the photodetector is decreased, but the intensity of the s-light reaching the photodetector is essentially unchanged. Thus, the difference between the maximum and minimum intensities is greater, and the average light intensity at the photodetector is slightly lower. The extinction of the p-light is related by Beer's law to the concentration of mercury. For the purposes of discussion, the difference between maximum and minimum light intensities can be considered as the "mercury signal strength." In the presence of SO_2, both p and s polarizations are attenuated, decreasing the mercury signal strength and the average light intensity.

Figure 3 is a graph of mercury signal strength versus average light intensity for concentrations of SO_2 from zero to 4500 ppm measured in the field during an SO_2 calibration. The mercury signal strength is seen to be a linear function of average light intensity for this broad band absorber. For the calibration shown in the figure, a least squares linear fit was applied to the data. The r^2 for this data set was 0.9991. Because the correlation is very strong in the range expected at coal-fired utilities, the analyzer can report the SO_2 concentration simultaneously with the concentrations of elemental and total mercury.

Figure 1. Zeeman splitting: Emission profile of natural mercury and mercury in a magnetic field.

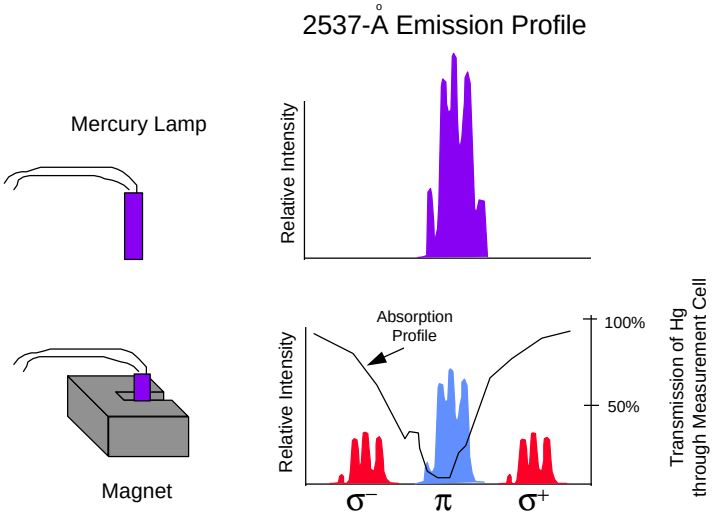

Figure 2. Ideal response of photodetector.

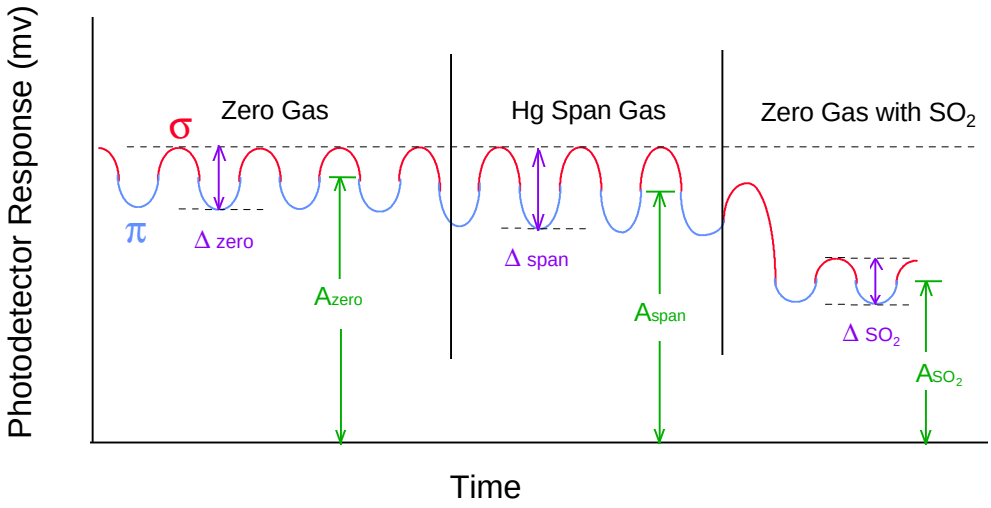

Figure 3. Linear response of analyzer to SO_2 concentrations from 0 to 4500 ppm.

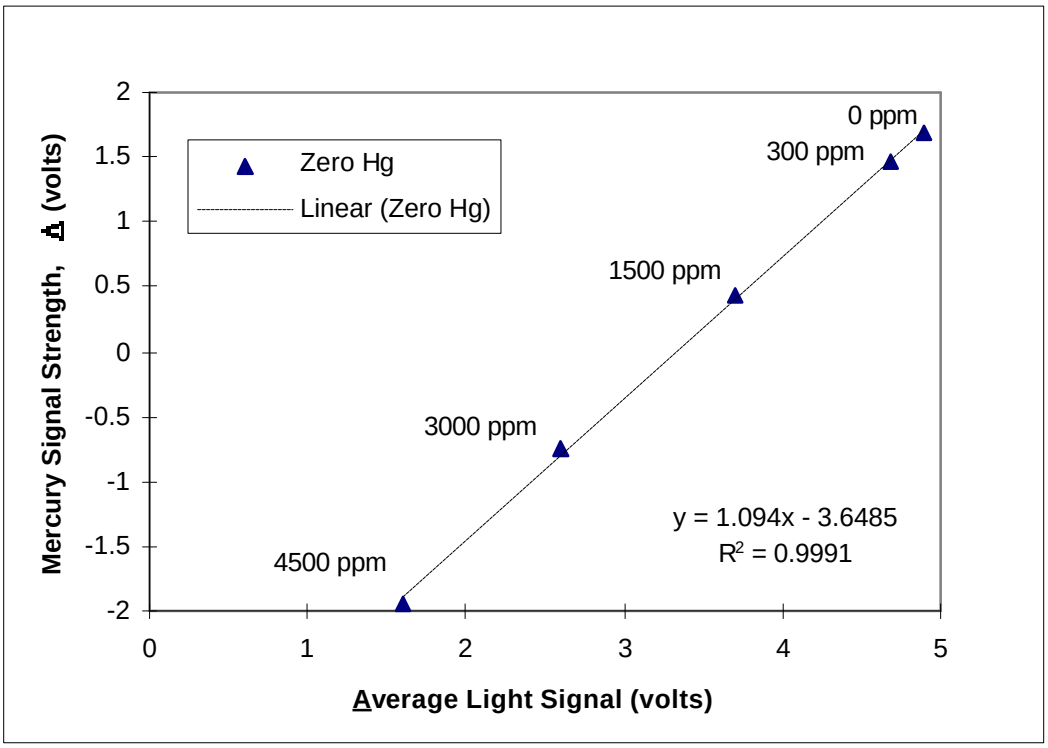

Appendix G

Laboratory Results with Monoliths Returned from the Field Test Unit

The appendix contains laboratory test results for monoliths that were taken from the field unit in April and in June.

On April 15, 1997, a single monolith was removed from Unit 1. At this point, Unit 1 had undergone 102 hours of sorption and 160 hours of desorption (seven cycles). The monolith had a thin film of ash coating its surface. To determine if the monolith had been fouled by this ash coating, the monolith was tested at ADA's lab with elemental and non-elemental mercury.

The tests were done with a synthetic flue gas as described in the main body of this report and with approximately 30 µg/m^3 of mercury. The automatic valving in the apparatus periodically passes the inlet gas to the analyzer so that we have a record of the constancy of the inlet mercury concentration. Figure G-1 shows complete up take of the mercury until breakthrough. At this point approximately 0.125 milligrams of mercury had been sorbed. There is one milligram of noble metal on the monolith, so the amount of uptake is the expected amount (10% to 15% mercury to noble metal mass ratio at breakthrough).

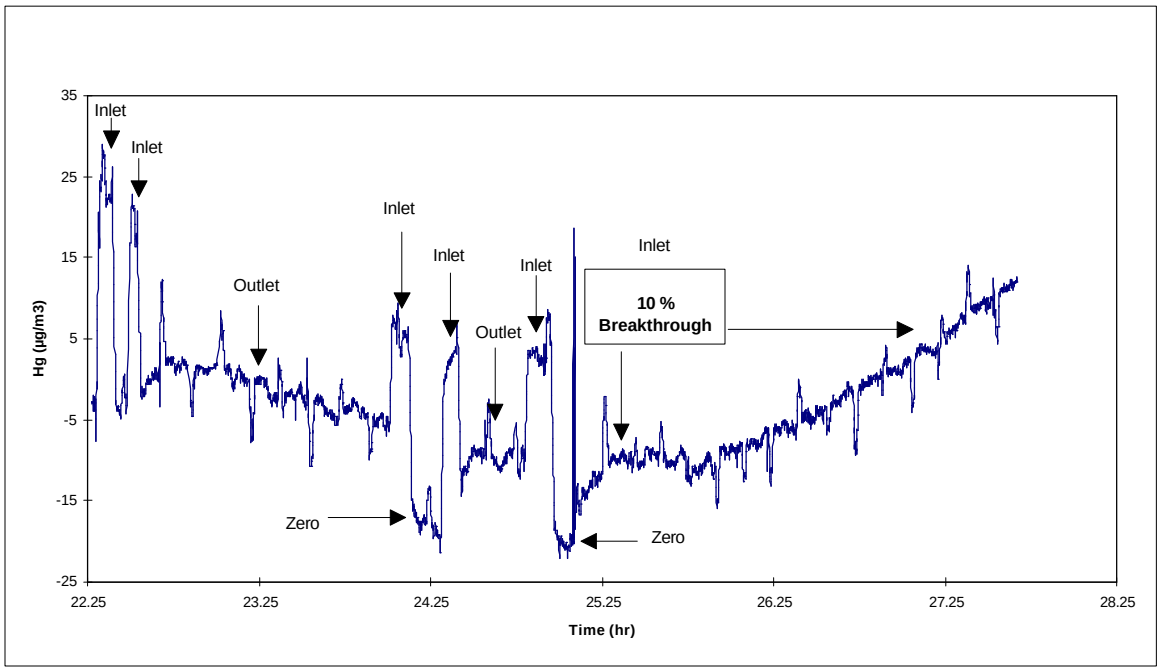

Figure G-1 – Sorption of Elemental Mercury with Monolith Removed from Unit 1

After the sorption, we regenerated the monolith and observed mercury coming off, although we were unable to get a good quantification of the amount that came off (Figure G-2).

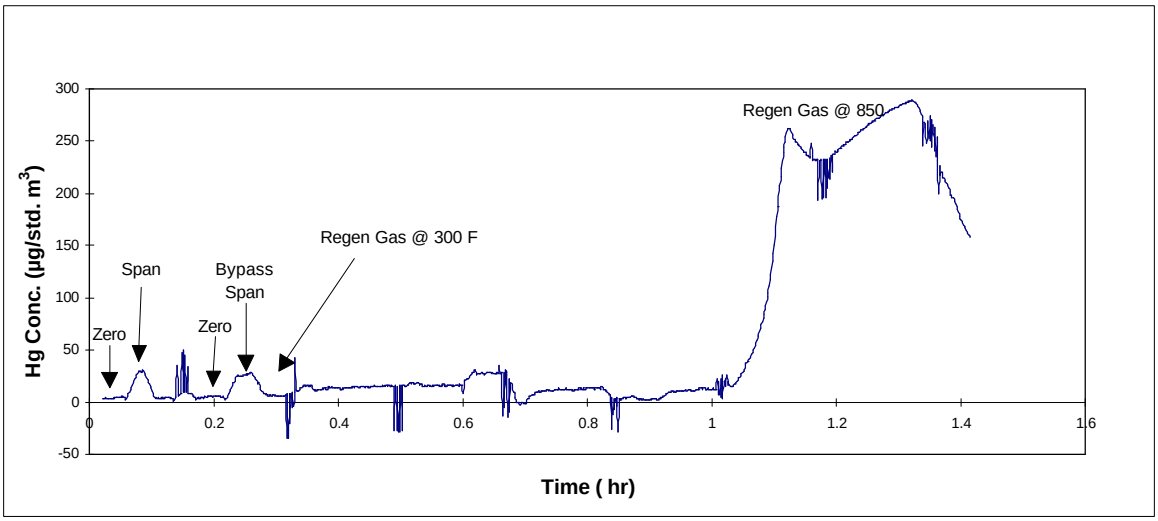

Figure G-2 – Regeneration of Monolith Removed from Unit 1

This monolith was then tested for sorption with $HgCl_2$. The gas phase concentration of $HgCl_2$ was 58.3 µg/std. m^3 (43 µg/m^3 of mercury). The monolith removed 100% of the mercury for at least two hours but had broken through at 24 hours. Because of computer problems, the data were not recorded between two hours and 24 hours. Therefore all we can say is that the monolith sorbed at least 0.018 milligrams of mercury but less than 0.22 milligrams of mercury before breakthrough. We would have expected breakthrough at about 0.1 milligrams of mercury sorbed.

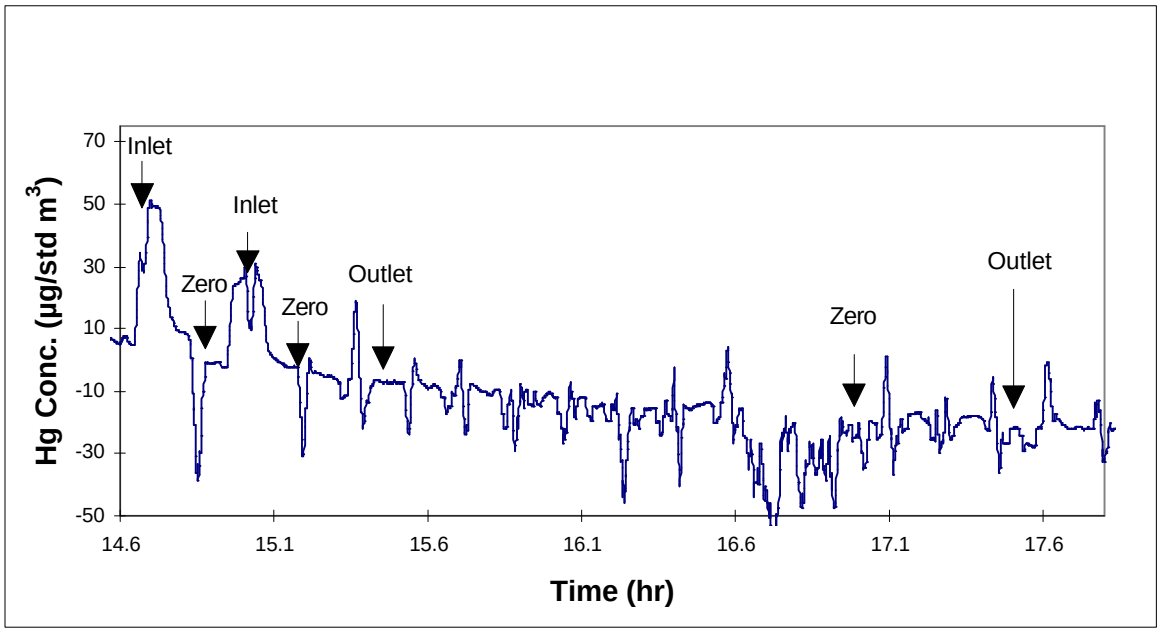

Figure G-3 – Uptake of $HgCl_2$ with Monolith Removed from Unit 1 in April

B) Lab Test on Monolith Removed from Unit 2 at end of June, 1997

On June 21 a monolith was removed from Unit 2 after 279 hours of sorption and 331 hours of desorption (12 cycles of sorption and desorption). This monolith also had a thin layer of ash coating its surfaces.

The tests were done with a synthetic flue gas as described in the main body of this report and with approximately 30 µg/m^3 of mercury. Again, the automatic valving in the apparatus periodically passed the inlet gas to the analyzer. Figure G-4 shows complete uptake of the mercury for the first six hours. In Figure G-5, we see that breakthrough occurred at approximately eight hours. At this point approximately 0.075 milligrams of mercury had been sorbed. This amount is a little less than what we would normally expect. Unit 2 was last desorbed for 20 hours before this monolith was removed. This result would seem to say that the monolith had lost 25% of its capacity in the five months at Consol.

However, we regenerated the monolith, tested it again, and found that it took up 0.16 milligrams of mercury (Figure G-6). This result is consistent with what we found in the laboratory (Figure 9 in main text) wherein a good strong desorption seemed to refresh the

monolith. This result therefore gives credence to the possibility that in a full-scale operating system, a periodically longer or stronger desorption will likely refresh the monoliths.

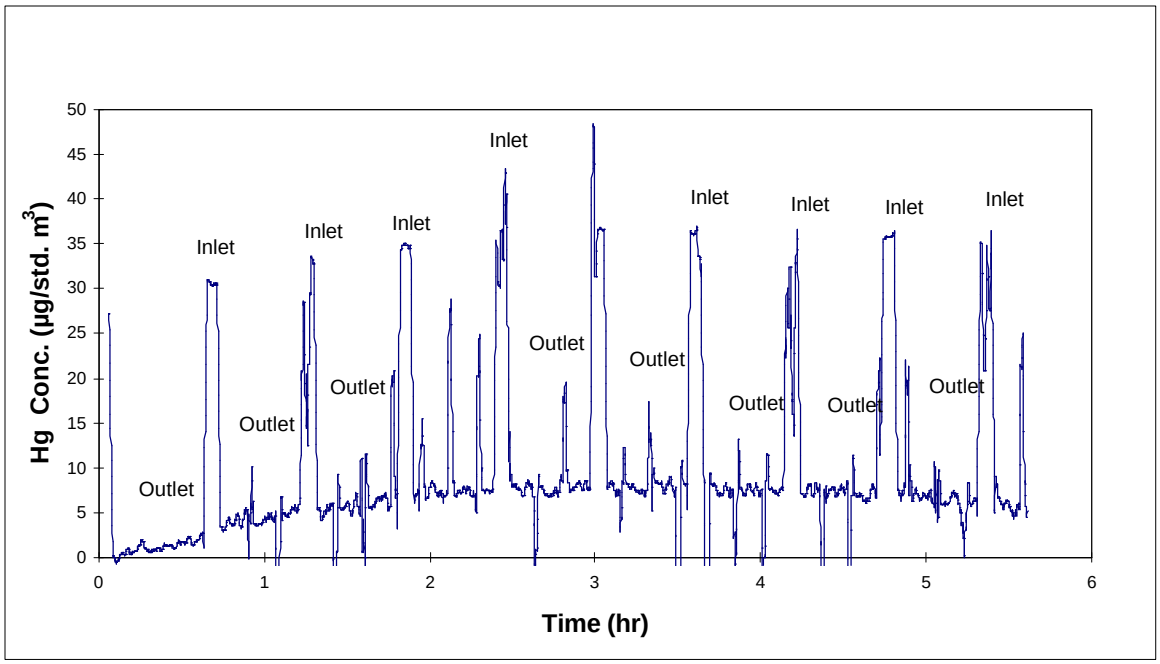

Figure G-4 – Sorption with Monolith Removed from Unit 2 in June

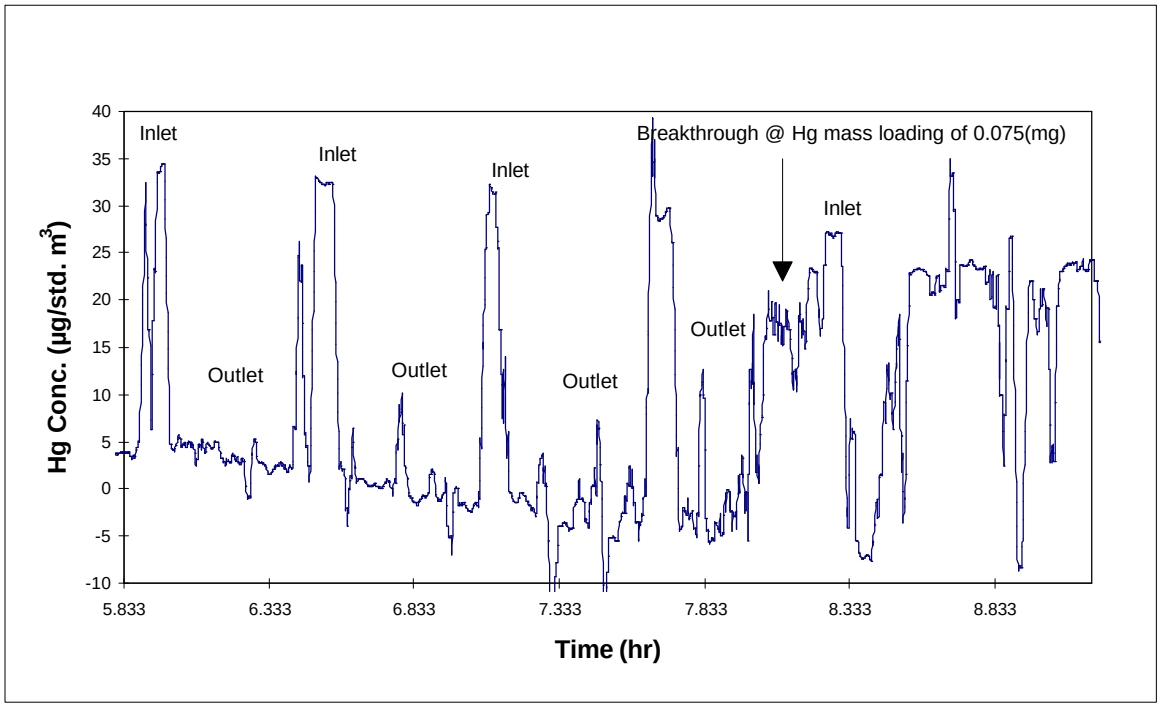

Figure G-5 – Breakthrough Point for Monolith Removed from Unit 2 in June

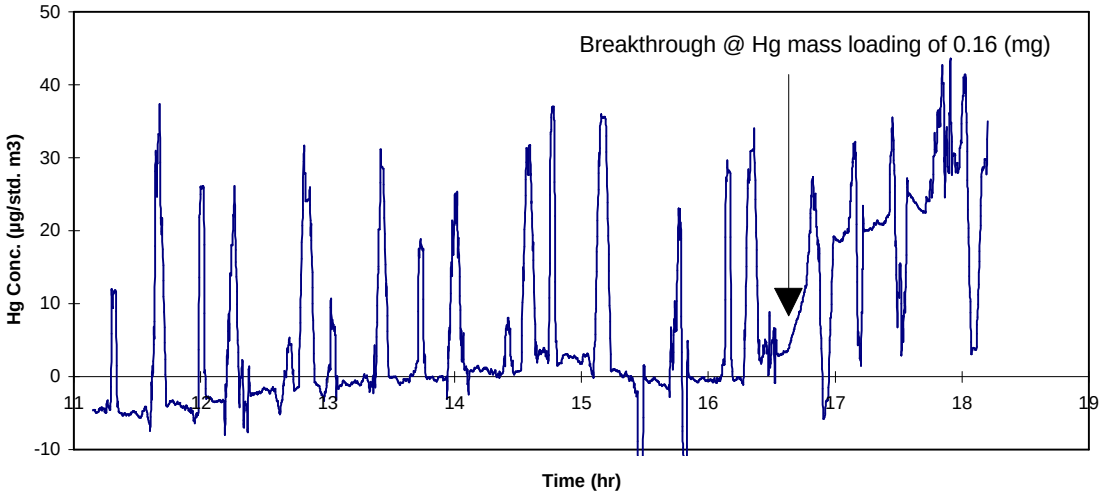

Figure G-6 – Second Sorption Test with Monolith Removed from Unit 2 in June